



Ricerca di Sistema elettrico

Valutazioni di rischio e scenari incidentali - PAR 2017

L. Burgazzi, R. Lo Frano, N. Muro, D. Del Serra, W. Ambrosini,
F. Mascari, F. Giannetti, M. Donorio, A. Giampaolo, L. Gramiccia,
G. Caruso



Valutazioni di rischio e scenari incidentali – PAR 2017

L. Burgazzi, F. Mascari (ENEA)
R. Lo Frano, N. Muro, D. Del Serra, W. Ambrosini (CIRTEN - UniPisa),
F. Giannetti, M. Donorio, A. Giampaolo, L. Gramiccia, G. Caruso (CIRTEN - UniRoma)

Settembre 2018

Report Ricerca di Sistema Elettrico

Accordo di Programma Ministero dello Sviluppo Economico - ENEA

Piano Annuale di Realizzazione 2017

Area: Generazione di energia elettrica con basse emissioni di carbonio

Progetto: Sviluppo competenze scientifiche nel campo della sicurezza nucleare e collaborazione ai programmi internazionali per il nucleare di IV generazione - Linea Progettuale 1

Obiettivo: Safety assessment e valutazioni d'impatto

Responsabile del Progetto: Federico Rocchi, ENEA

Il presente documento descrive le attività di ricerca svolte all'interno dell'Accordo di collaborazione "*Sviluppo competenze scientifiche nel campo della sicurezza nucleare e collaborazione ai programmi internazionali per il nucleare di IV generazione*"

Responsabile scientifico ENEA: Federico Rocchi

Responsabile scientifico CIRTEN: Marco Ricotti

Questo rapporto contiene i due seguenti Rapporti Tecnici ENEA:

- L. Burgazzi, R. Lo Frano, N. Muro, D. Del Serra, W. Ambrosini, Risk analysis of safety systems devoted to Severe Accident Management in nuclear power plants, ADPFISS-LP1-109
- F. Mascari, F. Giannetti, M. Donorio, A. Giampaolo, L. Gramiccia, G. Caruso, Analisi e valutazioni di Incidenti Severi in LWR, ADPFISS-LP1-122

Titolo

Risk analysis of safety systems devoted to Severe Accident Management in nuclear power plants

Descrittori

Tipologia del documento: Rapporto tecnico

Collocazione contrattuale: Accordo di programma ENEA-MSE: Piano Annuale di Realizzazione 2017, Linea Progettuale 1, Obiettivo B: Valutazione degli incidenti e delle loro conseguenze, Task B2-1

Argomenti trattati: Sicurezza nucleare
Analisi incidentale
Analisi di sicurezza probabilistica

Summary

This report presents the activities performed in the frame of LP1, Objective B (Accident consequences evaluation), task B2-1 of PAR 2017, ADP ENEA-MSE.

Main achievement is the risk analysis of the safety systems appointed to SAM (Severe Accident Management) actions, i.e. designed to prevent and mitigate the consequences of severe accidents. They include both systems for the residual heat removal from the containment and for molten core in vessel retention.

For the scope, deterministic as well as probabilistic approaches are applied.


Note:

This document has been prepared with the following main contributors:

- L. Burgazzi (ENEA)
- R. Lo Frano, N. Muro, D. Del Serra, W. Ambrosini (CIRTEN-Università di Pisa)

Ref. CERSE-UNUPI RL 5001/2018

2			NOME			
			FIRMA			
1			NOME			
			FIRMA			
0	EMMISSIONE	19/11/18	NOME	L. Burgazzi	F. Rocchi	F. Rocchi
			FIRMA	<i>L. Burgazzi</i>	<i>Federico Rocchi</i>	<i>Federico Rocchi</i>
REV.	DESCRIZIONE	DATA		REDAZIONE	CONVALIDA	APPROVAZIONE

Table Of Contents

List of Figures	3
List of Tables.....	4
List of Acronyms.....	5
Executive Summary	6
1. Introduction and scope.....	7
2. Passive containment cooling system operation and description (AP1000-like configuration).....	9
3. Reliability assessment of passive containment cooling system (AP1000-like configuration).....	12
3.1. Failure analysis.....	12
3.2. Fault tree failure probability.....	15
4. Interface with T-H analysis.....	18
5. Conclusions of the reliability analysis	20
6. Study of a new in-vessel corium retention strategy	22
6.1. Background and Introduction.....	22
6.2. IVR approach	24
7. Molten Pool Behaviour and Structural Integrity of RV.....	27
7.1. Analysis approach: assumption and modelling.....	28
7.1.1. Core accident progression	28
7.1.2. Boundary conditions of core melt	29
7.2. Thermal analysis	31
7.3. Thermal analysis: FEM analysis	33
8. Pool behaviour analyses: results' discussion	37
8.1. Analytical results.....	37
8.2. Numerical results.....	39
9. Final summary	48
References	50

List of Figures

Figure 1: AP1000 Passive containment cooling system	10
Figure 2: Flow chart of passive containment cooling system in AP1000.....	11
Figure 3: Functional failure fault tree of PCCS system	13
Figure 4: Fault tree for PCCS.....	16
Figure 5: Schematic IVMR phenomenology [9] and heat transfer processes in the melt progression.....	23
Figure 6: Heat flux vs. RV angular position of lower head in IVR	24
Figure 7: Schematic in-vessel melt progression sequence	25
Figure 8: Scheme of the internal core catcher (dashed surface at the vessel lower head on the left figure) and of the SiC-SiC structure with alumina pebble boxes (right figure).....	26
Figure 9: Scheme of the melt pool. Temperatures T_w , T_m and T_l or T_b refer the water, the molten core, the light metal layer and to the crust, respectively.....	30
Figure 10: Representation of the core debris relocated at the lower head, in a steady-state condition, and made of either solid oxidic crust and/or melt oxidic pool (left figure). Analytical model of core debris with outer RV insulator (instead of adiabatic boundary condition) [20], on the right figure. For this latter boundary conditions are $T(R_1)=T_{\text{corium}}$ and $T(R_5)=T_{\text{water}}$. The thermal insulation (layer C) is assumed 0.25 m thickness (0.15 W/m/K of thermal conductivity) as the real one in nuclear reactor [16-17].	32
Figure 11: Hypothetical representation of steel and Al_2O_3 contacting surface.	32
Figure 12: Strength and Young modulus behaviour vs temperature for the alumina	35
Figure 13: FEM model of the vessel lower head	35
Figure 14: Temperature trend for IVR with and without ICC solution.	38
Figure 15: Radial temperature in the bottom head for $T(R_4) = 100^\circ\text{C}$	38
Figure 16: Circumferential stress behaviour, in the A, B and C layers, as function of the corium temperature	39
Figure 17: Contour plot of temperature in the alumina and steel wall (a) in the case of external water cooling. In particular, the temperature distribution through the vessel wall is give in (b).	41
Figure 18: Contour plot of temperature in the alumina and steel wall in the case of absence of external water-cooling.....	41
Figure 19: Contour plot of temperature in vessel wall for 1m.....	42

Figure 20: Contour plot of temperature in the bottom head wall for 0.5m of relocated corium (a). In the figure (b) the distribution of temperature in the steel wall of vessel is also shown 43

Figure 21: Results of thermo-mechanical analysis: temperature (a) and stress (b) in the bottom head thickness (outward direction according to the arrow versus) in the case external water-cooling and full melt core relocation. In the Figure 20 (b) zooming of temperature trend in the alumina and steel thickness is given. 44

Figure 22: Stress distribution in the bottom head wall in the case external water cooling (a) and full melt core relocation. In the bottom figure (b) is given the countur plot in steel thickness. 45

Figure 23: Stress trend in the bottom head thickness in the case external water cooling and full melt core relocation. 46

Figure 24: Temperature (a) and stress (b) distribution in the bottom head of vessel, for 0.1m alumina thickness, in the case of external water cooling and full melt core relocation. 47

List of Tables


Table 1: Failure probabilities for the PCCS 14

Table 2: Geometrical and material properties used in the model [17-19]..... 32

Table 3: Material properties for FEM simulation 34

List of Acronyms

AP 600/1000	Advanced Passive
CCF	Common Cause Failure
CET	Containment Event Tree
CMC	Ceramic Matrix Carbide
DW	Drywell
ENEA	Italian National Agency for New Technologies, Energy and Sustainable Economic Development
ESBWR	Economic Simplified Boiling Water Reactor
EVR	Ex-Vessel melt Retention
FAPCS	Fuel and Auxiliary Pools Cooling System
FMEA	Failure Mode and Effect Analysis
GDCS	Gravity Driven Cooling System
HEX	Heat Exchanger
IAEA	International Atomic Energy Agency
IC	Isolation Condenser
ICC	Internal Core Catcher
ICS	Isolation Condenser System
IVR	In-Vessel Retention
IVCR	In-Vessel Corium Retention
IVMR	In Vessel Melt Retention
LOCA	Loss of Coolant Accidents
LWR	Light Water Reactor
MC	Monte Carlo
MFCI	Molten Fuel-Coolant Interaction
MELCOR	Methods for Estimation of Leakages and CONsequences of Releases
MSLB	Main Steam Line Break
NCF	Natural Circulation Failure
NPP	Nuclear Power Plant
PCC	Passive Cooling Condenser
PCCS	Passive Containment Cooling System
PCF	PCC Condenser Failure
PCCWST	Passive Containment Cooling Water Storage Tank
PSA	Probabilistic Safety Assessment, Probabilistic Safety Analysis
PWR	Pressurized Water Reactor
RMPS	Reliability Methods for Passive Systems
RPV	Reactor Pressure Vessel
R-S	Resistance - Stress
SAM	Severe Accident Management
SBWR	Simplified Boiling Water Reactor
SMA	Safety Margin Assessment
SSC	Structure System and Components
T-H	Thermal-hydraulic
WSF	Water supply failure

 Ricerca Sistema Elettrico	Sigla di identificazione	Rev.	Distrib.	Pag.	di
	ADPFISS-LP1-109	0	L	6	52

Executive Summary

The Fukushima incident highlighted, among other aspects, the need for the implementation of strategies for the management of severe accidents (SAM, Severe Accident Management), in the form of engineering safeguards aimed at minimizing the risk of radioactive substances leakage and likewise increase the level of protection of the plants.

In this regard, therefore, the objective of the international scientific community is to identify the engineering measures capable of increasing the capacity of the structure in the face of the updated demand, deriving from this type of severe events.

In light of the innovative reactor designs (such as AP1000) an activity is therefore proposed aimed at assessing the robustness of the various systems of protection of the plant, aimed at mitigating the consequences of severe accidents, such as, for example, for the disposal of heat from the Containment (PCCS, Passive Containment Cooling System), for the purpose of maintaining the function of confinement and containment of radioactive products, and to avoid the interaction of Corium with concrete (IVMR, In-Vessel Melt Retention). Specific systems are analyzed in terms both probabilistic (reliability) and deterministic (resistant capacity). For the proposed purposes, we will use preliminary analytical and / or numerical simplified models that will allow us to study the complexity of the incidental transient and highlight the benefits deriving from the implementation of the strategies for managing the severe incidents proposed; the same applies to assessments of newly developed safety safeguards in terms of performance and relative effectiveness.

The activity is intended as a completion and finalization of the two previous years, refer to ENEA report ADP-FISS-LP1-072 “Analysis relating to the implementation of the safety safeguards for the severe accident management in nuclear reactors”, issued in September 2016, which shows the design implementation through some specific passive concepts and ENEA report ADPFISS-LP1-096 “Assessment of the safeguards to cope with the consequences of severe accidents in nuclear power plants”, delivered in November 2017, where the safety and reliability assessment of any of the proposed systems is offered.

1. Introduction and scope

The extensive use of passive safety systems, designed to extend the coping period in the event of adverse situations such as occurred at the Fukushima Daiichi plant, is one of the most relevant strategy envisaged to meet the requirements to enhance the safety of nuclear power plants through increased safety system reliability, as devised in [1], which provides a list of systems, consistent with the available knowledge as emerging, for the most, from a literature survey.

IAEA-TECDOC-626 provides definitions for safety related terms as applied to advanced reactors [2].


The study deals with the assessment of passive systems, implemented in reactor designs to exercise and ensure the safety functions such as removing heat from the containment and the control and abatement of the amount of hydrogen that could break free, following a severe accident involving the melting of the core. As for this latter, the corium coolability (i.e., preventing melt-through of physical barriers) is recognized as the “Achilles-heel” of the Gen. II or earlier PWR designs such that to cope with this issue solutions adopted by Gen. III reactors consider the adoption of in-vessel melt retention (IVR) or ex-vessel melt retention (EVR) solution.

It has to remark also that the state of knowledge with respect to PWR in-vessel core-melt progression has not changed substantially from TMI-2. It is thought that a melt pool forms in the original core volume and then progress downwards into the lower plenum, to commence the thermal loading on the lower head. The new information is on the effects of accident-management actions, e.g., water addition to a hot core. This may increase the damage and the hydrogen generation, due to the Zircalloy oxidation.

The initial attack of the melt on the lower head is in the form of a jet, whose composition may well be fully oxidic.

Deeper consideration of these processes could provide a better understanding on how to assess and increase the thermal margin related to the in-vessel melt retention.

In particular, considering the specificities of their operation, a careful analysis is required to evaluate the vessel performance and ascertain the accomplishment of the required safety mission. Within a risk informed approach, the study proposes:

 Ricerca Sistema Elettrico	Sigla di identificazione ADPFISS-LP1-109	Rev. 0	Distrib. L	Pag. 8	di 52
--	---	------------------	----------------------	------------------	-----------------

- on the one hand, the assessment of the reliability of passive systems, conceived to maintain the function of containment of radioactive products, as a follow-on of [1], which shows some specific aspects of passive systems for further evaluation of safety in a reliability plane.
- on the other hand it is intended to study the behavior of the containment structures, such as the vessel, the containment system, etc., in order to assess from a deterministic point of view the safety margin (SMA) and propose engineering solutions/safeguards, based as well on the use of innovative materials for in-vessel retention, aimed at mitigating the effects of a severe accident scenarios.

To these aims, we will employ analytical and/or simplified numerical models, which allow to study the complexity of the transitional incidental and highlight the benefits of implementing the proposed strategies for the management of severe accidents.

2. Passive containment cooling system operation and description (AP1000-like configuration)

The passive containment cooling system in AP1000 [3] is a safety-related system that functions to reduce containment temperature and pressure following a loss-of-coolant accident (LOCA) accident, a main steam line break (MSLB) accident inside containment, or other events that cause a significant increase in containment pressure and temperature.

The function of the AP1000 passive containment cooling system (PCCS) is to prevent the containment vessel from overheating and exceeding the design pressure, which could result in a breach of the containment and the loss of the final barrier to radioactive release.

The PCCS consists of the following components (Figure 1):

- Air inlet and exhaust paths that are incorporated in the shield building structure
- An air baffle that is located between the steel containment vessel and the concrete shield building
- A Passive Containment Cooling (PCCWST) Water Storage Tank that is incorporated in the shield building structure above the containment
- A water distribution system.

In particular the passive containment cooling system water storage tank outlet pipe is equipped with three sets of redundant isolation valves. In two sets, air-operated butterfly valves are normally closed and open upon receipt of actuation signals. The third parallel supply line contains a normally closed motor-operated valve. And each valve fails open on loss of power or loss of air. In addition to these normally closed valves, there is a normally open motor operated valve in each of the three lines.

The PCCS is required to effectively cool the containment following an accident such that the design pressure is not exceeded and the pressure is rapidly reduced. The steel containment vessel itself provides the heat transfer surface that allows heat to be removed from inside the containment and rejected to the atmosphere. Heat is removed from the containment vessel by a natural circulation flow of air through the annulus formed by the outer shield building and the steel containment vessel it houses.

Outside air is pulled in through openings near the top of the shield building and pulled down, around the baffle and then flows upward out of the shield building.

The flow of air is driven by the chimney effect of air heated by the containment vessel rising and finally exhausting up through the central opening in the shield building roof.

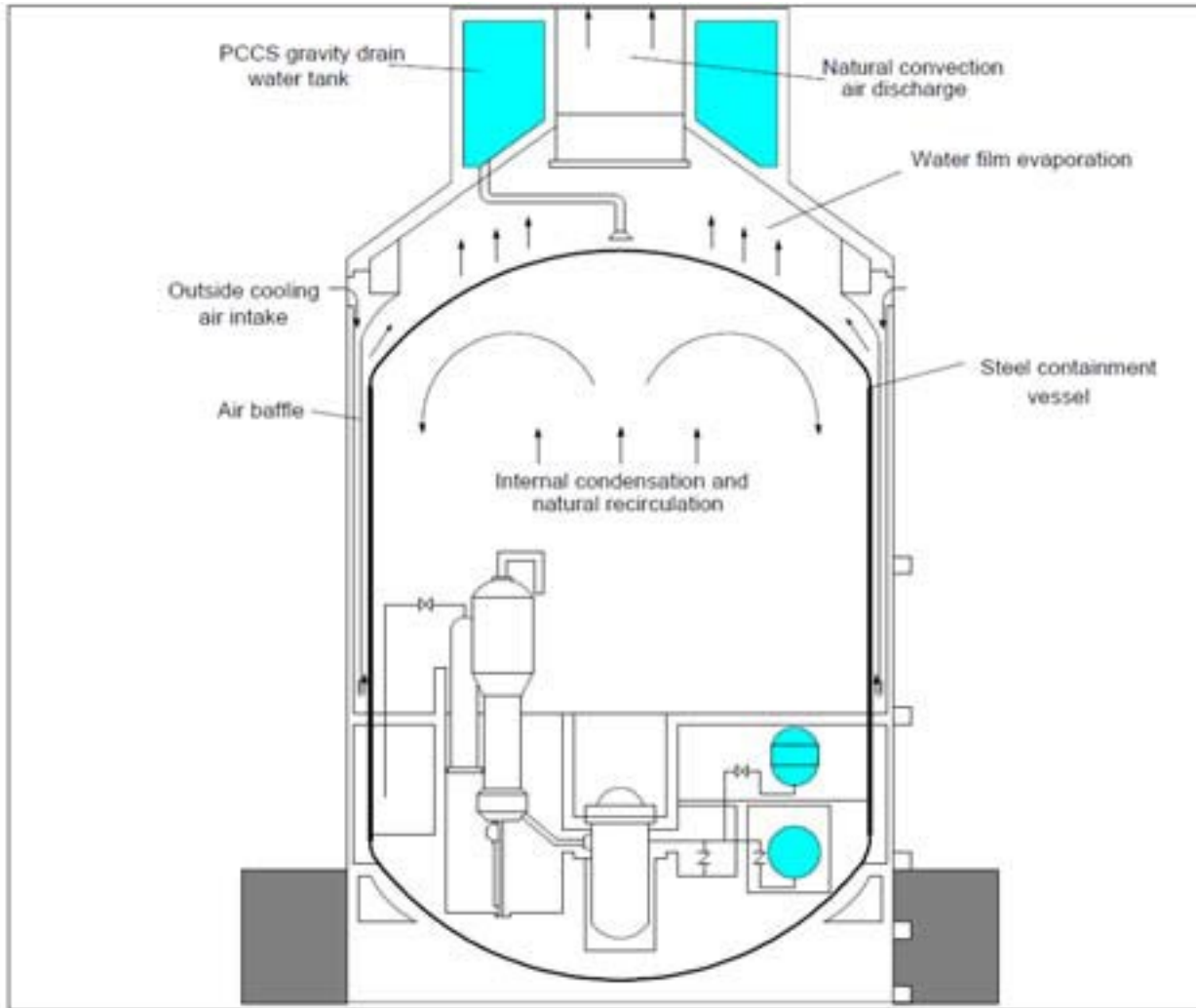


Figure 1: AP1000 Passive containment cooling system

If needed, the air cooling can be supplemented by water evaporation on the outside of the containment shell. The water is drained by gravity from a tank located on top of the containment shield building.

Three normally closed, fail-open valves will open automatically to initiate the water flow if a high containment-pressure threshold is reached. The water flows from the top, outside, domed surface of the steel containment shell and down the side walls allowing heat to be transferred

and removed from the containment by evaporation. The water tank has sufficient capacity for three days of operation, after which time the tank could be refilled, most likely from the ancillary water storage tank. The flow chart of the system illustrated in Figure 1 is shown in Figure 2.

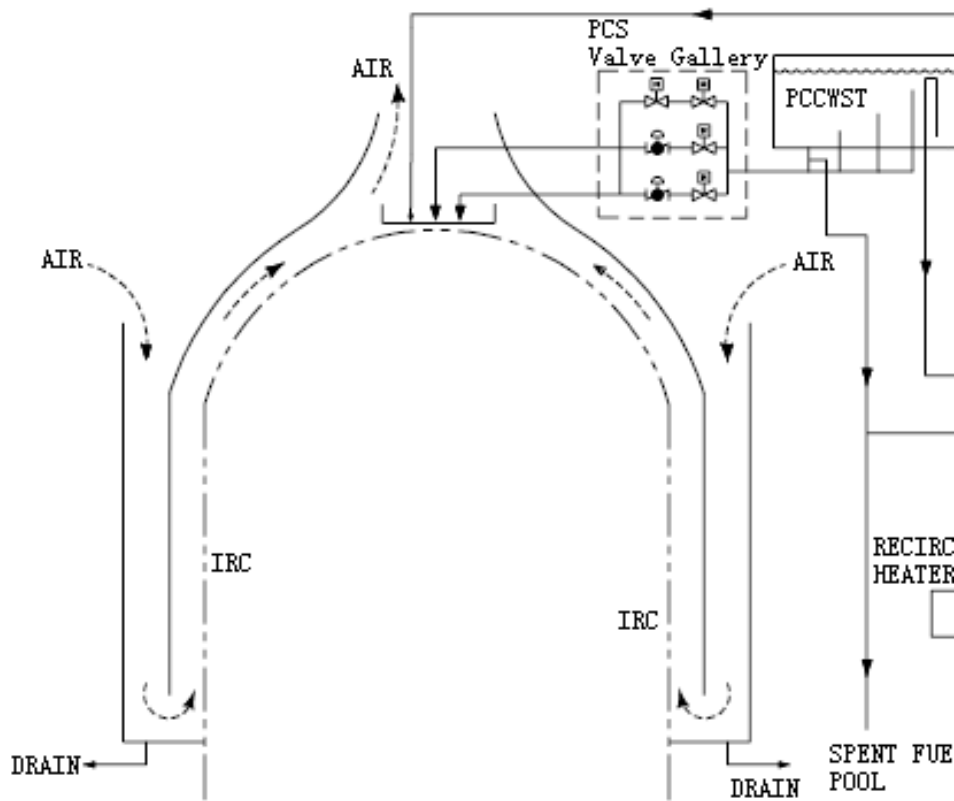



Figure 2: Flow chart of passive containment cooling system in AP1000

 Ricerca Sistema Elettrico	Sigla di identificazione	Rev.	Distrib.	Pag.	di
	ADPFISS-LP1-109	0	L	12	52

3. Reliability assessment of passive containment cooling system (AP1000-like configuration)

Alike the ESBWR case [4], AP1000 Passive Containment Cooling system assessment “appears” to be not very critical from the reliability viewpoint, since, as assessed in [1], the system operation doesn’t pose any relevant risk with respect to the expected performance.

To date in the open literature there are not studies focusing specifically on the reliability of the system, rather the available studies investigate the related efficiency/performance, that is the heat removal capacity of PCCS of advanced passive PWR during severe accidents.

Results show that the heat removal capacity of PCCS, during severe accident scenarios, can keep the containment pressure below the acceptance criterion for a range of severe accident challenges and the AP1000 containment is likely to remain intact and to not be bypassed: as a result, the plant has a significantly reduced frequency of release of large amounts of radioactivity following core damage [1]. Conversely, in this study the performance assessment in reliability terms is dealt with. In fact, since the system operation is based on natural circulation and air is the cold source, so physical process failure becomes one of the important failure modes, which should be considered in system failure prognosis.

3.1. Failure analysis

For the passive system reliability analysis, the success criterion adopted is $P_{\text{containment}} < \text{design value}$: here, $P_{\text{containment}}$ is the total pressure in the containment, and design value is the critical parameter if $P_{\text{containment}}$ exceeds such value it is considered that the containment will lose its function, in our case $P < 0.4\text{MPa}$ [3].

Actually the passive containment cooling systems introduced in AP600/AP1000 design are based upon heat exchange process of steam condensation/evaporation between the steel containment and the heat sink (i.e., atmosphere) and include condensation of steam in containment atmosphere, air convection, thermal conduction. The “functional” fault tree depicted in Figure 3, includes the likely failure modes impairing the PCCS system operation.

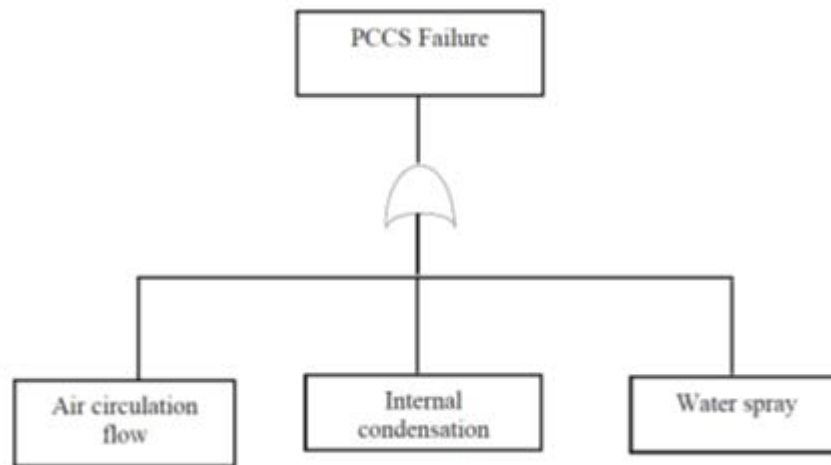


Figure 3: Functional failure fault tree of PCCS system

The preliminary qualitative safety analysis in [1] doesn't reveal relevant risk factors impairing the system performance such that the safety function is challenged, due to the fact that the corresponding probabilities of the modes of failure are very low if not negligible.

The underlying considerations are the following.

Both air circulation and internal condensation processes don't need any external activation and it is quite unlikely that their operation can be compromised by t-h factors which may reduce the heat exchange process like surface oxidation and cracking or decrease the rate of natural circulation like the envelope failure and fouling.

Finally as far as the water spray function is concerned, the level of redundancy and diversification (like the three redundant and diverse drain valves) contribute to improve the rank of safety and reliability of the system. However, the necessity for the quantification of the system reliability is recognized, in order to endorse and add credit to the outcome of the qualitative analysis.

As in the previous case, [4], the quantitative procedure involves the evaluation of the components needed for assuring the passive operation of the system.

The system failure can be induced by equipment default and physical process failure, and part of the equipment failing may increase the failure probability of the physical process.

Three main failure modes are identified to be the loss of air flow, the loss of natural circulation within the containment and the failure of the water supplemental system.

Loss of air flow is due to obstruction of the air ingress/outlet and is modelled by a component, like “strainer”, plugging.

For the system described in previous section, the air inlets are composed of three rows of air inlet holes, one or two rows failure may result in the decreasing of heat transfer capability as assessed in [5], which deals with the aspect related to the effect of air temperature on the failure prediction of the containment cooling system, by means of code simulations: again, as in previous case, due to the limited resources, this aspect is not addressed, while acknowledging its relevance.

We’ll assume the failure of the function upon two of the three rows of air inlet failure, independently of the external air temperature. Internal condensation and natural recirculation process is not estimated to be subject to failure by itself, since it is conditional upon cooling the external containment.

Finally the water spray supply system is evaluated in terms of train valves failures.

The reliability data for natural circulation failure modes are once again from [6] and [7] upon engineering judgment, as reported in Table 1, together with the corresponding failure probabilities. Failure probabilities are assessed taking a 72 hours value for the mission time T_m of the system consistently with the passive system requirement.

Note that single component failure probabilities are evaluated in the form of $\lambda * T_m$, which is acceptable for $\lambda * T_m < 0.1$ like in the present case. Note that loss of primary boundary is not accounted, since it is judged incredible.

Table 1: Failure probabilities for the PCCS

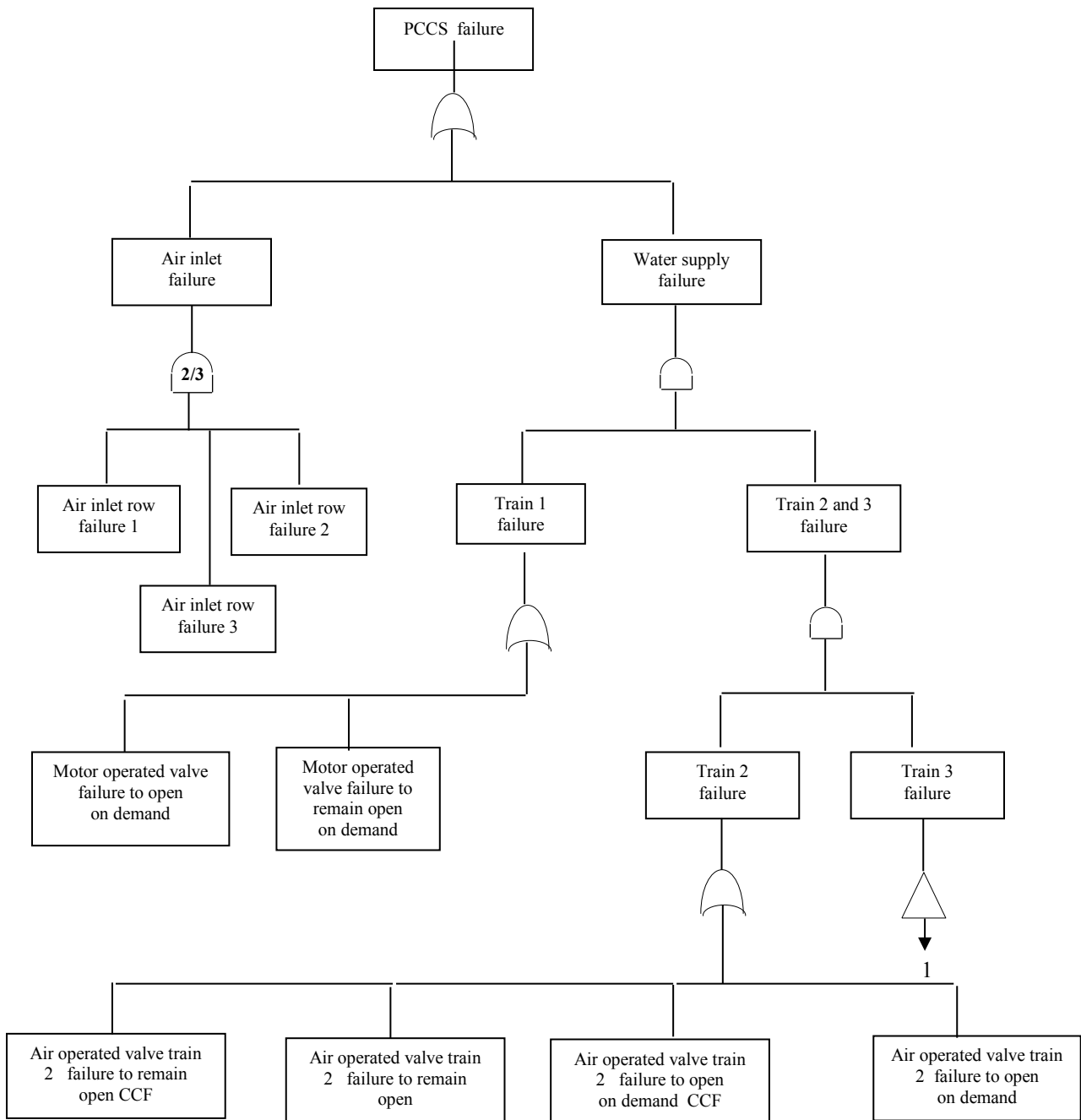
Component	Failure mode	Failure rate	Failure probability
Motor operated valve	Failure to open	$3.0 \cdot 10^{-3}/d$	$3 \cdot 10^{-3}$
Motor operated valve	Failure to remain open	$1.0 \cdot 10^{-7}/h$	$7.2 \cdot 10^{-6}$
Air operated valve	Failure to open	$3.0 \cdot 10^{-3}/d$	$3 \cdot 10^{-3}$
Air operated valve	Failure to open CCF	$3.0 \cdot 10^{-3}/d * 0.1^a$	$3 \cdot 10^{-4}$
Air operated valve	Failure to remain open	$1.0 \cdot 10^{-7}/h$	$7.2 \cdot 10^{-6}$
Air operated valve	Failure to remain open CCF	$1.0 \cdot 10^{-7}/h * 0.1^a$	$7.2 \cdot 10^{-7}$
Strainer	Plugging	$1.0 \cdot 10^{-9}/h^b$	$7.2 \cdot 10^{-8}$

^a: beta factor for CCF

^b: engineering judgement

3.2. Fault tree failure probability

In this paragraph the failure probability of the system is evaluated adopting the approach based on classical fault tree, which is constructed in Figure 4.



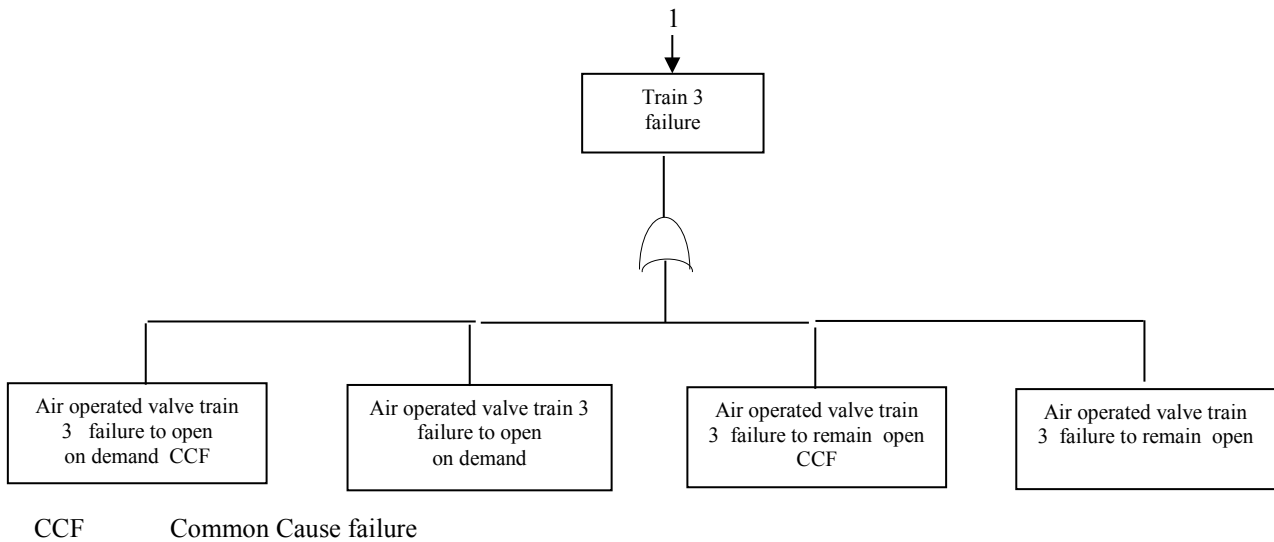


Figure 4: Fault tree for PCCS

The construction of the fault tree under discussion differs from the previous one, represented in Figure 2, in that the branch directly addressing the “natural circulation” and the relative modes of failure is not contemplated, as illustrated in the previous paragraph. Moreover, if, in case of ESBWR PCCS, all the events are linked by OR gates [2], making the assessment quite straightforward, this case presents, in addition, AND gates as well as a 2 out of 3 event.

The two out of three event for the air inlet occurs if two or three of the identical components fail and is calculated by means of the binomial distribution, so that:

$$P(\text{two components fail}) = 3P^2(1-P)$$

$$P(\text{three components fail}) = P^3$$

Where P is the individual probability of failure, with $P = 0.7 \cdot 10^{-7}$

Adding the probabilities of these mutually exclusive events in which the system will fail gives:

$$P = 3P^2(1-P) + P^3$$

This sum gives a negligible failure probability value of the order of 10^{-10} .

The events in the tree are denoted as follows, as regards the water supply water unavailability:

WSF	Water supply failure
A	motorized operated valve failure to open on demand
B	motorized operated valve failure to remain open
C	air operated valve failure to open on demand train 2
D	air operated valve failure to remain open train 2
E	air operated valve failure to open on demand CCF
F	air operated valve failure to remain open CCF
G	air operated valve failure to open on demand train 3
H	air operated valve failure to remain open train 3

$$WSF = (A+B) * (C*G+C*H+D*G+D*H+E+F)$$

$$WSF=A*C*G+A*C*H+A*D*G+A*D*H+A*(E+F)+B*C*G+B*C*H+B*D*G+B*D*H+B*(E+F)$$

$$WSF= 2.7 \cdot 10^{-8} + 6.4 \cdot 10^{-11} + 6.4 \cdot 10^{-11} + 1.5 \cdot 10^{-13} + 9 \cdot 10^{-7} + 6.4 \cdot 10^{-11} + 1.5 \cdot 10^{-13} + 1.5 \cdot 10^{-13} + 3.4 \cdot 10^{-16} + 2.1 \cdot 10^{-9}$$

Results from this reliability study present very low values for the probability of failure of the system under investigation, of the order of 10^{-6} , due to the CCFs, thus confirming the outcome of [1], which didn't reveal any relevant risk factors for the system to accomplish the safety function.

The study shows AP1000 PCCS reliability figure is affected mainly by the supplemental water system availability and in particular the Common Cause Failures of the train valves, whose occurrence decreases the system reliability.

4. Interface with T-H analysis

The connection of MELCOR simulations to reliability assessment and probabilistic safety assessment (PSA) provides both an opportunity and a challenge. In fact, it has to be noticed, that the simulations by the MELCOR code, do not relate directly to the reliability assessment of PCCS and the results are more useful to illustrate PCCS operation and performance. However, the information is valuable among other things for the determination of failure criteria for further reliability analysis and builds up the understanding of the phenomena involved.


For instance, quite obvious candidates for a failure criterion are the Containment pressure and temperature.

The reasons of this statement lies in the fact that MELCOR is intended primarily to model the progression of severe accidents. It is quite simple, approachable and flexible through its block based nature, but it may not be very effective in conducting analysis of performance or reliability for a single safety system such as PCCS. If intention is to obtain a numeric reliability estimate for PCCS, some more specific thermal-hydraulic codes could potentially be more practical for this purpose of use.

With MELCOR it is difficult to introduce probabilistic aspects into the analysis. It would be beneficial to conduct reliability assessment with a tool with which it is possible to sample system parameter values from given distributions, once the appropriate ones are determined. However, information gained via simulations can be exploited e.g. for determination of failure criteria. The simulation information can also be used in a dynamic approach to CET modelling, thus linking up with level 2 PSA. The result of the CET is then a probability distribution for the source term (consequence) of the CET.

If the objective of the analysis is to obtain a reliability estimate for PCCS, the reliability assessment would probably be more profitable with some other, more specific simulation tool, able to deal more effectively with some factors affecting PCCS function, like, for instance parameters such as pipe inclination and surface oxidation.


Obviously also the deterministic nature of the code poses some challenges, for probabilistic purposes. Maybe the most practical approach to simulation based reliability analysis would be to give system parameters some distributions from which to sample the values for them. The failure criteria would have been determined beforehand. This kind of Monte Carlo method

 Ricerca Sistema Elettrico	Sigla di identificazione	Rev.	Distrib.	Pag.	di
	ADPFISS-LP1-109	0	L	19	52

would require quite many simulation runs and the system reliability estimate would be determined according to the fraction of runs which do not exceed the chosen failure criteria. This is quite prohibitive to be performed with MELCOR, but as pointed out above, the MELCOR simulations can be advantageous for example in determination of reasonable failure criteria and in dynamic approach to CET modelling.

In the specific case of AP1000 PCCS, since the system operation is based on natural circulation and air is the cold source, so physical process failure becomes one of the important failure modes, which should be considered in system failure prognosis, and air temperature has important effect on system failure probability.

Monte Carlo (MC) simulation might be used to evaluate the system physical failure probability based on air temperature probability distribution, the effect of air temperature probability distribution on failure modes and the results of pressure distribution in the containment based on air temperature as illustrated in [5].

 Ricerca Sistema Elettrico	Sigla di identificazione	Rev.	Distrib.	Pag.	di
	ADPFISS-LP1-109	0	L	20	52

5. Conclusions of the reliability analysis

Natural circulation failure evaluation is included in the present study proposed for advanced LWR PCCS reliability assessment: this is attained through an approach aimed at the thermal-hydraulic performance assessment on the probability standpoint.

According to the previous section, some relevant methodologies for passive system reliability assessment, prompted so far, suggest propagation of important system uncertainties through Monte-Carlo simulation of a detailed best estimate mechanistic system, like MELCOR.

The main drawback consists in the requirement of a large number of system analyses using best estimate system code. Typically mechanistic thermal hydraulic codes of complex nuclear safety systems are computationally expensive and MC simulations using such models require considerable and often prohibitive computational effort to achieve acceptable accuracy. Consequently the issues pertaining to the natural circulation unavailability estimation suggest to approach the problem at the component level (see fault tree, figure 4), overlooking the failure modes related to the onset of thermal-hydraulic phenomena that would impair the passive function of the system, which appear to be negligible.


Consequently, as previously underlined, the outcome of the analysis represents a preliminary appraisal of the unavailability of a thermal-hydraulic passive systems for advanced GenIII+ reactors.

Qualitative analysis and fault tree construction are performed for safety-related systems that contribute to prevention or mitigation of severe accident events. The analysis identifies the importance of each component for each system.

Under the assumptions taken in the study results show a quite low value for the probability of failure, of the order of 10^{-6} .

The AP1000 design provides a passive means of maintaining the containment integrity by removing decay heat from the containment with water on the containment shell or through air cooling. This cooling ability reduces the potential of containment failure due to over pressurization after severe accident.

In particular, the diversity requirements adopted for the valves of passive containment cooling water storage tank minimize the consequences of Common Mode Failures to cause a loss of containment cooling.

 Ricerca Sistema Elettrico	Sigla di identificazione ADPFISS-LP1-109	Rev. 0	Distrib. L	Pag. 21	di 52
--	---	------------------	----------------------	-------------------	-----------------

The passive containment cooling system represents passive systems with thermal-hydraulic properties and therefore poses further challenges. The path forward includes the development of proper methods for reliability analysis of such systems becomes more urgent. If this study on PCCS reliability should be regarded as a preliminary analysis, it, however, lays the basis for further analysis to conduct the assessment with suitable tools, by leveraging the thermal-hydraulic simulations, and to yield any possible reliability estimate.

The features of suitable codes have to be examined in order to evaluate their appropriateness to effectively handle the issue for the given purpose.

6. Study of a new in-vessel corium retention strategy

6.1. Background and Introduction

Assuring the integrity of each NPP physical barriers becomes the corner stone of the defense-in-depth approach which is extensively employed in nuclear safety against the release of radioactivity to the environment. The understanding of severe accident (SA) phenomena and how to treat the phenomena evolving during SA are of meaningful importance to identify and propose (new) safety-oriented mitigation and/or retrofit measures.

The problem to deal with the safety systems, designed based on the “defense in depth” hierarchy, is to guarantee the design performance in the case of core damage (of frequency range 10^{-4} to 10^{-6} /reactor-year). For this reason a better understanding of core degradation phenomena, of interaction with the coolant of the behaviour of melt in contact with the primary circuit and its cooling potential is of meaningful importance.

As indicated in the ADPFISS-LP1-096, during a severe accident, the occurrence of reactor core meltdown may cause the failure of the first physical barriers, leading possibly to exothermic reactions (in absence of coolability) with ablation and metal attack of the reactor vessel lower head and to the release of a certain fraction of fission products to the pressure-bearing containment.

The corium coolability (i.e., preventing melt-through of physical barriers) has been in fact recognized as the “Achilles-heel” of the existing reactor designs. Therefore adequate performance (integrity and leak-tightness) of the containment in the aftermath of a postulated severe accident, thus, is of vital concern to avoid life-threatening event from the point of view of public safety.

The solutions proposed and adopted by Gen. III reactors are: in-vessel melt retention (IVR) or ex-vessel melt retention (EVR). They basically envisage the SA termination in the RPV or in the containment, respectively. The key strategy of IVR is to arrest and confine the corium in the lower head of the RPV by flooding the reactor pit (cavity), while EVR collects and cools the corium ejected from the RPV in a core catcher placed in the containment (like for the EPR and VVER).

The IVR strategy is considered the most effective measure to prevent the failure of the vessel bottom head, and of the containment and/or basemat melt-through, later. Consequently R&D

efforts spent in maximizing the safety this solution is able to assure (Figure 5) [8-9] should focus on the following open issues:

- vessel wall ablation due to the impingement of a melt jet,
- melt coolability in the presence of water,
- in-vessel melt retention process in the presence of crust,
- external cooling of the reactor vessel,
- critical heat flux (CFH) during external cooling,
- lower head melting or creep-rupture process, and
- vessel-hole ablation process.

Additionally, the following threats that these phenomena may pose to the containment integrity have to be investigated:

- Direct containment heating (re-hydration effects for $T_{cont} > 90^{\circ}C$);
- H_2 combustion or steam explosion;
- Containment long term over-pressurization, bypass and leakage; and
- Basemat melt penetration.

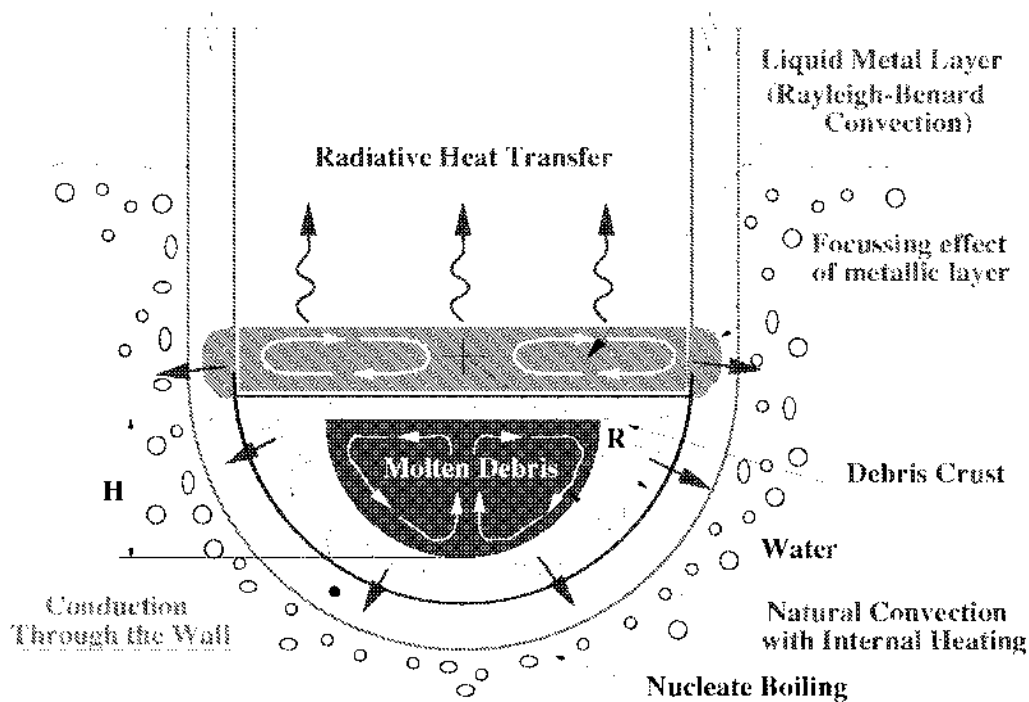


Figure 5: Schematic IVMR phenomenology [9] and heat transfer processes in the melt progression.

6.2. IVR approach

Conceptually the IVR approach benefits of external water cooling (flow normally driven by natural circulation) as it allows to remove the decay heat of the core melt relocated onto the reactor lower head [10÷13]. This solution is known as In-Vessel Corium Retention (IVCR).

By keeping the vessel wall cool the creep failure is prevented: this means to not exceed the limit of the external cooling capacity (or CHF) of boiling at all points around the vessel lower head (Figure 6). This latter emerged also in the analysis of the Fukushima accident: wider the CHF margin longer the time to manage plant emergency. On the contrary RPV melt-through may occur if water cooling/injection is not enough or unavailable for a prolonged period of time.

Figure 7 shows the most important phases (phenomena and possible interactions) of the in-vessel melt progression (IVMP) and the “expected” vessel failure modes that are typical for most existing/under deployment LWRs, which serve as a basis and rationale for identifying safety improvement. In this framework is inserted the CHF-reduction oriented solution that will be herein following investigated from a thermo-mechanical point of view.

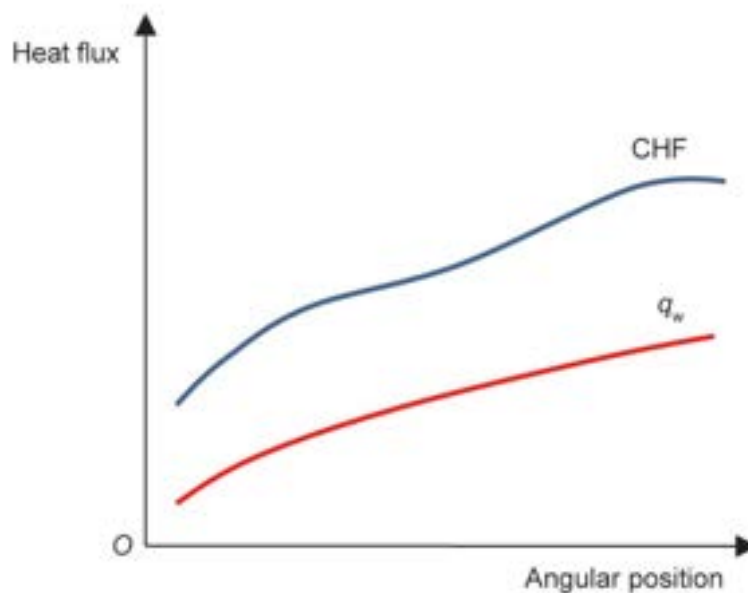


Figure 6: Heat flux vs. RV angular position of lower head in IVR

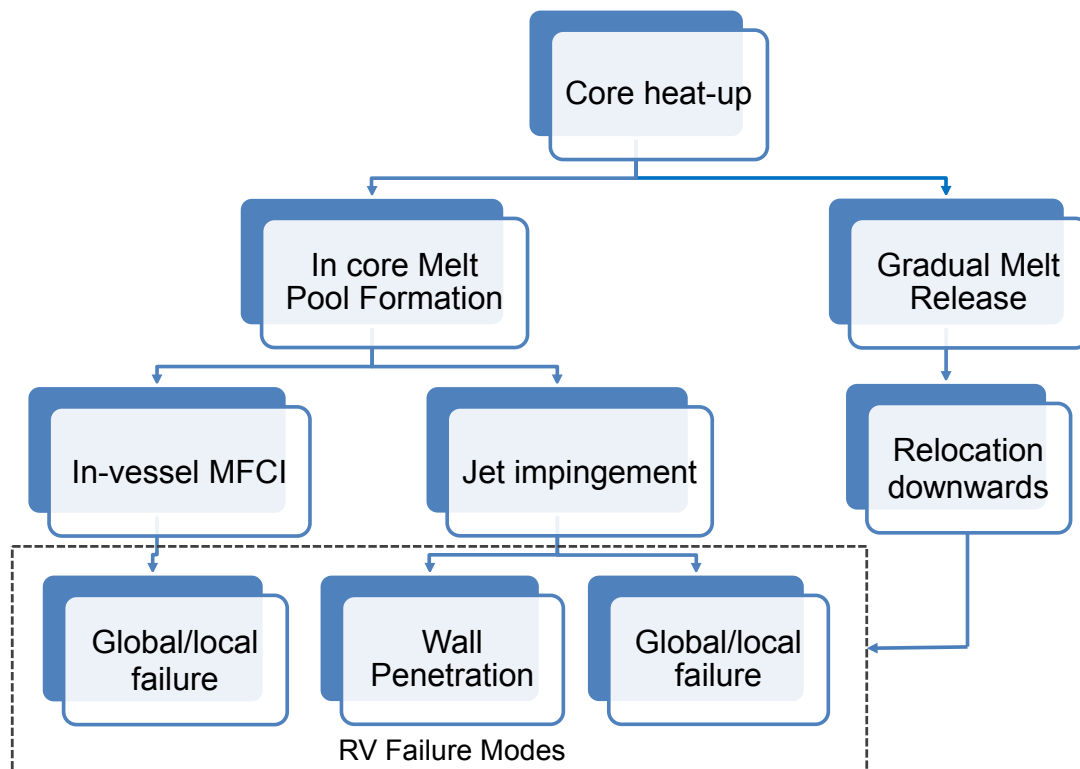


Figure 7: Schematic in-vessel melt progression sequence

The solution proposed to improve the safety and support the SAM consists of an internal core catcher (ICC), developed at the DICI- University of Pisa, made of a SiC-SiC matrix inside which are inserted boxes with pebble ceramic material (i.e. alumina).

Figure 8 shows a scheme of the proposed device. It is a passive component to install inside the lower head; this make it less prone to malfunctioning (“safety oriented solution”).

The material chosen as well as the geometrical configuration (‘thermal criterion’) make the ICC an innovative engineeristic system that could help in the SAM.

The internal and external liners of core catcher are made of high alloy steel.

The boxes instead are filled of alumina (Al_2O_3) in forms of pebbles. Al_2O_3 is chosen because of its high refractoriness, favorable thermal properties and capability to accommodate thermal expansion without high thermal stresses. This latter is strictly dependent on the thermal properties and may affect also packing factor of the boxes and as a result the thermal stresses.

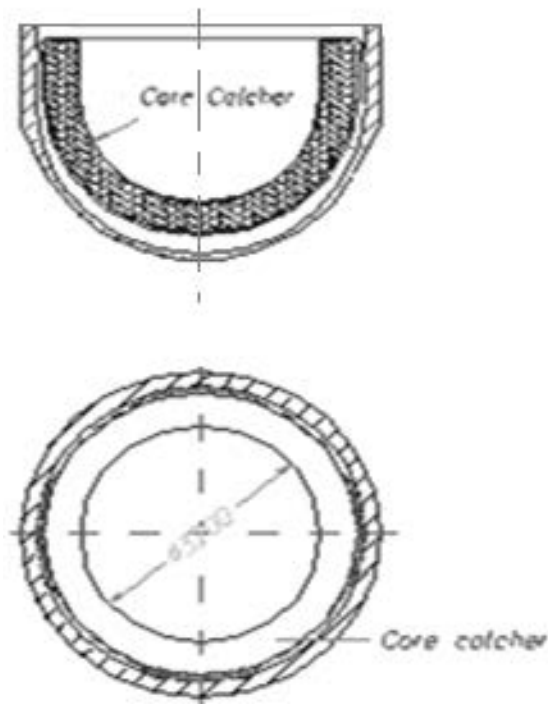


Figure 8: Scheme of the internal core catcher (dashed surface at the vessel lower head on the left figure) and of the SiC-SiC structure with alumina pebble boxes (right figure).

The way ICC will operate is theoretically simple: the alumina layer will not only increase the thickness of the bottom head of the RV but also will retard the core heat-up by acting as “thermal resistance” (in reason of its thermal conductivity lowering with the increase of temperature [13]). Accordingly, the thermo-chemical attack of the lower head, caused by the gradual decay-heated core melt (corium) relocation and/or inpingment downwards, is minimized or prevented (key benefit in SAM).

7. Molten Pool Behaviour and Structural Integrity of RV

Although the idea of ICC sounds quite simple, it is necessary to prove it with high confidence. In doing that the challenging task is determining precisely either the heat flux or the CHF, and especially the heat flux (q_w) of the melt pool convection which is largely affected by in-vessel severe accident phenomena and accident scenarios. Due to the uncertainties in the understanding of the physical phenomena and accident scenarios, a deterministic approach is introduced and used, and conservative scenario is taken into consideration. Therefore to assess (theoretically and numerically) the feasibility of the proposed ICC, the starting point is the analysis of the the most important phenomena affecting the core heat-up [14÷18].

To remark is that core heat-up condition is instaured once the water level inside the reactor vessel drops, and, as widely known, the fuel clad temperature rises rapidly due to the decay heat in the fuel. After that the fuel heat-up accelerates beyond about 1500 K, when the Zr-H₂O reaction is violent and the rate of heat generation may be much much greater than that of the decay heat. Reached the melting point, the molten material starts to relocate to the lower head of the RPV in form of oxidic or metallic jet.

“Being in contact with colder solid structures, the melt may solidify again, forming a barrier for the molten material coming later (“candling” and “blockage” processes)” [9].

In such a scenario, it has been recognized that vessel wall ablation (melting) due to jet impingement heat transfer could be a vessel failure mode, which has to be evaluated for assessment of the resulting containment loadings [11-12]. In addition, it emerged from the past 15 years of research on the IVMR that melt pool, if formed, may subsequently separate into 2 layers (i.e. lower oxidic layer and upper liquid metal layer) or 3 layers (heavy metal, oxidic and light metal layers), each of which is responsible of complex phenomena, suc as the global and local creep rupture, the focusing effects of metallic layer, the ablation of thw wall with water ingression or gap coling, molten fuel-coolant interaction (MFCI), etc.

Furtermore as indicated in [9], the in-vessel MFCI may cuase destructive energetic in-vessel steam explosions (' α -mode'), that is a source of potential threat for vessel and containment integrity, and fragmentation of the core melt jet ('debris' behaviour).

Additionally, another concerns may be posed by the superheated metallic melt layer and by the freezing temperatures of both the metallic melt and the vessel wall (carbon steel) that are

close to each other (the large driving temperature difference for sidewall heat removal may result in vessel wall meltthrough).

Based on that it is possible to observe that the ICC issues to face are mostly affected by the heat-up of vessel wall and the heat removal capacity.

In general, the vessel heat-up will result in a reduction of mechanical strength of the vessel material; as a consequence, the lower head wall can be subjected to significant thermal and pressure loadings, and the lower head could fail due to creep rupture. In consideration of that, benefits the proposed ICC are clear, since a thin layer of it will serve as a thermal insulation, preventing the vessel wall from melting, and increasing the safety margin of plant.

Finally in the proposed study, the gap colling or the effects due to the resulting water ingress are not taken into account.

7.1. Analysis approach: assumption and modelling

7.1.1. Core accident progression

Briefly the degraded core accident progression that lead to core damage is dependent on large number of phenomena that can be extended over long periods of time. However, some common chemical and physical phenomena may be identified in their progression.

[14] identifies the following four time intervals, each of which is characterized by an own dominant phenomena:

- (a) Initiation of accident until superheat in core;
- (b) Superheat in core until core temperature exceeds 1500 K;
- (c) Core temperature exceeding 1500 K until corium slumping (more likely to occur in PWRs than in BWRs, as learned from TMI-2 accident); and
- (d) Formation of molten pool in lower plenum until vessel failure.

Phase (a) is very short, less than 10 min in case of LB-LOCA, or very long ranging from about 6 to 10 h in case of long-term LOSP or TMLB.

The phenomena in (a) are accompanied by a variation of pressure varies. After the core is uncovered - phase (b) -, heat transfer from the fuel to the steam is low compared with decay heat, and the fuel temperature increases till to clad ballooning and rupture (oxidation of Zircalloy and H₂ generation).

Temperature may reach 1500 K for low-pressure sequences and 1700 K for high pressure sequences.

As clearly indicated in [14], at low pressure the stainless steel clad fails before reaching its melting point due to internal pressure, deformation, and contact/interaction effects. In BWRs, VVERs and some PWRs with boron carbide (B₄C) as absorber, the major low-temperature reaction may occur at about 1500 K [16-17-18].

Phase (c) results in other core degradation phenomena; the reduced natural circulation between the core and the upper plenum may cause reduced heat transfer and hence a rapid heat-up of the core. In general, the core slumping or relocation into the lower plenum has to be described deterministically for all possible kinds of scenario and by adopting conservative assumptions regarding melt superheat, relocation rate, melt fragmentation etc. because of the low understanding of the complex phenomena occurring during this long time phase.

Phase (d) deals with the long-term behaviour of the corium relocated in the lower plenum. It is important for the estimation of RPV failure and the consequences for the thermal loads to the containment. If sufficient water is available in the lower plenum and the corium mass limited as in TMI-2, it might protect the wall from thermal loads. Otherwise local/global wall failure may occur.

7.1.2. Boundary conditions of core melt

The proposed internal core catcher approach is based on the successful coolability of the core melt: considered temperature is higher than 2273.15K, since the solidification temperature of melt corium jet may range from 1700K (for metal jets) to 3000K (for oxidic jets) at the bottom head, allowing the stabilization of the severe accident.

In such a scenario, the vessel wall ablation due to the jet impingement heat transfer is not considered because of the results obtained from the RIT/NPS experiments.

They showed that the stagnation zone, where the corium may relocate, should not be affected by the turbulence, which is the major physical mechanism governing the physics of fluid flow and heat transfer in the impingement area under phase change conditions.

Moreover it was observed that the rapid progression of the melt front and the increased heat transfer due to the surface roughness are tricky phenomena more for thin jet than for thick jet, are the case under investigation. Consequently, to evaluate efficacy of the ICC, the physical

situation of interest is, at this first stage, that characterising the relocated melt corium upon a meltable solid wall, i.e. vessel steel plus the layer of alumina.

The instauration of heat transfer processes will ensure that at least the bottom layers of the RPV wall are not undergoing “heat flux focusing effects” [18-19].

Based on the data obtained from the AP-600 accident scenario evaluation (specifically provided from COPO (Kymalainen et al., 1994), UCLA (Asfia and Dhir, 1994) and the mini-ACOPO (Theofanous et al., 1995) experiments, it is possible to assume that the reactor layer would be quite thick and the focused heat flux at the vessel wall was lower than the critical heat flux at the vessel outer wall.

The metal layer resident on top of the oxidic pool (see the scheme of Figure 9) was found to focus the heat added to it from the oxidic pool towards. However, since in the analysis it is assumed that the core is entirely molten, the contribution of radiative heat transfer becomes lesser important than the contribution of conduction through the wall.

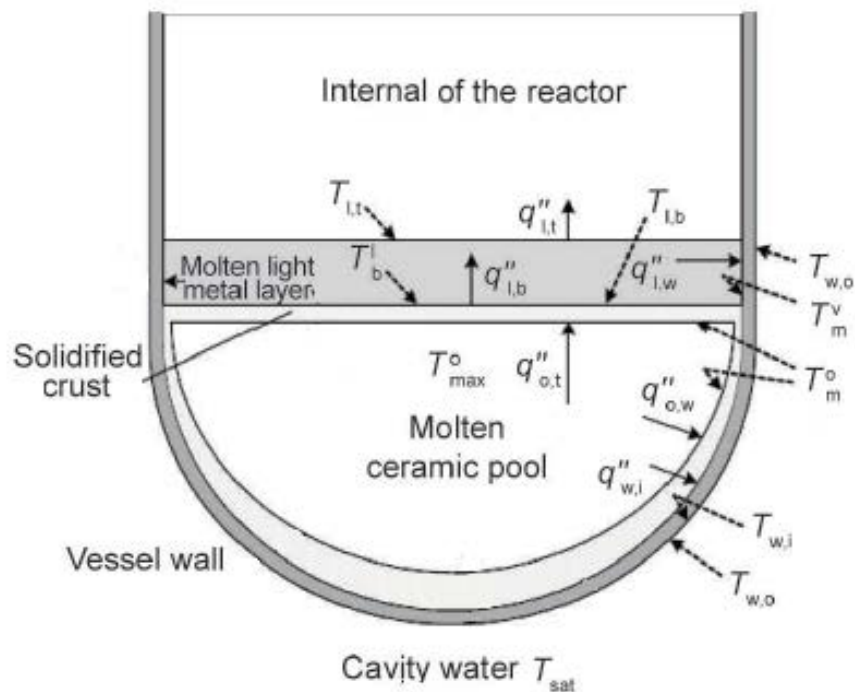


Figure 9: Scheme of the melt pool. Temperatures T_w , T_m and T_l or T_b refer the water, the molten core, the light metal layer and to the crust, respectively.

Summarising, the upward/downward splitting heat flux is affected by the stratification; indeed more heat is transferred downwards. Moreover, the heat flux towards the debris wall is

determined primarily by conduction and not by boundary layer flows, as for the unstably stratified regions.

The proposed ICC concept, by thickening the bottom head wall, may contribute to delay effects and consequences of the heat-up and, hence, avoid the “boiling crisis”.

7.2. Thermal analysis

The arrest of lower head heat-up and eventual quenching is the key to the survival of the RPV and for an appropriate SAM. To attain the aim it is needed to determine thermal loadings on acting on the lower head on the basis of the knowledge of progression of the core melt and degradation.

For the thermo-mechanical analysis performed, homogeneous pool condition and stratified condition with an upper metallic layer and a lower oxide layer covering the RV wall are considered. In the analysed cases, very high temperature gradients occurred at the hemispherical boundary, the heat flux across this boundary reaching its maximum close to the upper pool surface.

The reference model for the calculation of the heat flow effects is shown in Figure 10, while the material properties are given in Table 2. Despite in reality the physical shape of relocated corium and of the melt RV internals are several; they may fall in the category of one-dimensional systems because of the identified boundary conditions, made assumptions and also because the temperature in the “body” is function of the radial distance (and is independent from the axial distance or azimuthal angle).

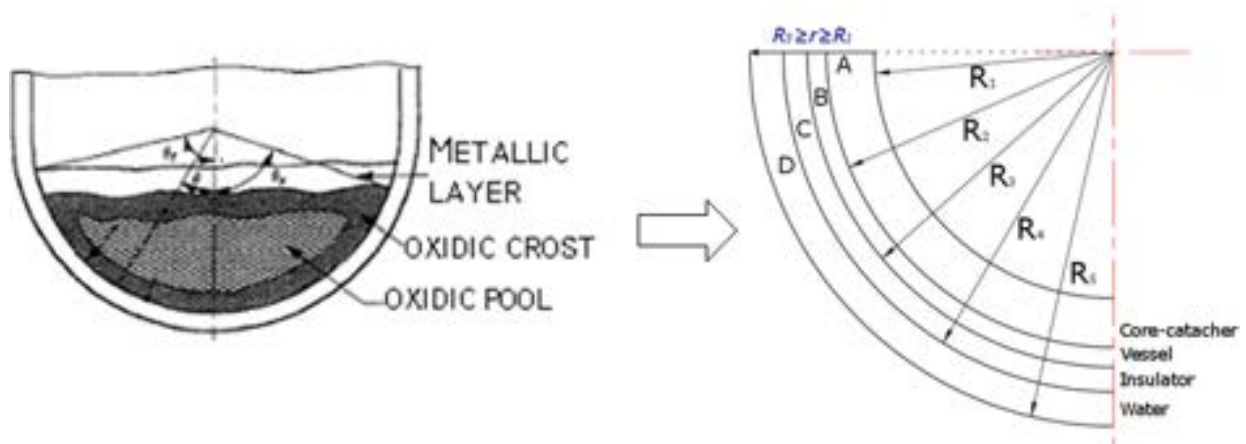


Figure 10: Representation of the core debris relocated at the lower head, in a steady-state condition, and made of either solid oxidic crust and/or melt oxidic pool (left figure).

Analytical model of core debris with outer RV insulator (instead of adiabatic boundary condition) [20], on the right figure. For this latter boundary conditions are $T(R_1)=T_{\text{corium}}$ and $T(R_5)=T_{\text{water}}$. The thermal insulation (layer C) is assumed 0.25 m thickness (0.15 W/m/K of thermal conductivity) as the real one in nuclear reactor [16-17].

Table 2: Geometrical and material properties used in the model [17-19]

Component	Radius [m]	Thickness [m]	Thermal conductivity [W/m/K]
Core-catcher	2.50÷3.00	0.5	0.50
Vessel	3.00÷3.20	0.2	18.00
Insulator	3.20÷3.45/3.50	0.25/0.30	0.15
Water	3.45/3.50÷3.80	0.30/0.35	0.60

Another aspect to account for a proper description of the IVR heat processes is the thermal contact resistance, which arises along the junction formed by steel and Al_2O_3 (they have dissimilar thermal conductivity mainly) or contacting surface.

If a heat flux is imposed across it, the homogenised (“uniform”) heat flow may be generally restricted to the conduction through the contact area, as shown in Figure 11.

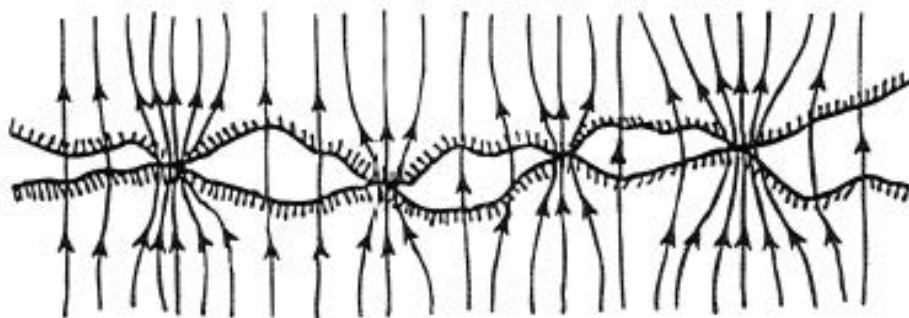



Figure 11: Hypothetical representation of steel and Al_2O_3 contacting surface.

The presence of a solid medium between the contacting surfaces (with reference to Figure 10, corium-alumina, alumina-steel and steel-water sub-systems) may contribute to or restrict the

 Ricerca Sistema Elettrico	Sigla di identificazione	Rev.	Distrib.	Pag.	di
	ADPFISS-LP1-109	0	L	33	52

heat transfer, depending mostly upon the thermal conductivity, thickness, and hardness of the material. Since no gaps are expected between the contacting surfaces, any heat radiation is therefore prevented.

As for the energy balance across the corium-alumina-steel system, the heat contributions of the axial, azimuthal and time-dependent terms may be neglected.

Steady-state conditions is so assumed in the debris pool; the temperature is so represented by a continuous function that account for /equates heat generated and heat lost as well as the several and different materials thermal conductivities.

In this assessment the heat flux imposed at the lower head is assumed less than 1.5 MW/m^2 (about 1.3 MW/m^2 for 1000 MWe PWR, as confirmed by the ULPU-2000 experimental data); the thermal resistance along the upward thermal radiation path is maximized.

The set up model treats the case of a uniform composition, initially quenched, debris bed of zero porosity.

The hemispherical lower head wall is included in the modeling, its melt-through due to the thermal attack of the melt pool is calculated first analytically and numerically [20÷24].

The heat transport to the hemispherical boundary is through conduction, and, then, through a boundary layer created by the downward flow along the curved wall from the upper part of the pool: Fourier problem with direct integration solution.

No chemical reactions are considered for either the evaluation of proper thickness of pebble bed or temperature trend within the pool.

As for the latter, it was evaluated by assuming: (1) primary system depressurized; (2) lower head fully submerged in cavity water before that core debris reaches the lower head, and (3) water level in the cavity pit maintained indefinitely.

The lower head vessel integrity is calculated by considering several corium temperatures such to provide a wider overview of the core melt progression effects. The boundary conditions are consequently the core melt temperature and the water temperature ($40 \text{ }^\circ\text{C}$).

7.3. Thermal analysis: FEM analysis

Numerical analyses for analysing thermal performance of the ICC are performed by FEM code MSC©Marc. The preliminary model is implemented based on the scheme of relocation the core debris given in the previous Figure 10. In the modelling the presence of water in the

reactor lower plenum is not represented; this is a conservative assumption since the presence of gap cooling in the lower plenum vessel may be considered as a mechanism of keeping the vessel wall cool. The lower head wall is assumed subjected to thermal and pressure loads represented in terms of core melt temperature and pressure acting on the top surface.

For assessment of core meltdown accident progression, mode, timing and the possible vessel failure becomes of paramount importance [23÷27].

To the purpose of the thermo-mechanical simulation the following assumptions and restrictions are imposed:

- adiabatic condition on the core catcher external surface (no radiation flux surface)
- no top surface cooling of corium cooled the by passive emergency cooling systems;
- with and without insulator;
- isothermal boundary condition for the external vessel surface ($T \sim 390\text{K}$) cooling;
- elasto-plastic behaviour for the vessel.

The initial conditions of 2000K for the oxidic debris and 1550K for the metallic layer become of minor importance because the thermal load to the vessel lower head is maximized when debris pool reaches a steady thermal state.

Additionally, Table 3 provides the specific material properties implemented as input for the simulation.

Figure 12 provides instead the trend of the stress and of the modulus of elasticity, respectively, as function of the temperature.

The alumina thermal conductivity trend is instead that obtained experimentally in [13].

Finally Figure 13 shows the set up and implemented FEM model used for the thermal safety margin assessment.

Table 3: Material properties for FEM simulation

Property	Alumina	Carbon Steel
Density	3970 kg/m ³	7800 kg/m ³
Specific heat	1560 J/kg K	514 J/kg K
Conductivity	10.5 W/mK	30 W/mK
Latent fusion heat	3577 kJ/kg	
Young Modulus	380000 MPa	196500 MPa

Yielding strength	3000 MPa	173 MPa
-------------------	----------	---------

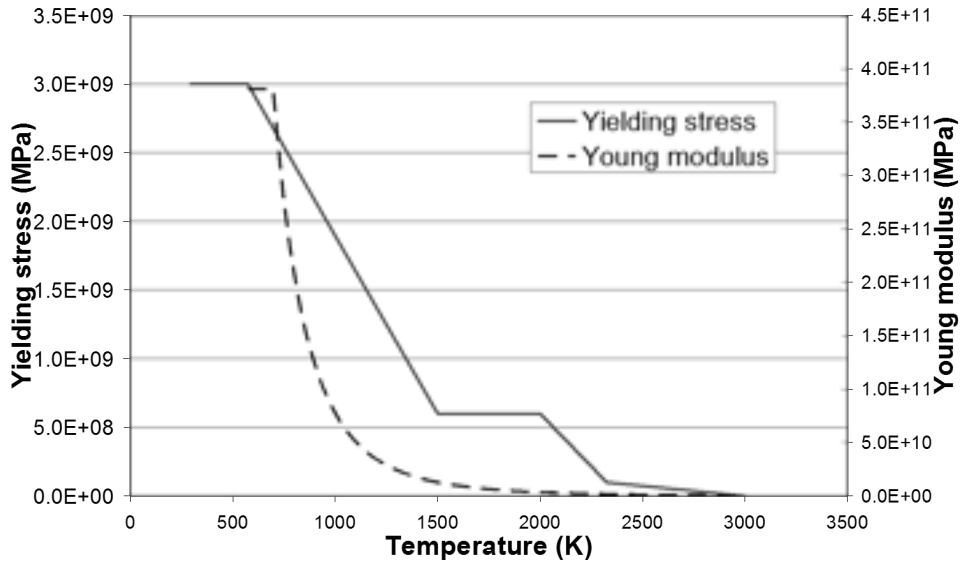


Figure 12: Strength and Young modulus behaviour vs temperature for the alumina

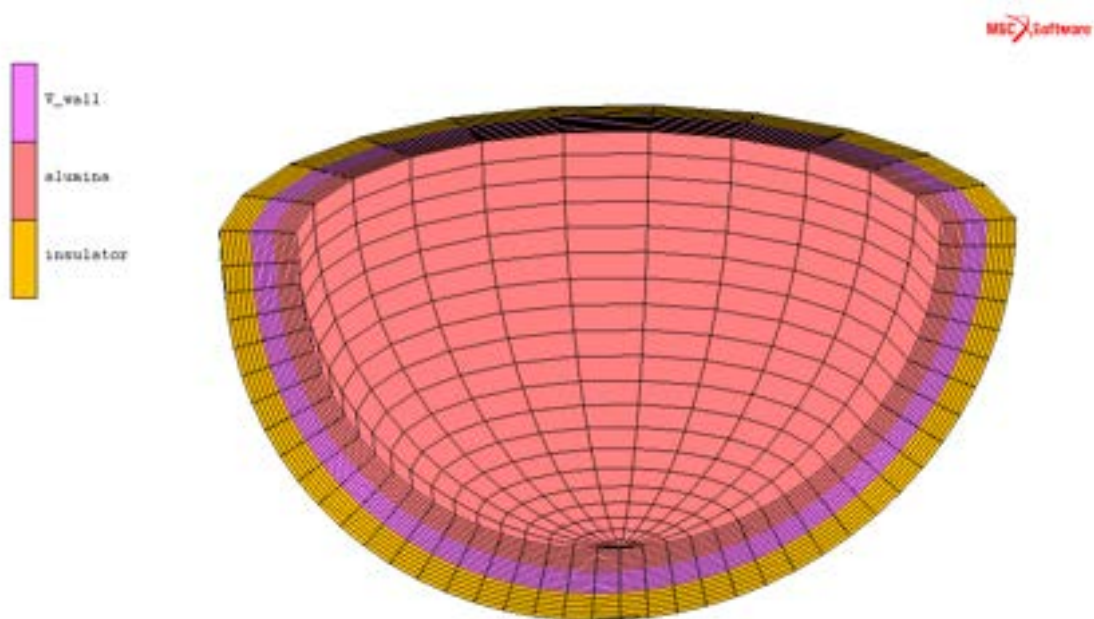



Figure 13: FEM model of the vessel lower head

The model is implementing element type 43, which is an eight-node, isoparametric, arbitrary hexahedral suitable for three-dimensional heat transfer applications. The conductivity of this

 Ricerca Sistema Elettrico	Sigla di identificazione ADPFISS-LP1-109	Rev. 0	Distrib. L	Pag. 36	di 52
--	---	------------------	----------------------	-------------------	-----------------

element is formed using eight-point Gaussian integration. The analyses performed have been the steady state and the thermal/mechanical transient. Direct integration method is used.

8. Pool behaviour analyses: results' discussion

In this section we first briefly summarise results quoted in available literature, subsequently they are provided the stresses calculated with the reference model of previous Figure 10 right. FEM analyses results are also provided in what follows and critically discussed in terms of safety margin [28-29]. Moreover, based on the ultimate stress, the thermal endurance (γ) is calculated such to be able to measure the performance of the proposed core-catcher solution. It is obtained as:

$$\gamma = \frac{\sigma_u}{\alpha E} \left(\frac{k}{\rho c_p} \right)^{\frac{1}{2}} \quad (1)$$

In Eq. (1) σ_u is the ultimate tensile stress, α is the thermal expansion coefficient, ρ is the density, k is thermal conductivity, and c_p is the specific heat capacity.

8.1. Analytical results

It was highlighted that 20 cm of alumina results in about 12% reduction of the average vessel wall temperature: thicker this protective layer lower is the average vessel wall temperature.

Moreover the parametric study performed to identify for which the temperature at R₄ is less than 100 °C (t_∞ condition) suggested that R₅ be less than 0.15 m. In this case, the solution of Laplace equation is consistent with the problem and the steady-state solution can be used directly; no transient analysis is thus required.

Indeed, ICC reduces the heat-up from the lower head of vessel as shown in Figure 14: this positive effect immediately results in an increase of thermal safety margin.

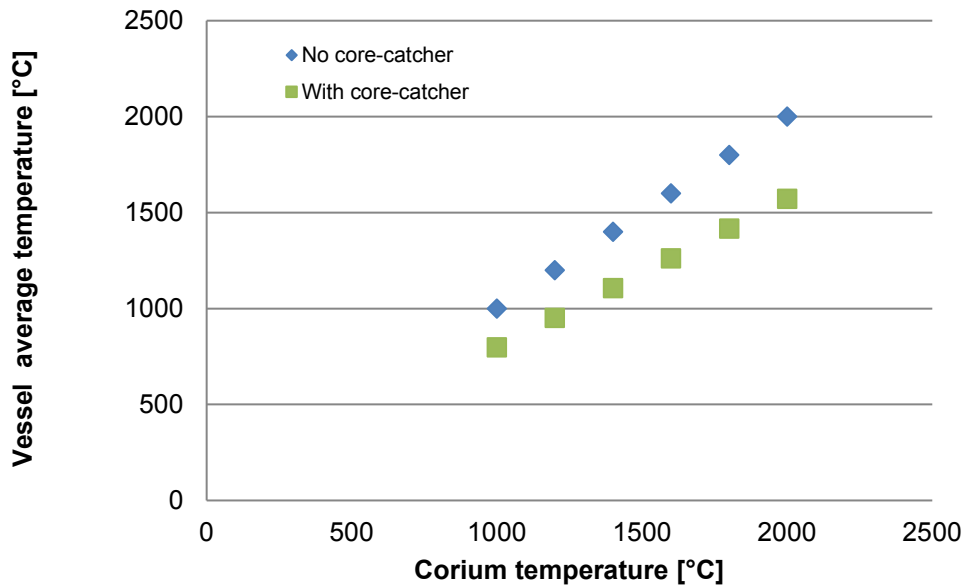


Figure 14: Temperature trend for IVR with and without ICC solution.

Secondarily, Figure 15 shows the temperature behaviour calculated by ranging T_{corium} from 1000 °C to 2000 °C for the worst heat transfer condition [20]. The circumferential stress are instead shown in Figure 16: thermal stresses are relevant inside the core-catcher and become negligible in the vessel wall. No stress state characterise the external vessel insulator.

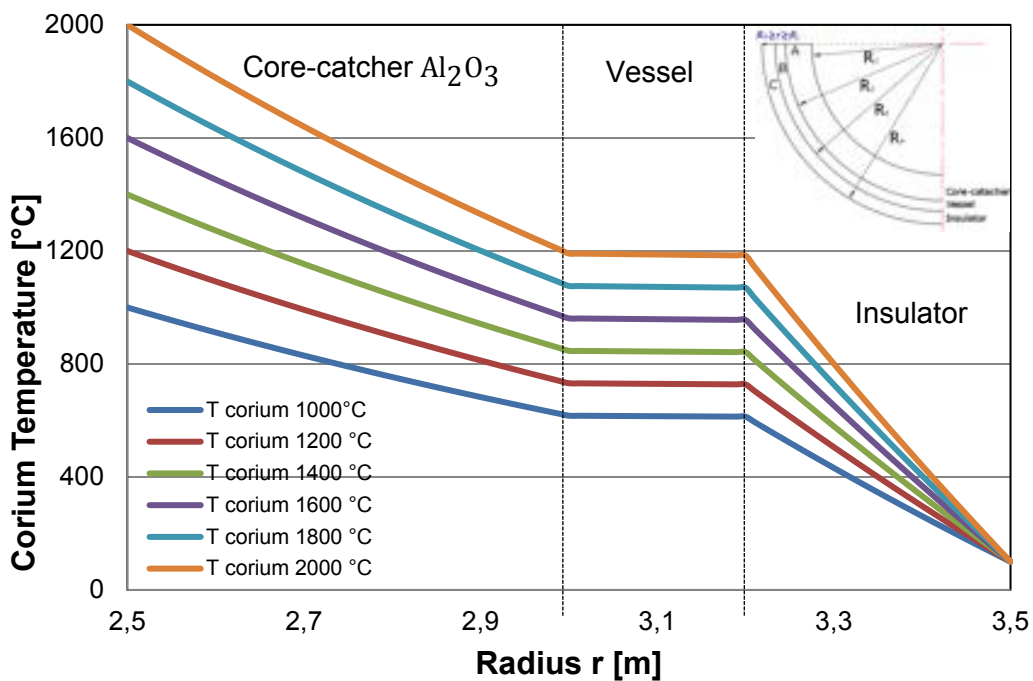


Figure 15: Radial temperature in the bottom head for $T(R_4) = 100^\circ\text{C}$.

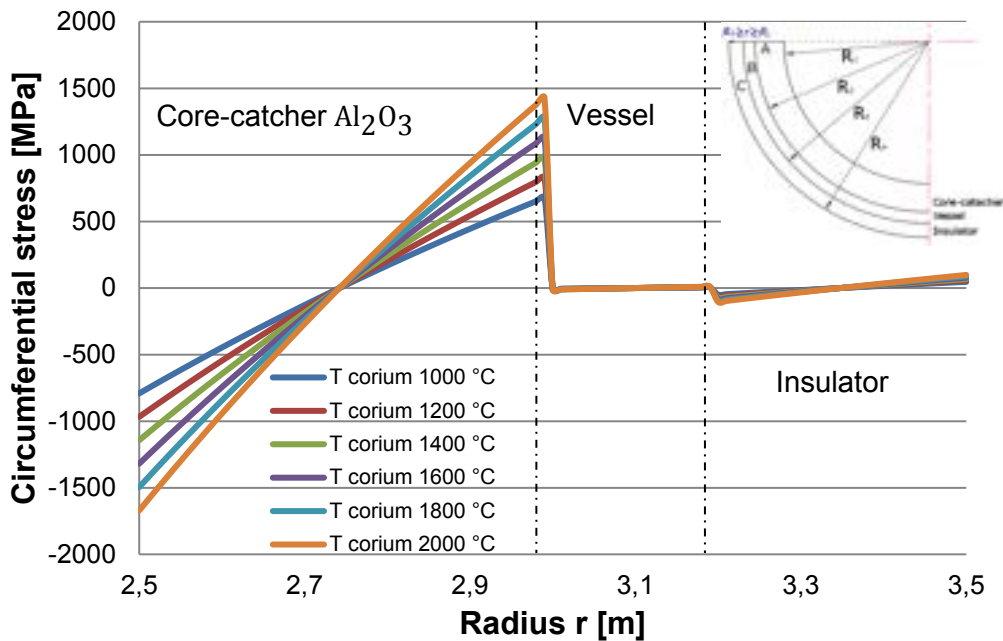


Figure 16: Circumferential stress behaviour, in the A, B and C layers, as function of the corium temperature

8.2. Numerical results

In general, the heat, transferred from the debris to the vessel wall, causes the lower head heat-up and in the long time may be responsible of the weakening of the vessel strength.

This occurs because of the degraded material properties caused by the high temperature.

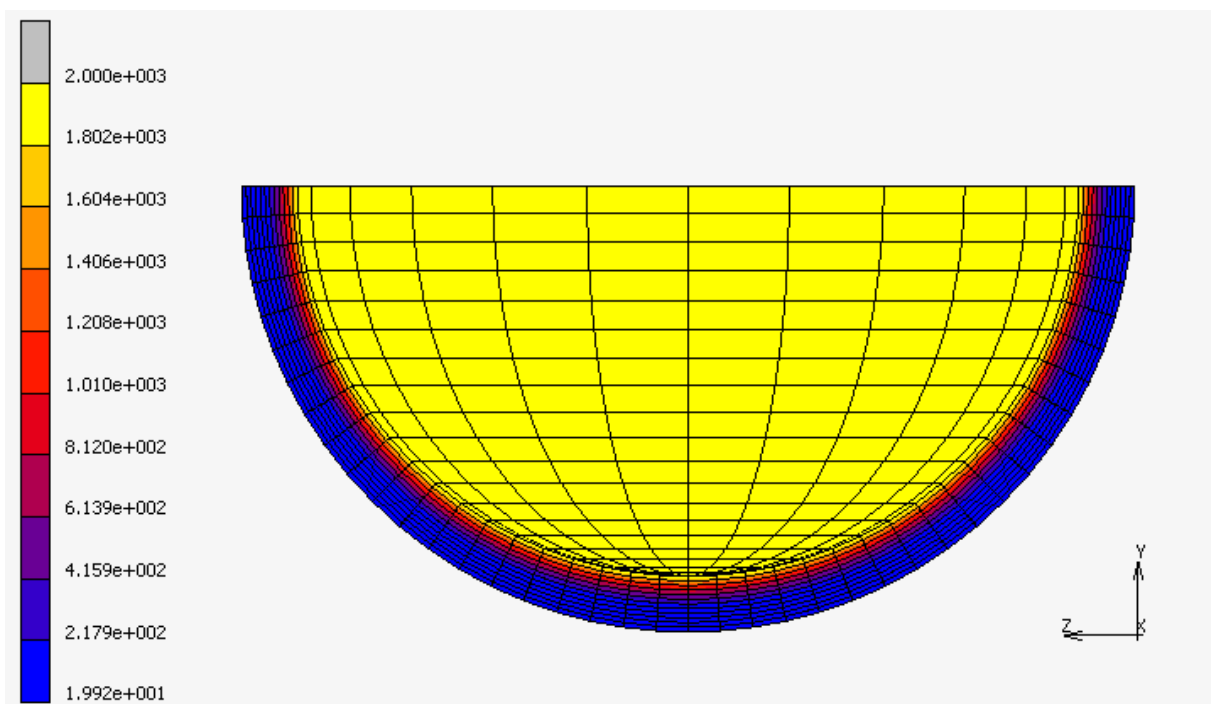
Figure 17 and Figure 18 show the distribution of the temperature as numerically calculated for thermal steady state condition.

They provide the temperature distribution in the assumed case of presence or absence of water external cooling. These contour plots clearly indicate the benefit of the allumina is delaying the heat transefer to the vessel wall also when the external cooling is exhausting. In addition, by comparing the obtained results with the previous analytical results, it appear that results are in good agreement each others.

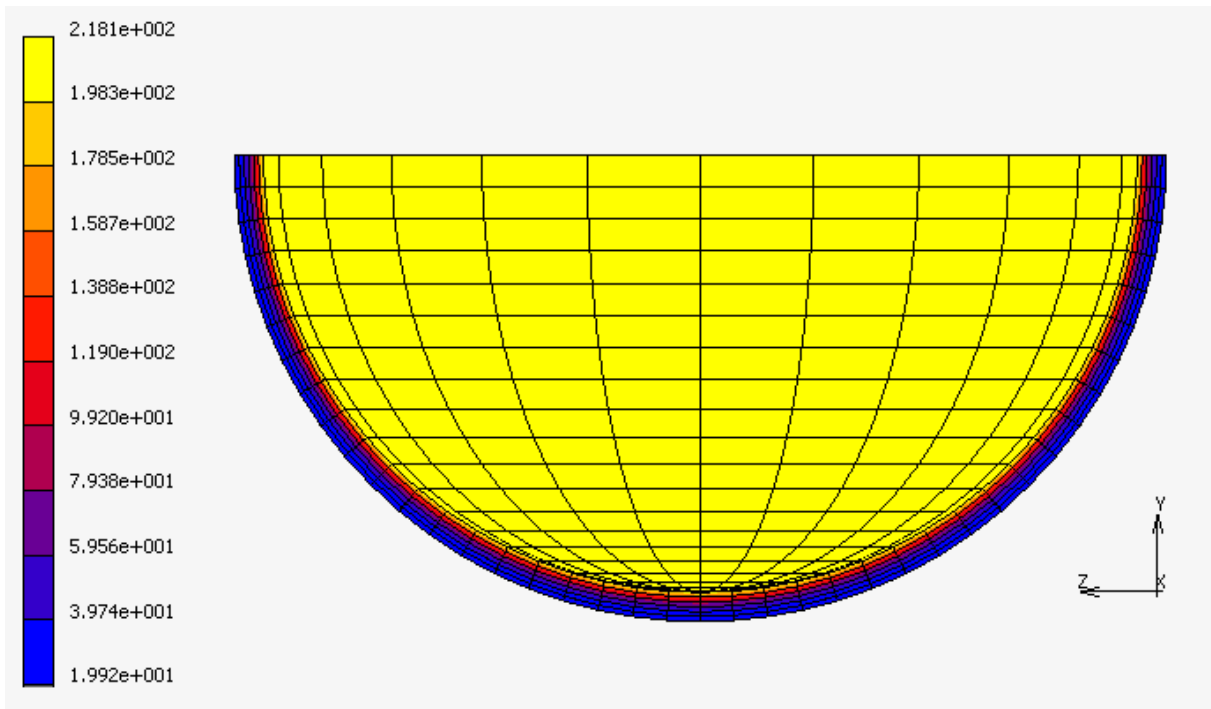
Without ICC, the heat conduction leads very soon to pre-heating of the solid vessel, due to the high conductivity of steel. When the removed heat flux is overwhelmed by the corium heat flux, the vessel ablation starts and in absence of external cooling increases slightly.

Figure 19 and Figure 20 show the behaviour of the temperature within the overall bottom head wall and in the steel vessel when the relocation of melt core are 1m and 0.5m respectively. The simulated case envisages the external water cooling.

After 1 hr from SA, it is possible to observe that the maximum value of the temperature is below the limit for which localized failure may appear. By analysing and comparing the showed temperature distributions it emerges clearly the positive role of the ceramic material in retarding the wall heating.



(a)



(b)

Figure 17: Contour plot of temperature in the alumina and steel wall (a) in the case of external water cooling. In particular, the temperature distribution through the vessel wall is give in (b).

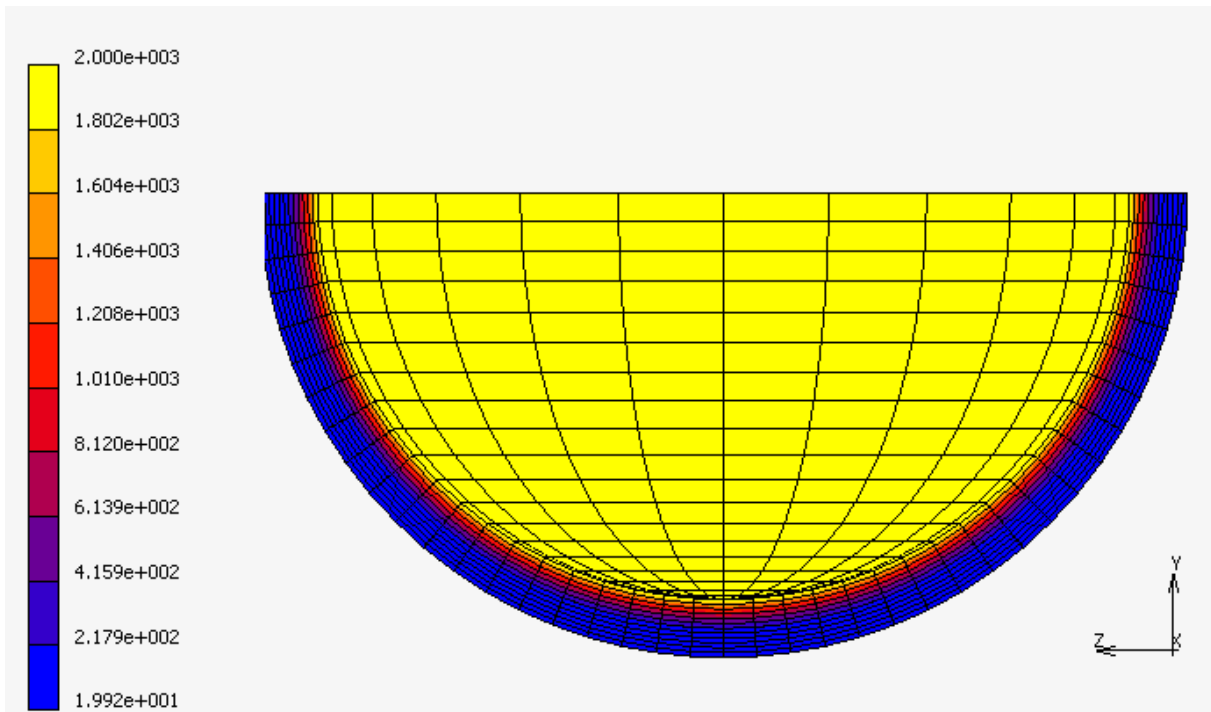


Figure 18: Contour plot of temperature in the alumina and steel wall in the case of absence of external water-cooling.

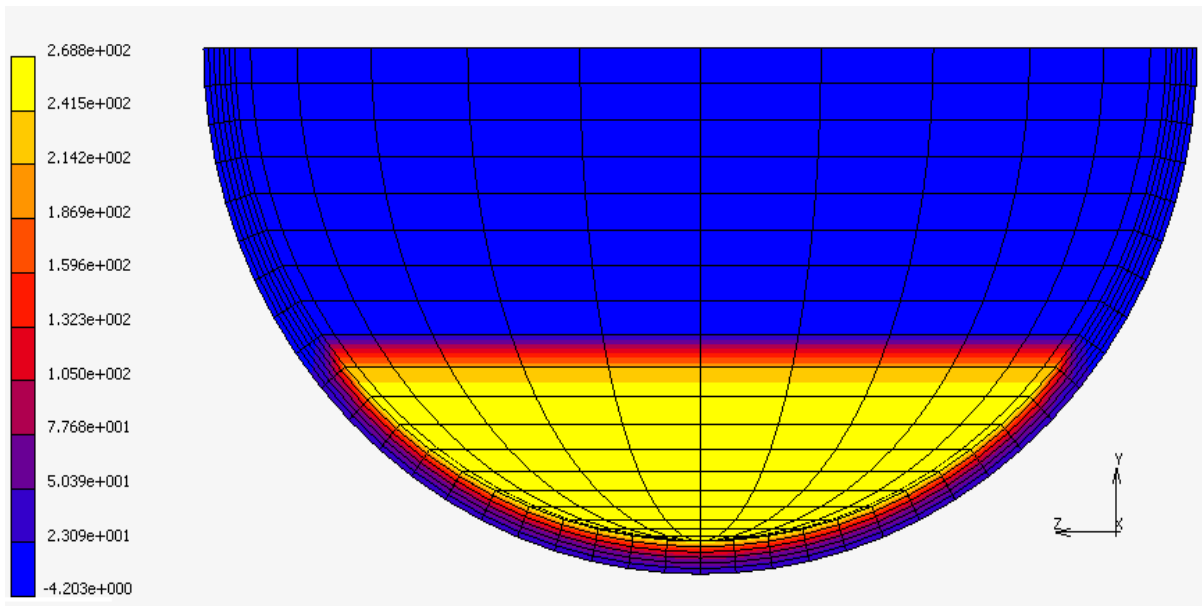
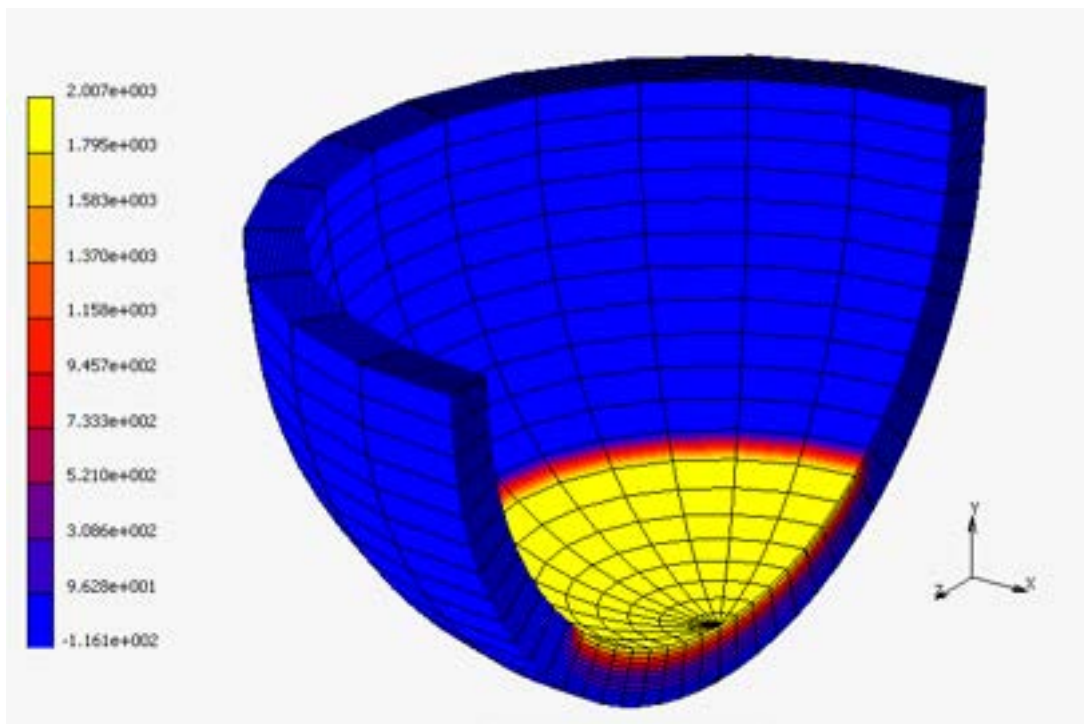
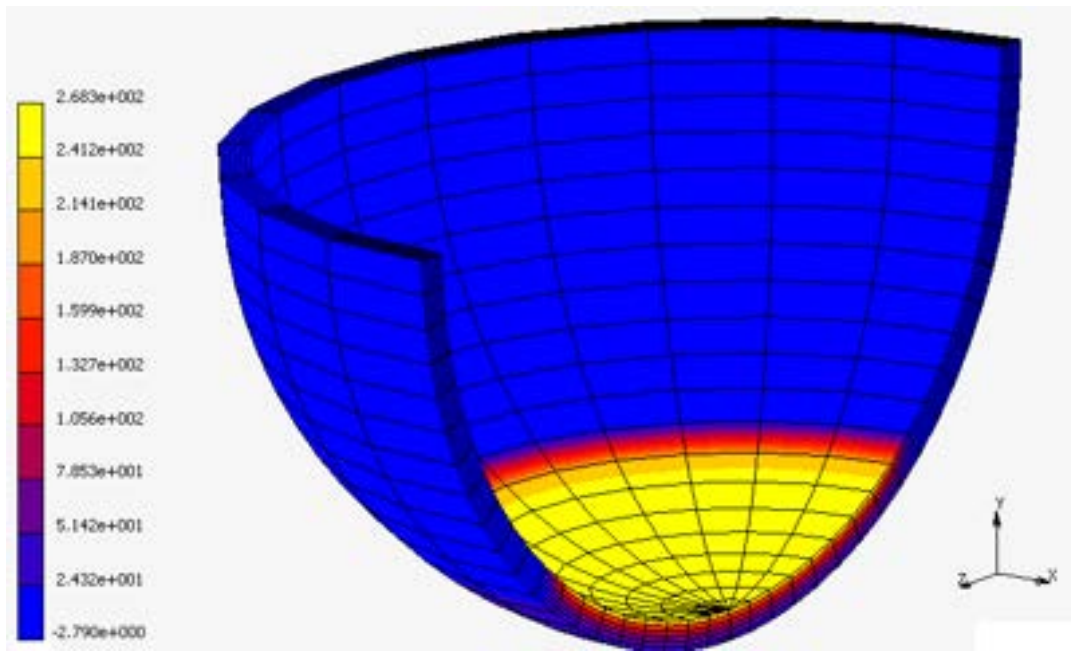


Figure 19: Contour plot of temperature in vessel wall for 1m.



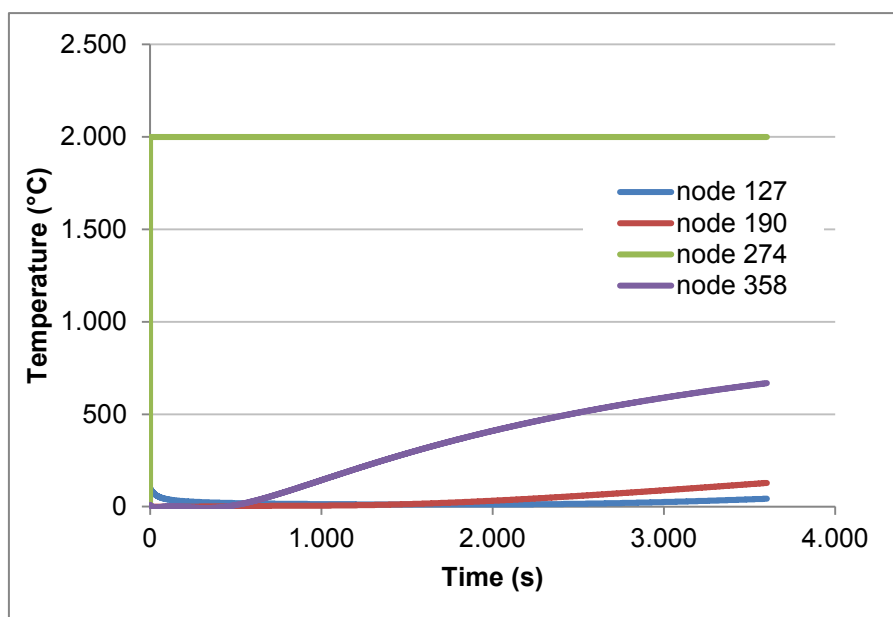
(a)



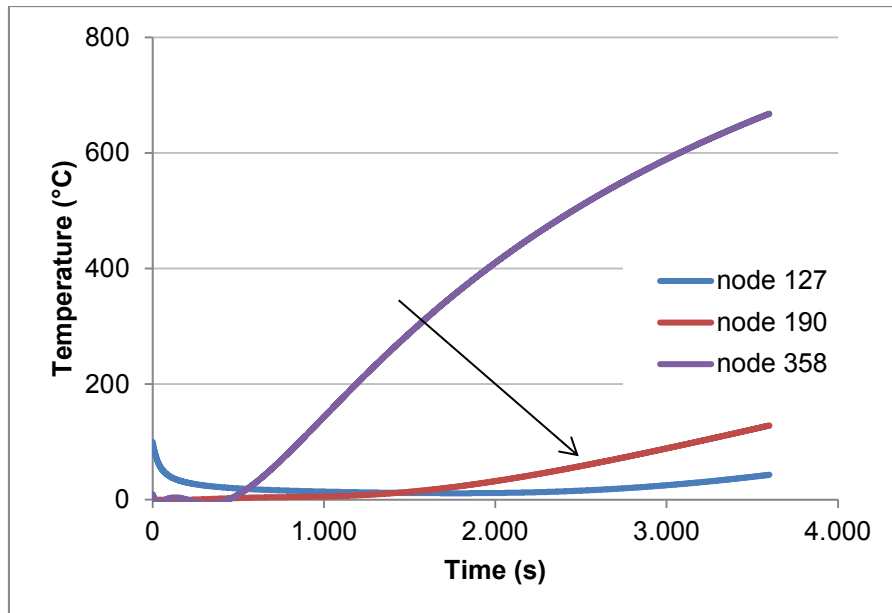
(b)

Figure 20: Contour plot of temperature in the bottom head wall for 0.5m of relocated corium (a). In the figure (b) the distribution of temperature in the steel wall of vessel is also shown

The lower head wall, as highlighted by FEM analyses' results is undergoing to significant thermal (Figure 21 and Figure 23) and pressure loads, and therefore it is liable to failure due to melting or creep rupture in the long term. In addition, vessel creep due to prolonged exposure at high temperatures could potentially develop into a breach of the lower vessel steel wall.



(a)



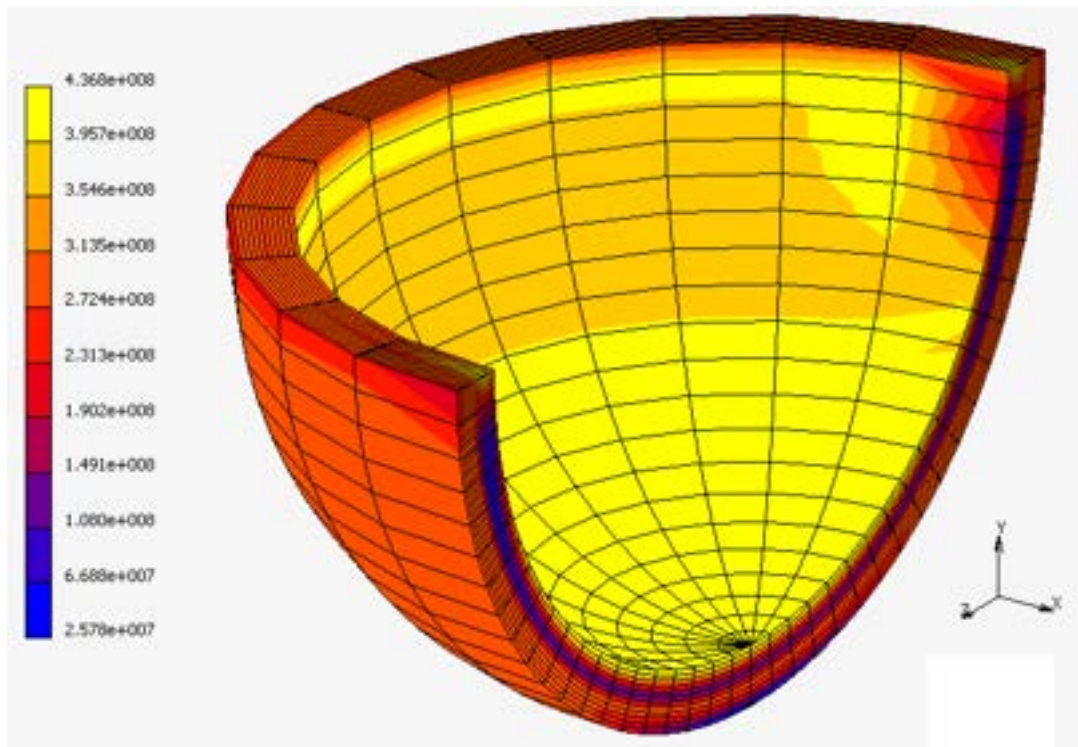
(b)

Figure 21: Results of thermo-mechanical analysis: temperature (a) and stress (b) in the bottom head thickness (outward direction according to the arrow versus) in the case external water-cooling and full melt core relocation. In the Figure 20 (b) zooming of temperature trend in the alumina and steel thickness is given.

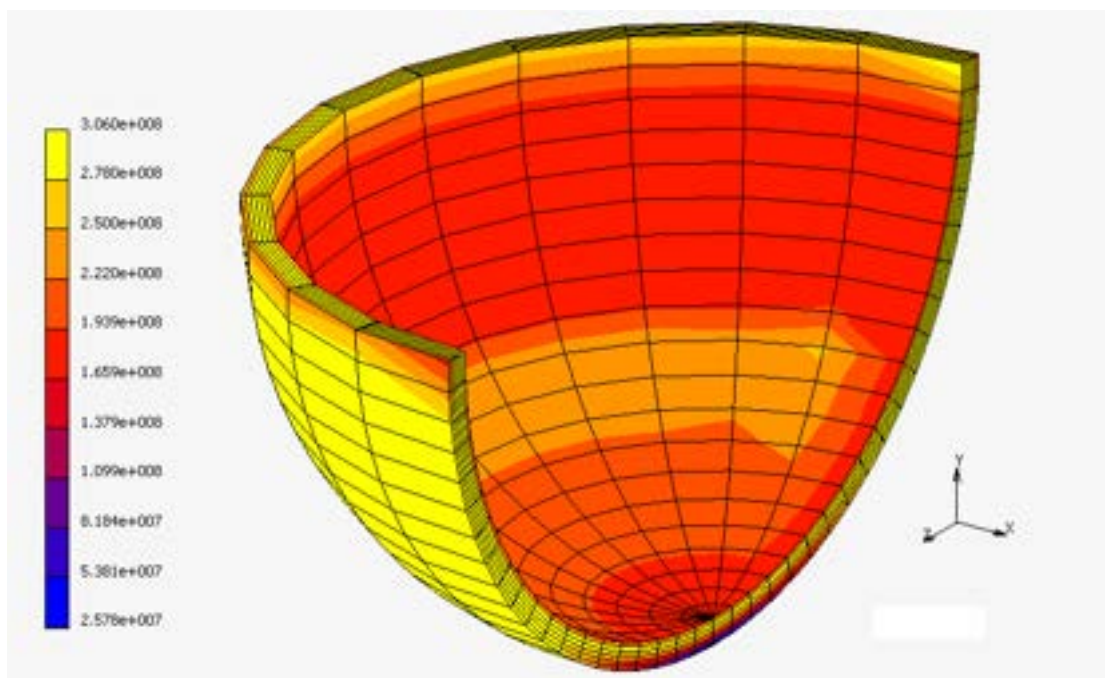
Analysing the stress distribution along the bottom head wall (alumina plus steel) and the Von Mises stress plot, it is possible to observe that the inner part of alumina facing the corium reaches quite soon the allowable stress limit.

Due to high level of stresses, plastic deformations appear at the vessel wall. They resulted directed mainly downwards even if deformations appear also at the corners of the lower head because of restraints (reaction forces exerted on the structure).

The consequence that such deformations may cause is localised wall thinnings, while the bottom part should be mostly intact.



(a)



(b)

Figure 22: Stress distribution in the bottom head wall in the case external water cooling (a) and full melt core relocation. In the bottom figure (b) is given the countur plot in steel thickness.

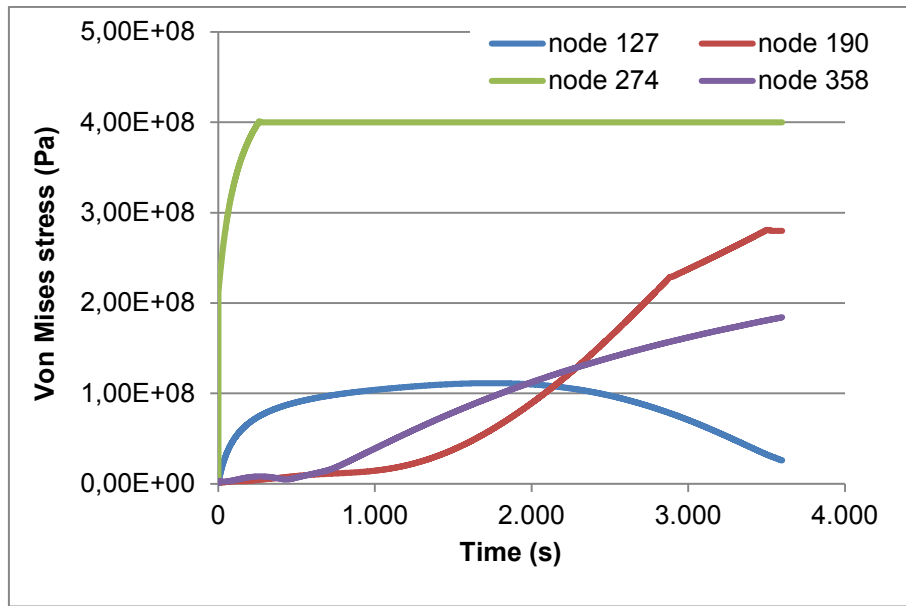
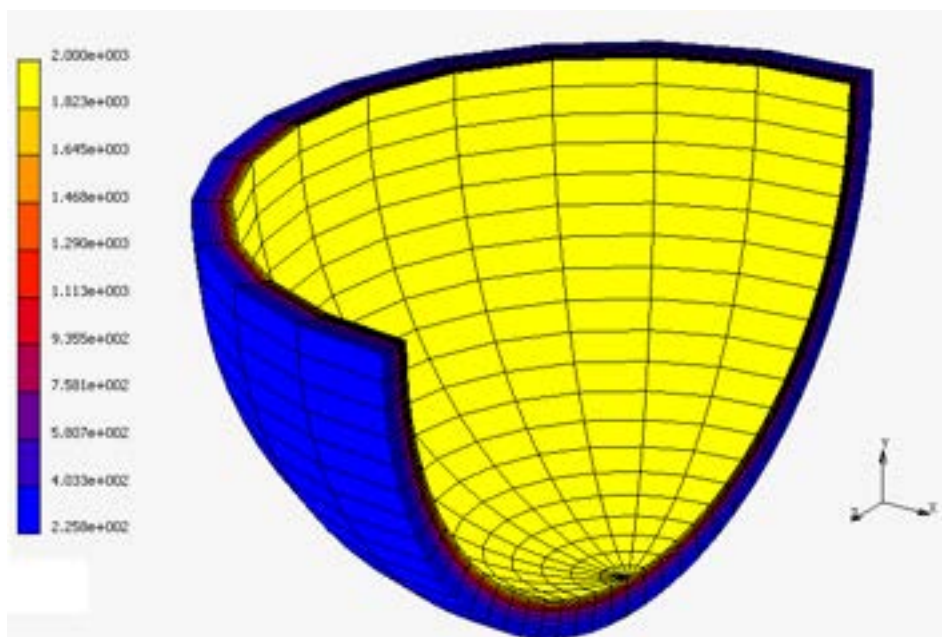


Figure 23: Stress trend in the bottom head thickness in the case external water cooling and full melt core relocation.

Finally simulation have been performed varying the thickness of alumina. The results obtained are provided in what follows in terms of temperature and stress (Figure 24). They show that reducing the alumina layer at 0.1m the temperature of the lower head increases. This poses a serious risk in terms of structural integrity and for the SAM. After 1 hour, the temperature of the outer surface of the vessel ranges about 220°C even in presence of external cooling, while the alumina is going to face thermal degradation,



a)

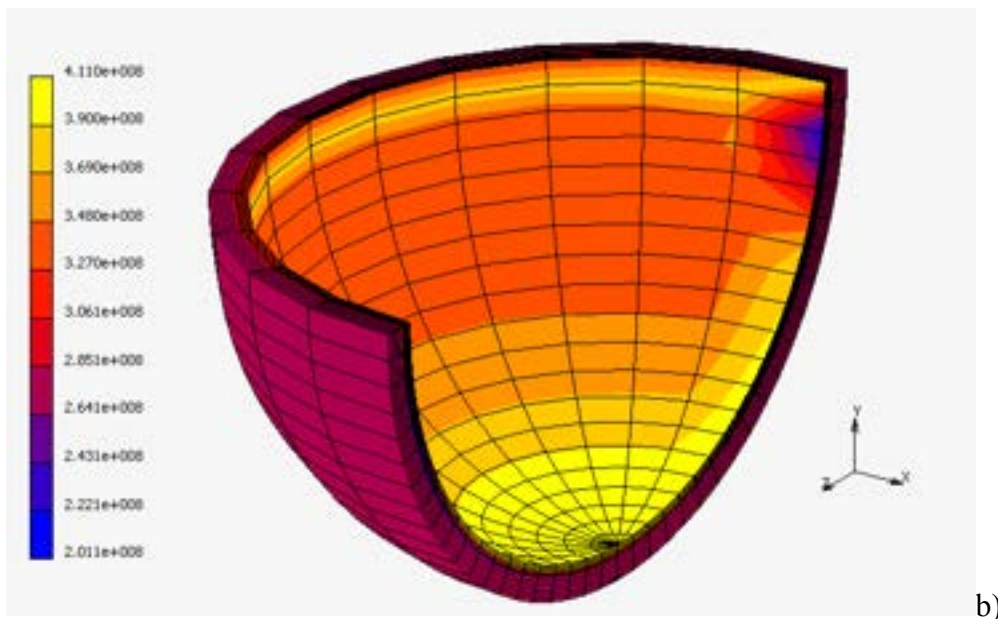


Figure 24: Temperature (a) and stress (b) distribution in the bottom head of vessel, for 0.1m alumina thickness, in the case of external water cooling and full melt core relocation.

We may reasonably desume that, as a consequence of that, the cavity pit of reactor could be heated-up in short time: temperture and pressure may increase accordingly posing serious structural problem for the containment building (the heating of water inside the cavity may result e.g., in H₂ production). Plastic deformation is about 8E-3.

9. Final summary

The first part of the study has examined passive nuclear safety, concentrating on the reliability aspect. Special emphasis is given on the passive containment cooling system, a thermal-hydraulic passive safety system, designed for LWR advanced reactor. Tools such as failure analysis and fault tree analysis are used to conduct reliability assessment for PCCS. Component reliability data is taken from available literature. Estimate for failure probability is obtained, but it must be regarded only as a suggestive approximation, as the main point was to show how to use classical methods in reliability assessment of passive systems.

The study shows the reduction in risk of containment heat removal failure and demonstrates a very low risk profile, because PCCS are highly reliable, due to, e.g., the redundancy configuration of components and passive design.


Additional effort is required aimed both at a deeper investigation on the thermal-hydraulic performance of the system and at the assessment of the relative uncertainties, with help of a suitable tool. Simulations by suitable codes for system performance assessment during severe accidents in order to achieve reliability figures of merit is suggested as a valuable means to merge both thermal hydraulic and probabilistic aspects.

This is in order to add credibility and validate the passive system reliability analysis.

Furthermore a new IVCR strategy to face issues due to the relocation of the corium in the pressure vessel lower head is presented, by proposing and investigating a new technological system based on an original designed core catcher (made of batch of ceramic multi-layered pebble of low thermal conductivity). The feasibility and positive effects of this system, in terms of SA management, are analysed by performing analytical and numerical simulations.

In doing that different thicknesses are analysed and level of corium relocation taken into account. Numerical modelling allows to investigate the core catcher at the final state of corium relocation (including characterization of material properties at severe accident conditions); FEM model allows for thermo-mechanical evaluation of RV bottom head capacity. The transient duration in the simulation lasts 1hr.

Results show that in general, the heat transferred from debris to the vessel wall, causes the lower head heat-up and in the long time may be responsible of the weakening of the vessel strength. After 1 hr from SA, the maximum value of the temperature is below the limit for which localized failure may appear. Moreover, results clearly indicate the benefit of the


 Ricerca Sistema Elettrico	Sigla di identificazione	Rev.	Distrib.	Pag.	di
	ADPFISS-LP1-109	0	L	49	52

alumina core catcher is delaying the heat transefer to the vessel wall also when the external cooling is going to exhaust.

Without ICC, the heat conduction leads very soon to pre-heating of the solid vessel, due to the high conductivity of steel. When the removed heat flux is overwhelmed by the corium heat flux, the vessel ablation starts and in absence of external cooling increases slightly.


Finally, it is worthy to remark that, in absence of water-cooling and for prolonged exposure at high temperatures, plastic deformations appear may cause localised wall thinning as well ascreep could potentially develop into a breach of the lower vessel steel wall.

Further investigation are however necessary to account mainly for focusing effects and ablation, which may play an important role in the SAM and for the assessment of structural reactor vessel capicity.


 Ricerca Sistema Elettrico	Sigla di identificazione	Rev.	Distrib.	Pag.	di
	ADPFISS-LP1-109	0	L	50	52

References

1. R. Lo Frano, L. Burgazzi, Analysis relating to the implementation of the safety safeguards for the severe accident management in nuclear reactors, ENEA report ADP-FISS-LP1-072, September 2016
2. IAEA-TECDOC-626 International Atomic Energy Agency, IAEA. 1991. Safety related terms for advanced nuclear plants
3. J.L.Foret., “AP1000 Probabilistic Safety Assessment”, chapter 13, Pittsburgh, PA, Westinghouse Electric Company LLC (2003)
4. R. Lo Frano, L. Burgazzi, Assessment of the safeguards to cope with the consequences of severe accidents in nuclear power plants”, ENEA report ADPFISS-LP1-096, November 2017
5. Yu Yu et al., “Effect of Air temperature on Failure Prognosis of Passive Containment Cooling System in AP1000”, Chemical Engineering Transactions, Vol. 33, 2013
6. N. C. RASMUSSEN, “Reactor Safety Study: An Assessment of Accident Risks in US Commercial Nuclear Power Plants,” WASH 1400, NUREG-750014, U.S. Nuclear Regulatory Commission, Oct. 1975
7. S.E. Mays, EG&G Idaho. 1982. Interim Reliability Evaluation Program: Analysis of the Brown Ferry Unit 1, Nuclear Power Plant, Appendix C—Sequence Quantification
8. Nuclear Safety in Light Water Reactors, Severe Accident Phenomenology, Academic Press, Elsevier, chapter 6, 519-588, 2012
9. 4th EU FP, “Final report for the Melt-Vessel Interactions”, EU, 1999
10. W. Ma et al., In-Vessel Melt Retention of Pressurized Water Reactors: Historical Review and Future Research Needs, *Engineering 2 (2016), 103–111*
11. J.L. Rempe, et al., Light Water Reactor Lower Head Failure Analysis, Technical Report, NUREG/CR-5642 EGG-2618, October 1993.
12. T.G.Theofanous, , et al., 1995, In-Vessel Coolability and Retention of a Core Melt, DOEIID-10460, v.2 (July 1995).
13. R. Lo Frano, et al., Thermo-mechanical test rig for experimental evaluation of thermal conductivity of ceramic pebble beds, *Fusion Eng. and Design 89, (2014), 1309-1313*.
14. NEA/OECD Nuclear Safety, In-vessel core degradation code validation matrix NEA/CSNI/R(2000)21, 31 October 2000.

 Ricerca Sistema Elettrico	Sigla di identificazione	Rev.	Distrib.	Pag.	di
	ADPFISS-LP1-109	0	L	51	52

15. S. K. Spencer, et al., Fragmentation and Quench Behavior of Corium Melt Streams in Water, NUREG/CR-6133 ANL-93/32, 1994.
16. T.G. Theofanous, et al., In-Vessel Coolability and Retention of a Core Melt, DOE/ID-10460, vols. 1 and 2, October 1996.
17. T. G. Theofanous, et al., In-vessel coolability and retention of core melt, *Nuclear engineering and design* 169, (1997), 1-48.
18. O. Kymäläinen, H. Tuomisto, T. G. Theofanous, In-vessel retention of corium at Loviisa, *Nuclear Engineering and Design* 169, (1997), 109-130.
19. R. Kolbe and E. Gahan, Survey of Insulation Used in Nuclear Power Plants and the Potential for Debris Generation, NUREG/CR 2403 Supplement n. 1, SAND82-0927, May 1982.
20. R. Lo Frano et al., Integrity of pressure vessel lower head in case of corium relocation: identification of loads and failure modes, Transactions of SMiRT-24, Division V, BEXCO, Busan, Korea - August 20-25, 2017.
21. B.K. Singh et al., Coupled thermo-structural analysis for in-vessel retention in PHWR using ABAQUS, *Nuclear Engineering and Design* 323 (2017) 407–416
22. J.-W. Park et al. Vessel wall conjugate heat transfer and solution procedure, *Annals of Nuclear Energy* 88 (2016) 57–67.
23. Ott, L. Hoge, Failure Modes of the BWR Reactor Vessel Bottom Head. Oak Ridge National Laboratory, Tennessee, 1989.
24. R. Chambers, A Finite Element Analysis of a Reactor Pressure Vessel during a Severe Accident. NUREG/CR-5046, 1989.
25. R. S. Chambers, A Finite Element Analysis of a Pressurized Containment Vessel during Core Melt Down, SAND87-2183, 1987.
26. S.A. Chavez, and J. L. Rempe, Finite Element Analyses of a BWR Vessel and Penetration under Severe Accident Conditions, *Nuclear Engineering and Design*, 148,(1994), 413-435.
27. T. Y. Chu, et al., An Assessment of the Effects of Heat Flux Distribution and Penetration on the Creep Rupture of a Reactor Vessel Lower Head, Twelfth Proceedings of Nuclear Thermal Hydraulics, 1997 ANS Winter Meeting, November 16-20, 1997, Albuquerque, NM, 135-144.

 Ricerca Sistema Elettrico	Sigla di identificazione ADPFISS-LP1-109	Rev. 0	Distrib. L	Pag. 52	di 52
--	---	-------------------------	-----------------------------	--------------------------	------------------------

28. P. Tusheva, et al., Investigations on in-vessel melt retention by external cooling for a generic VVER-1000 reactor. *Ann. Nucl. Energy* 75,(2015), 249–260.
29. Y.P. Zhang, et al., Analysis of safety margin of in-vessel retention for AP1000. *Nucl. Eng. Des.* 240, (2010), 2023–2033.

Titolo
ANALISI E VALUTAZIONI DI INCIDENTI SEVERI IN LWR
Descrittori
Tipologia del documento: Rapporto Tecnico

Collocazione contrattuale: Accordo di Programma ENEA-MISE su Sviluppo Competenze Scientifiche nel Campo della Sicurezza Nucleare e Collaborazione ai Programmi Internazionali per il Nucleare di IV Generazione.

Argomenti trattati: Reattori ad Acqua Leggera, Incidenti Severi, MELCOR, RAVEN, Incertezza

Sommario

Nel presente rapporto tecnico vengono riportati i risultati dell'attività di ricerca sviluppata nella linea LP1 (Sviluppo Competenze Scientifiche nel Campo della Sicurezza Nucleare), obiettivo B (Safety Assessment e Valutazioni D'impatto) task B2 (Valutazioni di Rischio e Scenari Incidentali) topic 2 (Calcolo Integrale di Scenari Incidentali) del PAR 2017, Accordo di Programma ENEA-MISE. In relazione ai reattori di tipo BWR, l'analisi del transitorio, che si è destato nell'Unità 1 del reattore di Fukushima Daiichi (conseguente al terremoto e allo tsunami che si sono verificati il giorno 11 Marzo del 2011) è stata effettuata con il codice MELCOR. Un'analisi di incertezza, utilizzando il software RAVEN, è stata sviluppata al fine di caratterizzare l'incertezza del codice nel predire la pressione del vessel e del drywell, selezionate come figure di merito dell'analisi, durante il transitorio scelto e identificare i parametri di input che hanno una maggiore influenza su di esse. In relazione ai reattori PWR un transitorio non mitigato dovuto a una postulata perdita d'acqua d'alimento del generatore di vapore in un generico PWR da 900 MWe è stato analizzato con il codice MELCOR. Si sottolinea una completa revisione della nodalizzazione del core e del vessel al fine di avere una risposta più dettagliata dei fenomeni di degradazione. I risultati di queste analisi sono qui riportati. Il rapporto è redatto in lingua inglese.

Note


Il presente lavoro è stato preparato con il contributo del personale ENEA e CIRTEN:

 Authors: F. Mascari (ENEA),
 F. Giannetti, M. Donorio, A. Giampaolo, L. Gramiccia, G. Caruso (CIRTEN)
 ref. Doc.: CERSE-UNIRM RL 6001/2018

Copia n.
In carico a:

2			NOME			
			FIRMA			
1			NOME			
			FIRMA			
0	EMISSIONE	23/11/18	NOME	F. Mascari	F. Rocchi	F. Rocchi
			FIRMA	<i>F. Mascari</i>	<i>F. Rocchi</i>	<i>F. Rocchi</i>
REV.	DESCRIZIONE	DATA	REDAZIONE	CONVALIDA	APPROVAZIONE	



 Ricerca Sistema Elettrico	Sigla di identificazione ADPFISS-LP1-122	Rev. 0	Distrib. L	Pag. 3	di 56
--	--	------------------	----------------------	------------------	-----------------

**ANALISI E VALUTAZIONI DI INCIDENTI
SEVERI IN LWR**


**(ANALYSES AND EVALUATION OF SEVERE
ACCIDENT IN LWR)**



CONTENTS

1.	INTRODUCTION.....	9
2.	FUKUSHIMA DAICHII UNIT 1 SENSITIVITY AND UNCERTAINTY ANALYSIS	11
2.1	MELCOR Code	11
2.2	RAVEN software tool	11
3.	BWR FUKUSHIMA DAICHI UNIT I SEVERE ACCIDENT MODEL	12
3.1	Boiling Water Reactors NPP description	12
3.2	Fukushima Daiichi NPP site layout	13
3.3	The accident.....	14
3.4	Sequence of events at Fukushima Daiichi Unit 1	15
3.5	MELCOR nodalization approach.....	16
3.6	CORE Model	18
3.7	Thermal hydraulic model	21
3.8	Containment model	23
4.	RAVEN – MELCOR coupling development.....	24
4.1	Variables and sampling	26
5.	RESULTS.....	27
6.	UNMITIGATED LOSS OF FEED WATER TRANSIENT ANALYSIS IN A GENERIC PWR THREE LOOPS DESIGN LIKE of 900 MWe.....	30
6.1	Unmitigated LFW - Loss of feedwater transient	30
7.	MELCOR nodalization.....	30
7.1	RPV – Reactor Pressure Vessel	31
7.1.1	Core	32
7.1.2	Upper Plenum	33
7.2	Hot Legs, Pressurizer, Steam Generator, Cold Leg	34
7.3	Secondary System	36
7.4	Containment.....	36
7.5	Natural Circulation Flows	37
7.5.1	HL Flow Rates and a Discharge Coefficient.....	37
7.6	Core Degradation Modelling.....	39
7.6.1	Core blockage model	39
7.7	Vessel Lower Head Failure and Debris Ejection	39
7.8	Reactor SCRAM.....	39
8.	Steady State Results.....	40
9.	RESULTS.....	42
10.	Conclusions.....	47
11.	ABBREVIATIONS	48
12.	REFERENCES.....	51




 Ricerca Sistema Elettrico	Sigla di identificazione ADPFISS-LP1-122	Rev. 0	Distrib. L	Pag. 7	di 56
--	--	------------------	----------------------	------------------	-----------------

ABSTRACT

This report presents the activity performed in the framework of LP1 (Sviluppo Competenze Scientifiche nel Campo della Sicurezza Nucleare), Objective B (Safety Assessment e Valutazioni D'impatto) task B2 (Valutazioni di Rischio e Scenari Incidentali) Topic 2 (Calcolo Integrale di Scenari Incidentali) of the PAR 2017, ADP ENEA-MiSE. In relation to the BWR reactors, the analysis of the transient that took place in Unit 1 of the Fukushima Daiichi reactor (following the earthquake and tsunami that occurred on 11 March 2011) was carried out with MELCOR code. An uncertainty analysis, using the RAVEN software, was developed in order to characterize the uncertainty of the code in predicting vessel and drywell pressure, selected as figures of merit of the analysis, during the selected transient and identify the input parameters that have a major influence on them. In relation to the PWR reactors, a unmitigated transient due to a postulated loss of feed water of the steam generator in a generic PWR 900 MWe was analyzed with the MELCOR code. It is to underline a complete revision of the core and vessel nodalization in order to have a more detailed prediction of the degradation phenomena.



	Ricerca Sistema Elettrico	Sigla di identificazione ADPFISS-LP1-122	Rev. 0	Distrib. L	Pag. 9	di 56
---	----------------------------------	--	------------------	----------------------	------------------	-----------------

1. INTRODUCTION

After the Fukushima accident, the interest of each country using nuclear energy as a part of its national energy mix has been more focused on severe accident [1-7] mitigation strategies. Several severe accident management analyses have been performed to analyze the accident progression, the core damage, the grace period and the fission product release demonstrating the accident management strategy adequacy.

When a postulated event determines an unmitigated transient, due to postulated several concurrent malfunctions, the core cooling could be not enough to maintain the fuel and flow channel geometry and the core and the related structural materials could start their degradation and consequent relocation phenomena along the core and the lower plenum. In these scenarios the core material and the cooling flow paths could lose their original geometry, well known in term of core cooling capability, and the new configuration is characterized by a mixture of molten corium and debris with a consequent geometry determining an uncertain core cooling capability. Then the evolution of the severe accident starts and will evolve considering the different postulated extreme boundary conditions and mitigation actions that are postulated to do not succeed during the accident evolution.


Considering the complexity and mutual different interacting phenomena along a severe accident progression and the possible source term release to the environment, the research on severe accidents is fundamental in order to characterize the main phenomena determining the transient evolution of the plant and to support SAM assessment. Within this regard a key role is done by the State-of-Art severe accident codes (as ASTEC [8], MAAP [32], MELCOR [9], etc), [10] that storing all the knowledge developed in the last decades from the experimental activities, permit the prediction of the transient behaviour of a plant, during a severe accident, and qualitatively and quantitatively can support the assessment of SAM.

These codes storing all the knowledge developed in the last decades from the experimental activities, permit the prediction of the transient progression of the modeled plant, during a postulated severe accident, characterizing the main severe accident phenomena taking place in the Reactor Pressure Vessel (RPV), the Reactor Cavity (RC), the Containment (PCV), and the confinement buildings typical of LWRs. Several models/correlations have been implemented in these State-of-Art severe accident codes and have to be set by code-user during input-deck development.

In relation to the code model/correlations implemented in the State-of-Art severe accident codes, even though several experimental campaigns in the field of severe accident phenomena [13-17] have been performed and provided valuable “assessment database [18]” as references to assess severe accident simulation tools, the analyses of the current State-of-the-Art shows that there is the need to reduce some uncertainties still present [19] and a consequent investigation of phenomena/processes, up to day not investigated in detail in geometric prototypical experimental facility with prototypical material, should be addressed.

Considering the need to reduce some uncertainties still present and considering the reached level of development and maturity of severe accident codes and their application on SAMG assessment the discussion and application of severe accident progression analyses with uncertainty (uncertainty is used as a measure of the error made with the code in prediction plant behavior) estimation is currently a key topic in the BEPU framework.

In term of research and development on severe accidents, ENEA is involved in the maintenance of a nuclear safety culture in order to have a high level technical point of view to support independent Italian national evaluations. Infact, though nuclear energy is not part of Italian energy mix, several NPPs are at the Italian border areas. Therefore, Italian capability to analyse possible postulated plant accident progressions is of strategic interest for our national emergency preparedness strategy. Infact these analyses are the basis for technical-scientific prediction of potential risk scenarios, planning of response activity and possible prevention in order to minimize damage in the event of potential contamination of Italian territory. Within this regards uncertainty estimation with the probabilistic method are in progress to support DBA [12] and BDBA [11] analyses.


 Ricerca Sistema Elettrico	Sigla di identificazione ADPFISS-LP1-122	Rev. 0	Distrib. L	Pag. 10	di 56
--	--	------------------	----------------------	-------------------	-----------------

1.1 Probabilistic Method to Propagate Input Uncertainty

In general the sources of uncertainty can be grouped as a) code uncertainty (e.g. approximation in the conservative equation and in the closure models and correlations) b) representation uncertainty (nodalization effect), c) scaling (the code are validated against scaled down facilities), d) plant uncertainty (e.g. initial and boundary conditions), e) user effect .

Several methodologies have been developed in the past to perform Uncertainty Analysis. In particular this uncertainty methodologies can be grouped in a) methods to propagate input uncertainty, divided in probabilistic (e.g. CSAU, GRS, IPSN, etc.) and deterministic methods (e.g. AEAW, EDF-Framatome, etc.); and b) method to extrapolate output uncertainty (e.g. UMAE) [98].

The probabilistic method to propagate the input uncertainty [95] is, in brief, based on a random sampling of the input uncertain parameters selected by the user; a set of N code runs having in the input a combination of the uncertain parameters is created and solved with the selected code and then, by using regression analysis, it is computed the effect of the input parameters uncertainty on the results uncertainty. The main advantages of this method are that the number of code runs does not depend on the number of input uncertain parameters and it is not necessary a prior Phenomena Identification and Ranking Table (PIRT) that is a long process. The number of code runs N depends on the probability content and on the confidence level set by the user and on the number of Figure of Merits (FOMs) selected for the analysis and it is computed using the Wilks formula [96-97]. Each input uncertain parameter should be defined by its range of variation and its Probability Density Function (PDF); this means that even if the exact value of a parameter is uncertain, some values are more likely to be close to the real one than others. This is one of the main task to be tackled because the evaluation of the correct PDF for each parameter it is not a trivial task and a careful study is required. The selection of the most suitable PDF for each parameter depends mainly on the physical quantity and on the availability of reduced-scale or full-scale measured data. If data are available, it is possible to build a histogram and to derive the PDF [12]. A comprehensive overview of PDF derivation and types is provided in [99].

 Ricerca Sistema Elettrico	Sigla di identificazione ADPFISS-LP1-122	Rev. 0	Distrib. L	Pag. 11	di 56
--	--	------------------	----------------------	-------------------	-----------------

2. FUKUSHIMA DAICHI UNIT 1 SENSITIVITY AND UNCERTAINTY ANALYSIS

Sapienza University of Rome together with ENEA plans to conduct sensitivity and uncertainty analyses on the Fukushima Daiichi unit 1 plant with the MELCOR code. The MELCOR model to be used was developed for previous deterministic safety analyses reported in [29], [30] and [31]. In order to perform this sensitivity and uncertainty study Sapienza University of Rome has developed a new Python interface to couple the MELCOR code with the RAVEN (Reactor Analysis and Virtual control ENvironment) software tool. The goal of this study is to evaluate the effects of some selected parameters on the melt progression behavior of the core and show the capabilities of the coupling between RAVEN and MELCOR performing statistical analysis to estimate the range of evolution of severe accident scenarios.

2.1 MELCOR Code

MELCOR [33][34] is a fully integrate, engineering-level computer severe accident code able to simulate the thermal-hydraulic phenomena in steady and transient condition and the main severe accident phenomena characterizing the RPV, the reactor cavity, the containment, the confinement buildings typical of LWR and the source term estimation. It has been developed at Sandia Laboratories (SNL) for the U.S. Nuclear Regulatory Commission..

The code is based on the “control volume” approach. MELCOR can be used with the Symbolic Nuclear Analysis Package (SNAP) [35] in order to develop the nodalization and for the post processing data by using its animation model capabilities.

MELCOR has a modular structure and it is composed of an executive driver and a number of major modules, or packages, that together model the major systems of a reactor and their interactions.

The Core (COR) package models the relocation of core and lower plenum structures during melting and debris formation and ejection into the reactor cavity consequently the reactor vessel failure. This package also calculates the thermal-hydraulic response of core internal structures, considering energy transfer to and from Control Volume (CVH) and Heat Structure (HS) packages.

The Control Volume Hydrodynamics (CVH) and Flow Path (FL) packages model the thermal-hydraulic behavior of liquid water, water vapor and gases. The CVH input defines the initial state of each volume, requiring geometry and composition. FL package is instead concerned with connections between control volumes, through which control volume masses may flow. The Radionuclide (RN) package: models the release of fission products from fuel and debris, and aerosol dynamics with transport through flow paths and deposition on structure surfaces. Boundary conditions, like fluid parameters, structures surface temperatures and source terms are provided by other MELCOR packages. It is also possible to consider the wash-off of radionuclides deposited on heat structures from the drainage of water films and the aerosol removal by safety features.

The Control Function (CF) package where user can define functions of variables that can be used by other packages in the code. There is a series of available types of control functions that can have a several number of uses, some of which contains a difficult control logic; it is for example used to control the opening of a valve, or the pump head associated with a flow path. It is also important to underline that control functions (CF) or tabular functions (TF) can be associated with CVH and FL packages, in order to simulate for example sources and sinks of mass or energy, valves, pumps, etc.

2.2 RAVEN software tool

RAVEN (Reactor Analysis and Virtual control ENvironment) is a software tool, developed at the Idaho National Laboratory (INL), that acts as the control logic driver and post-processing tool for different applications [37]. RAVEN has been developed to perform parametric and probabilistic analysis based on the response of complex system codes, in order to quantify the safety margins related to safety-related events [38]. The initial development of RAVEN has been focused on providing dynamic risk assessment capability to RELAP-7 [94], however the modular software structure made possible the coupling with other any system codes.

Nowadays RAVEN is a multi-purpose probabilistic and uncertainty quantification platform.

RAVEN is composed of three main software systems that can operate either in coupled or stand-alone mode:

- Graphical User Interface
- Control Logic System
- Probabilistic and Parametric framework

The control logic system is currently available for RELAP-7 only, but Sapienza University of Rome plans to extend this feature also to the MELCOR code.

The two basic elements of RAVEN useful to perform a sensitivity or uncertainty analysis are:

- Distributions: necessary to produce sampling of the input parameters and initial conditions, based on their probabilistic distribution. A large library of probability distribution functions is available in RAVEN: Bernoulli, Binomial, Exponential, Logistic, Lognormal, Normal, Poisson, Triangular, Uniform, Weibull, Gamma, and Beta. All distributions are also available in their truncated form when this is mathematically feasible.
- Sampler: necessary to connect a set of variables to their corresponding distributions and produces a sequence of points in the input space. There are three main classes of samplers: blind samplers, dynamic event tree samplers, and adaptive samplers [39].

3. BWR FUKUSHIMA DAIICHI UNIT I SEVERE ACCIDENT MODEL

3.1 Boiling Water Reactors NPP description

Boiling water reactor is characterized by a closed, direct steam cycle loop (Figure 3-1), using water as coolant and as moderator to control reactivity. The working fluid boils in the reactor core and drives turbines to generate electricity. The steam is then condensed, cooled by the condenser tubes, filled with water taken from a heat sink. The water is finally pumped back to the reactor building in the Reactor Pressure Vessel (RPV) as feed water.

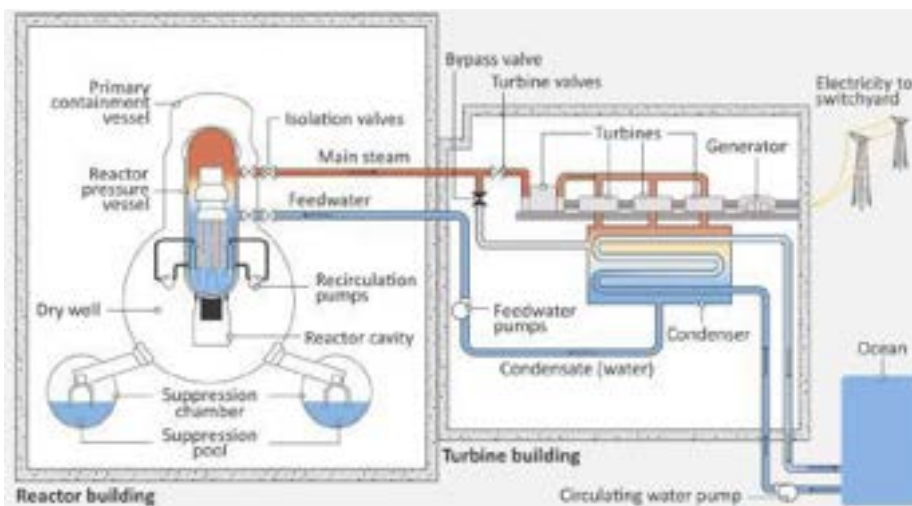


Figure 3-1: BWR Plant [40]

Fukushima Daiichi Nuclear Power Plant is composed by 6 units which cover the evolution of BWR technology during the 12 years from the construction of Unit 1 in 1967 until the complete operability of Unit 6 in 1979. After Unit 1, which was a BWR/3 design, Units 2-5 were BWR/4 while Unit 6 was a BWR/5 design.

Description	Unit 1	Unit 2	Unit 3	Unit 4	Unit 5	Unit 6
Reactor type	BWR/3	BWR/4	BWR/4	BWR/4	BWR/4	BWR/5
Electrical output (MWe)	460	784	784	784	784	1100
Thermal output (MWth)	1380	2381	2381	2381	2381	3293
Commercial operation start	March 1971	July 1974	March 1976	October 1978	April 1978	October 1979

Table 3-1: Fukushima Daiichi Nuclear Power Plant Specifications

The main differences between BWR types regard Recirculation Loops, Reactor Isolation Pressure and Inventory Control, Emergency Core Cooling Systems and Containment.

The containment of a BWR is a pressure suppression containment. It is composed by a wetwell, a drywell and a vent system.

The detail of the main emergency systems of Fukushima Daiichi BWRs is reported in [41] and [46].

3.2 Fukushima Daiichi NPP site layout

The site was located 220 km north of Tokyo, on the Pacific coast of Fukushima Prefecture.

Before the construction of the NPP, the site elevation was about 35 m referring to the average sea level at Onahama port ("OP" level); consequently, a great excavation plan was necessary, as shown in Figure 3-2.

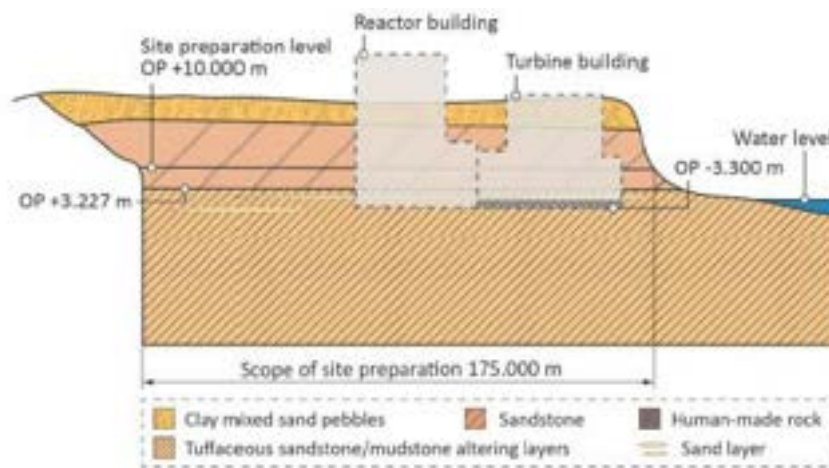


Figure 3-2: Cross section of the Fukushima Daiichi construction site [41]

The plant and building of Units 1-4 were built at an elevation of 10 m, in order to provide an acceptable and stable bedrock foundation. Considerations and security features against tsunami were present in the Establishment Permit (EP), the Japanese equivalent of the safety analysis report. Tsunami events were considered in the tidal water level for plant design, influencing NPP's project and construction. At the beginning the design basis tide level was OP +3.122 m, and referring to this value the Nuclear Power Plant was projected. This initial EP design value was re-evaluated several times during years, whose countermeasures are summarized in the following table.

Year	Tsunami height evaluation	Countermeasure
1996	Establishment permit OP +3.122m (observed height resulting from Chilean tsunami in 1960)	-
2002	Japan Society of Civil Engineers (JSCE) assessment method. OP +5.7m	Raise elevation of pumps Make buildings watertight
2007	Disaster Prevention Plan by Ibaraki Prefecture Government approx. OP 4.7m	Unnecessary
2007	Disaster Prevention Plan by Fukushima Prefecture Government approx. OP 4.7m	Unnecessary
2009	Latest bathymetric and tidal data on the basis of the JSCE assessment method. OP +6.1 m	Raise elevation of pumps

Table 3-2: Fukushima Daiichi Tide Level's evaluation [42]

After the last evaluation in 2009 the NPP could face a tide water level of OP +6.1 m (lower than the 14 m tsunami wave occurred during the accident).

At the end of construction works, the Nuclear Power Plant had six different reactors, two of which, Unit 5 and 6, were separated from the other four. Following a simplified plan of Fukushima Daiichi NPP [42].

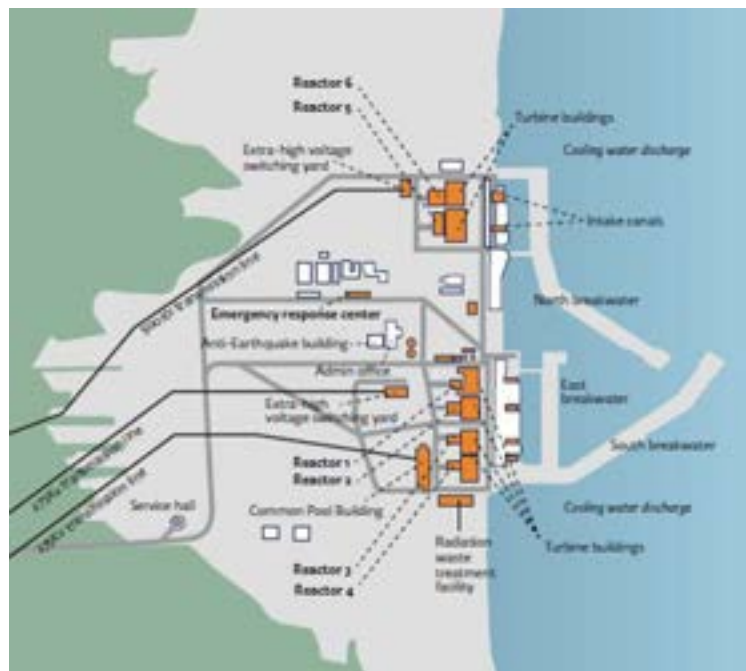


Figure 3-3: Layout of Fukushima Daiichi NPP [42]

3.3 The accident

On March 11 2011, at 14:46, the Great East Japan Earthquake and its consequences caused an extreme situation which carried to the severe nuclear accident at Fukushima Daiichi Nuclear Power Plant, owned by the electric company TEPCO (Tokyo Electric Power Company). When the accident occurred the Unit 1, 2 and 3 were in normal operation, while Units 4 to 6 were stopped, under periodical inspections. After the beginning of the earthquake, SCRAM (emergency shut-down system) was immediately provided in all operating Units. However, the earthquake damaged the electricity

transmission system between the NPP and external facilities, causing the total loss of off-site electricity (Station Black Out-SBO). From this point Emergency Core Cooling Systems started operating through emergency diesel generators, providing heat removal from nuclear reactors. The tsunami generated by the earthquake flooded in the NPP's site, making totally unavailable the seawater pumps, diesel generators and the DC powered facilities, projected, with all the other systems, to face a design basis tide water level of 6.1 m; in particular, Units 1, 2 and 4 lost all power, while Unit 3 only AC power, and later on March 13 lost direct current.

The damages of the tsunami were not only to power supplies, but also to buildings, machineries and equipment installations, causing an extremely difficult access and movement within the plant, precluding the immediate and continuous injection of water through alternative systems.

3.4 Sequence of events at Fukushima Daiichi Unit 1

At 14:47 of 11 March 2011, after the earthquake, acceleration sensors initiated the automatic reactor scram. Emergency Diesel Generators (EDGs) started automatically at 14:48 in response of loss of all off-site power, restoring AC power.

Meanwhile the RPV was isolated through the closing of Main Steam Line Isolation Valves (MSIVs). Consequently, the reactor pressure increased due to the continuous steam generation, until both loops of the isolation condenser system automatically started. The IC is designed to have capacities to remove decay heat by heat exchange at 5 minutes after the scram by its one subsystem. Therefore, under the current operation conditions (longer than 5 minutes after the SCRAM and simultaneous operation of two subsystem), more decay heat is removed than necessary. The operation of both isolation condenser loops lowered the reactor pressure and temperature so rapidly that the operators manually stopped them, in accordance with procedures, in order to prevent thermal stress on the reactor pressure vessel. Afterwards, only one of the loops was used by the operators to control the cooling rate in a range prescribed by the procedures. The reactor pressure was controlled by manually repeating the start-up and shutdown of the IC subsystem-A.

It should be noted that the IC automatic start-up pressure is set lower than the lowest SRV activation pressure, therefore the reactor coolant inventory in the reactor doesn't decrease, as long as the IC is in operation.

Maneuvering actions such as the starting up of the suppression chamber (S/C) in the cooling mode of the containment cooling system (CCS) were also being taken in parallel for cold shutdown of the reactor.

At 15:36 a tsunami wave 14 m high reached the site, flooding the plant and damaging EDGs located in the basements of the Turbine Building (TB) and the Control Building (CB), causing the total loss of AC power at 15:38 Station Blackout-SBO).

All coolant capabilities were lost and all displays of monitoring instruments and various display lamps in the Main Control Room went out due to the station black out caused by tsunami.

Approximately from 16:42 to 17:00 of 11 March 2011, part of the DC power supplies was temporarily recovered.

Concerned about the water inventory left in the IC shell side tank, at 18:25 the operators closed the isolation valve outside the containment on the return pipe. Post-accident surveys of the water in the IC shell side tank revealed that the water level indicator of subsystem-A had been 65% (normal level is 80%) and water in the tank had been sufficient. If the isolation valve had not been closed at 18:25 on March 11 reactor cooling by the IC might have been continued.

Local measurements (in the reactor building) at 20:07 indicated that the reactor was still near the operating pressure of 70 bar (7 MPa), which prevented water injection by alternative methods that would only be possible below 8 bar (0.8 MPa).

Meanwhile, the reactor pressure became low enough to allow alternative water injection. An alternative cooling method, that is, freshwater injection from the fire engines into the Unit 1 reactor to restore core cooling, started at 04:00 on 12 March, about 12.5 hours after the station blackout. Water injection from a single one-tonne truck continued intermittently for approximately 5.5 hours with the

truck having to return to the freshwater tank periodically to be refilled. At the same time, work on establishing a direct line from the tank continued. Later, just over 17.5 hours after the station blackout, continuous freshwater injection into Unit 1 started directly from the tank.

The measurement of Unit 1's containment pressure at 04:19 on 12 March showed that pressure in the containment had decreased since the last measurement (at 02:45) without any operator action and without an established vent path, indicating that some unintentional containment pressure relief had occurred through an unknown path. Furthermore, the radiation levels measured at the main gate shortly afterwards showed an increase. This was also an indication of some uncontrolled radioactive release from the primary containment.

Because of the higher pressure in the reactor system the suppression pool was vented out (as per picture g of Figure 3-4). The venting was started too late and the atmosphere within the containment reached a too high hydrogen gas concentration. This caused at 15:36 on March 12, the explosion of the reactor building allowing radioactive materials to be released into the environment (as per picture h of Figure 3-4). Less than an hour after the explosion, radiation dose along the site boundary had reached 1.015 $\mu\text{Sv/hr}$. Later, on March 12, the operators started to inject seawater into the reactor through the core spray system in order to cool the reactor; boron was then added to the water to control the reactor criticality.

This situation continued over the next several days as site personnel attempted to restore electrical power to the unit (as per picture i of Figure 3-4). Off-site power was restored to Unit 1 on March 20, nine days after the event.

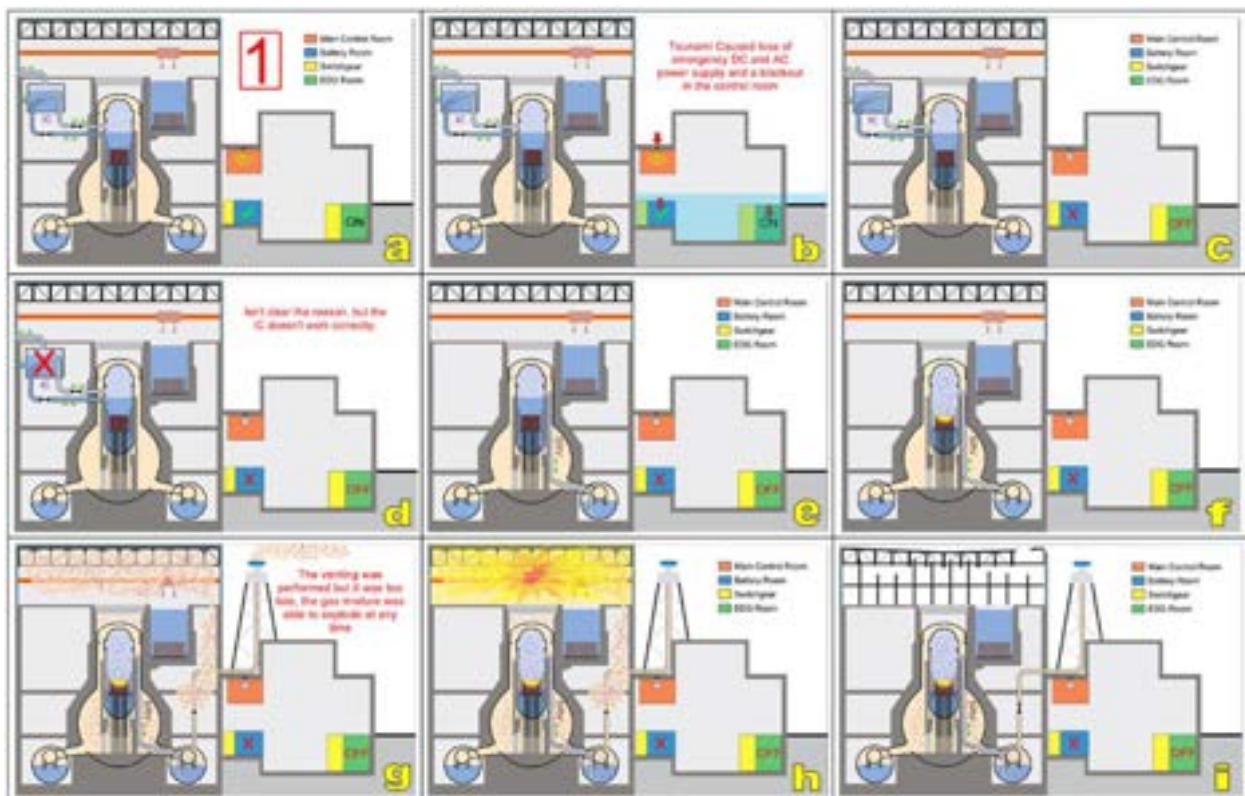


Figure 3-4: Fukushima Daiichi Unit 1 - accidental sequence.

3.5 MELCOR nodalization approach

In order to develop the Fukushima unit 1 MELCOR nodalization [43], following the SANDIA approach reported in the Fukushima Daiichi Accident Study (SAND2012-6173) [44], the nodalization

has been based on the Peach Bottom reactor (different power but similar reactor). The references used to develop the BWR Peach Bottom nodalization are [43] and [45].

Starting from this model, the Fukushima Daiichi Unit 1 input was built with the data reported in [46] and applying a reasonable scaling factor for each component, as pointed out in the following table, if the data are not available.

DATA	UM	Peach Bottom	Fukushima Daiichi 1
BWR type	-	BWR4-MARK1	BWR3-MARK1
Thermal output	MW	3514	1380
R inner vessel	m	3.2	2.4
RPV wall thickness	m	0.164	0.16
RPV lower head thickness	m	0.21	0.2
Height vessel	m	22.2	20
Radius lower head	m	3.188	2.391
Length FAs	m	4.35	4.35
Active length	m	3.66	3.66
NS mass	kg	33866	17730 2
UPPER PLATE mass	kg	24144	12640
SS mass	kg	46000	
CORE PLATE mass	kg	14998	7852 2
CR housing mass	kg	12041	6304 2
CRGTs mass	kg	30000	
CRs mass	kg	9722.205	5090 3
Zircaloy mass	kg	61700	32330
Steel mass	kg	121180	63500
Poison mass	kg	1785	935

Table 3-3: Peach Bottom and Fukushima Daiichi 1 Power Plants specifications

Fuel information were taken from [46], directly reported in the following table.

Reactor core	Length of active fuel		366	mm
	Hydraulic equivalent diameter		3.44	m
	Total amount of uranium		68	t
	Steam flow rate		2400	t/h
	Core temperature		558	K
	Averaged uranium enrichment		STEP2 (8x8): 3.4 9x9: 3.6	wt%
	Burnup (STEP2)-Averaged		39.5	GWD/t
	Burnup (9x9)-Averaged		45.0	GWD/t
Fuel (STEP2)	Diameter of pellet		10.4	mm
	Outer diameter of cladding tube		12.3	mm
	Thickness of cladding (zirconium liner)		0.86(0.1)	mm
	Fuel assembly (STEP2)	Number of FA	68	mm
Number of fuel rod in one FA		8x8 – 4 (water rod)	-	
Material of channel box		Zircaloy-4	-	
Fuel (9x9)	Diameter of pellet		9.4	mm
	Outer diameter of cladding tube		11	mm
	Thickness of cladding (zirconium liner)		0.70(0.1)	mm
	Fuel assembly	Number of FA	332	-
		Number of fuel rod in one FA	9x9 – 9 (water channel)	-
		Material of channel box	Zircaloy-4	-
Control blade	Control material		B4C	-
	Configuration		Cross shape	-
	Number of control blade		97	-
	Pitch		305	mm

Table 3-4: Unit 1, Fuel information [46]

3.6 CORE Model

The core geometry was slightly modified compared to the previous one, in particular the lower plenum nodalization has been modified.

Moreover, following the MELCOR best practices [47] the thickness of the gas gap between fuel pellets and cladding to simulate fuel swelling.

The core axial and radial division is necessary to define different “Core cells” in which the code requires to specify masses of fuel (UO₂), supporting structures (SS), non-supporting structures (NS) and related adjacent core channel and core bypass control volumes. Core cells individuate exclusively volumes related with the lower plenum and inside the core shroud. It is important also to underline that bottom of RPV has been taken as the reference level.

The axial core division can be done by splitting into two different regions, one below the bottom of active fuel (BAF) and one above (top of active fuel, TAF).

The first one (see Table 3-5) has been divided into 13 levels. The transition from spherical to cylindrical vessel shape has been set at +2.76585 m.

The division of the active core region is based on the reference [46], which calculates average axial and radial peaking factors that must be inserted in cells containing fuels. Consequently following the reference, in order to use verified power peaking factors, the active core region has been divided into 10 levels, from the Bottom of active fuel (BAF), deduced by the top of active fuel (+9.1543 [1]) minus the active fuel length (3.66 m), to the top of the core (assumed 0.5 m above TAF). It is important to notice that the last axial level does not contain fuel and consequently its axial peaking factor has been set equal to zero.

Number	Bottom of the Level	Level thickness	Axial peaking factor
1	0.0	0.25908	0
2	0.25908	0.25908	0
3	0.51816	0.25908	0
4	0.77724	0.25908	0
5	1.03632	0.25908	0
6	1.2954	0.49015	0
7	1.78555	0.6145	0
8	2.4	0.36585	0
9	2.76585	0.49015	0
10	3.256	0.49015	0
11	3.74615	0.49015	0
12	4.2363	0.49015	0
13	4.72645	0.49015	0
14	5.2166	0.2777	0
15	5.4943	0.4575	0.705882353
16	5.9518	0.4575	1.103562552
17	6.4093	0.4575	1.088649544
18	6.8668	0.4575	1.082021541
19	7.3243	0.4575	1.08533554
20	7.7818	0.4575	1.08699254
21	8.2393	0.4575	1.06876553
22	8.6968	0.4575	0.77879039
23	9.1543	0.51	0.0

Table 3-5: MELCOR CORE Nodalization

The axial power profile is reported in the following figure.

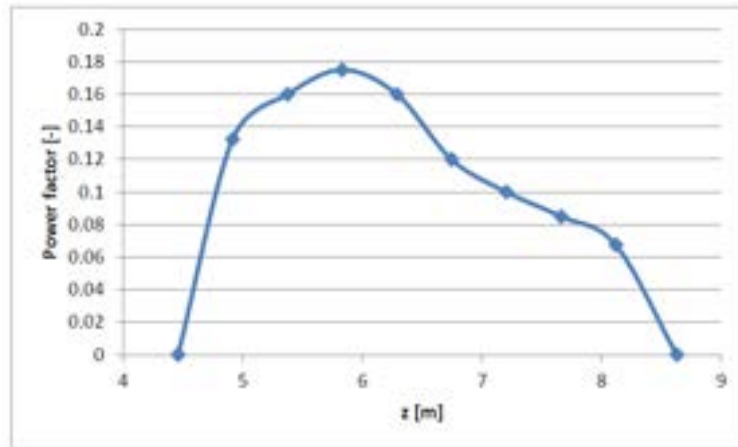


Figure 3-5: Axial relative power factor

The radial division is based on the reference [48], which provides radial peaking factors of core radial sections identified by the number of FAs contained, but without providing any information about dimensions. Consequently, since MELCOR requires radius of the radial rings division, an equivalent diameter of the total area of FAs associated with one peaking factor has been determined. The square lengths of channel boxes are unknown, consequently Peach Bottom channel box dimensions are assumed both for 8x8 and 9x9 FAs.

	Number of FAs	Total Area of FAs	Outer Radius	Peaking Factor
Radial Ring 1	100	2,884775	0.884	0.35
Radial Ring 2	100	6,046625	1.25	0.3
Radial Ring 3	100	9,395525	1.531	0.225
Radial Ring 4	100	12,74443	1.768	0.125
Radial Ring 5	0	0	1.972	0
Radial Ring 6	0	0	2.4	0

Table 3-6: MELCOR Radial Nodalization

An equal distribution of material in the active part has been set.

The 5th radial ring simulates the outer bypass region, the annular region between the active core and the internal surface of the core shroud, while the 6th radial ring simulates the downcomer region. In these two regions there aren't fuel rod, but only refrigerant. So this portion of the core, has a strong discontinuity with respect to the most inner rings, where there are the fuel rods, and other structural materials. The outer radius of the Fukushima reactor (2.4 m) has also been used to estimate the thickness of the cylindrical wall and the hemispherical shell of the vessel (data not reported in the references). Starting from the thickness of the reference reactor, and using the correlation of Mariotte has been estimated, for example, a thickness value of the hemispherical shell of the vessel of 0.165 m instead of 0.22 m. This parameter has a great importance both in terms of heat exchange (as the thickness increases, clearly increases the thermal resistance), both for the influence that would have on a possible resistance to breaking in incidental simulations.

The 3D vision of the model is the one below.

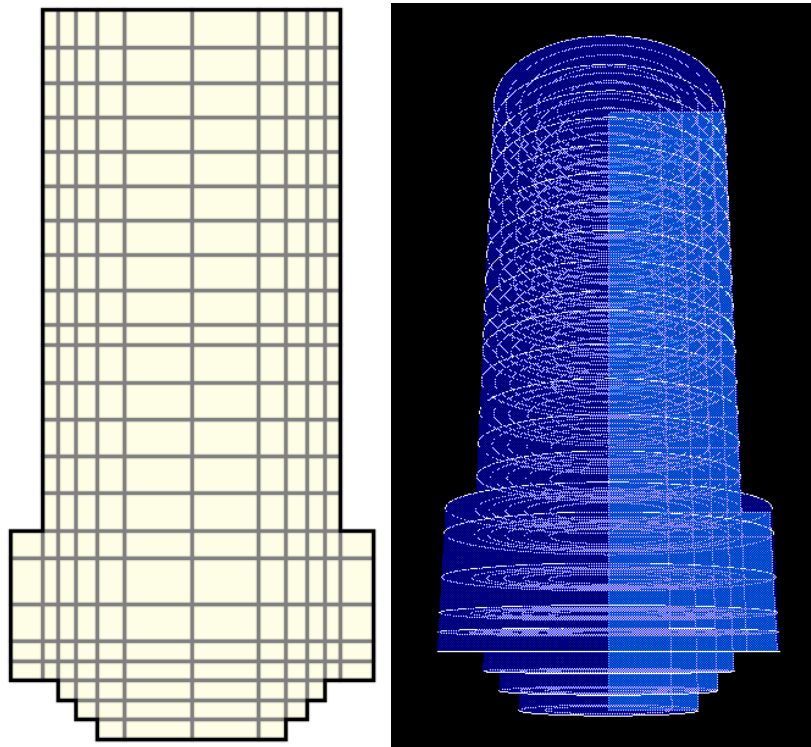


Figure 3-6: Fukushima Unit 1 Axial & Radial Core Nodalization (made with SNAP)

The SS failure model selected is the “Stress Based”, inserting SS number and inner/outer diameter.

Particular attention was dedicated to the modeling of lower head of the core. The detailed nodalization of the lower part of the core, allowed to optimally simulate the spherical head profile behavior. The default heat transfer coefficients are used in the current model, they are order-of-magnitude parameters that should be varied in sensitivity studies to determine their impact on lower head heat transfer and failure. The default failure temperature (1273.15 K) is instead an approximate value for the transition to plastic behavior for steel. This temperature value is then considered with the structure thickness and load to evaluate its failure. However, since BWR penetrations are thinner than LH, the debris ejection preferably occurs through penetrations open areas.

3.7 Thermal hydraulic model

The detailed thermal hydraulic nodalization is reported in [31]. The MELCOR nodalization was designed to have a reasonable computational time and a realistic prediction of the phenomena involved during the transient assuring a reliable and accurate transient simulation.

The control volumes adjacent to core cells have been splitted in order to better simulate local heat transfer process for a wide range of fluid conditions and structure surface temperatures. Core nodalization is always much finer than the CVH nodalization, each hydrodynamic volume contains two core cells. In earlier versions of MELCOR, limitations in several models made it difficult to perform calculations using a fine CVH nodalization with one control volume for each core cell or each small number of core cells. MELCOR 1.8.4 or later versions of the code include improvements in the dT/dz model and incorporates a core flow blockage model (in the FL package). These make such calculations more practical, although some penalty in terms of increased CPU time requirements should still be expected.

The RPV MELCOR nodalization, made by using SNAP and shown in Figure 3-7, comprises the lower plenum, the core, the core bypass, the upper core plenum, the standpipes, the steam separator, the steam dome, the upper downcomer, the middle downcomer, the lower downcomer and the steam

line. The 2 external recirculation loops are modelled separately, while the jet pumps are modeled with two equivalent jet pumps.

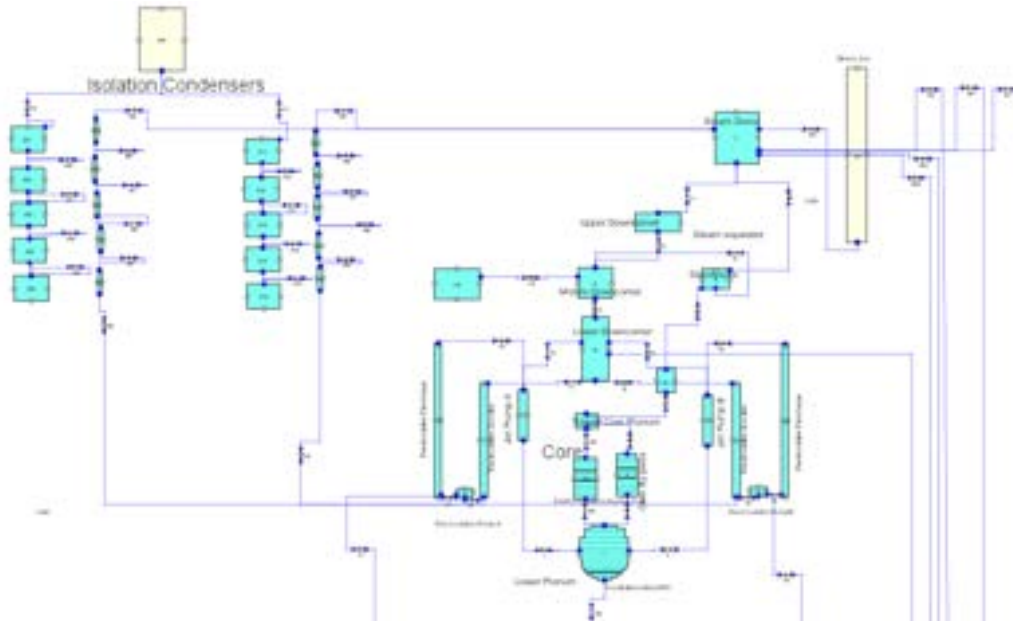


Figure 3-7: Fukushima Unit 1 - Thermal Hydraulic model (made with SNAP)

The Unit 1 of Fukushima NPP have two ICs for removing the decay heat when the main isolation valve (MSIV) is closed and the main condenser is isolated. This passive system were originally designed to prevent over pressure in the RPV without activation of the SRV.

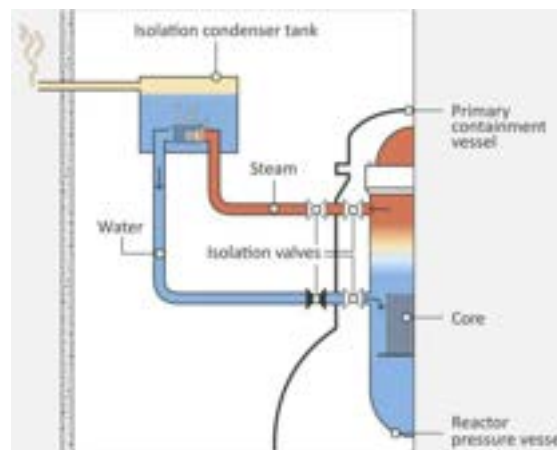


Figure 3-8: Isolation condenser circuit [49]

When the pressure is higher than 7.13 MPa the IC goes in operation and continues more than 15 seconds, while the SRV activation pressure is about 7.27 MPa.

Considering the heat removal capacity of the two ICs after the reactor scram, in order to avoid thermal stress due to cold water inflow in the RPV, the line valves opening is adjusted in order to have a temperature change of the RPV less than 55 °C/hr (operator manual states) [1]. For time a short step problem, a detailed nodalization was implemented with five volumes and five junctions for each side, instead the one volume per side initial nodalization. With this nodalization, a time step of about 0.1 s is possible without any problem.

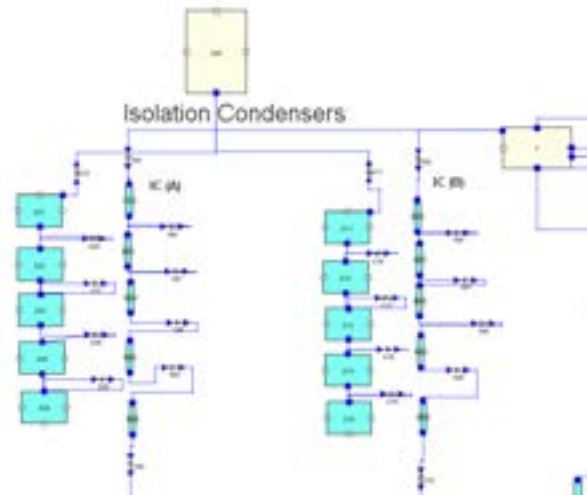


Figure 3-9: Isolation Condenser Model (made with SNAP)

3.8 Containment model

The primary and the secondary containment are modeled with the following nodalization, as represented in Figure 3-10.

The primary containment of the Mark-I design is modeled with of six separate regions:

- Drywell-In-pedestal;
- Drywell-Ex-pedestal;
- Drywell-Top;
- Drywell-Annulus;
- Vent pipes;
- Wetwell.

The secondary containment is modeled with nine separate regions:

- Torus room
- South 135 level
- North 135 level
- South 165 level
- Remain 165 level
- South 195 level
- Remain 195 level
- Refueling Bay
- Turbine Building.

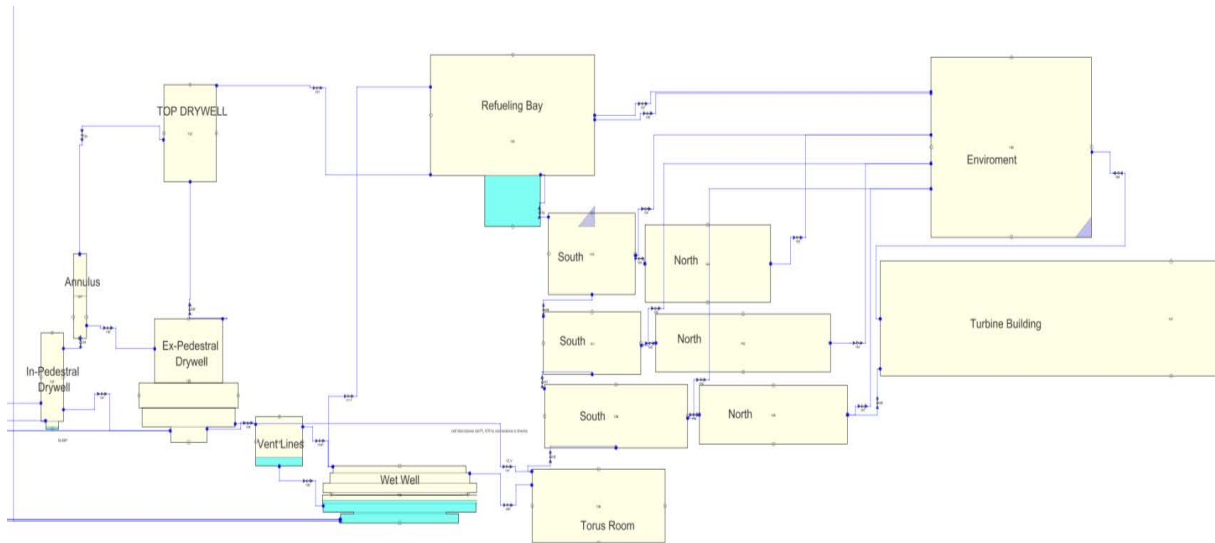


Figure 3-10: Fukushima 1 Containment nodalization (made with SNAP)

The containment passive heat structures are modeled, in particular for the evaluation of the aerosol deposition.

4. RAVEN – MELCOR coupling development

A Python interface has been developed to allow the interaction between RAVEN and MELCOR. The Python interface allows to perturb all the parameters accessible through the MELCOR input deck. In such a way RAVEN is capable of investigating the system response as well as the input space using Monte Carlo, Grid, or Latin Hyper Cube sampling schemes, but its strength is focused toward system feature discovery, such as limit surfaces, separating regions of the input space leading to system failure, using dynamic supervised learning techniques.

The interface has three main functions, interpret the information coming from RAVEN, translate such information in the input of the driven code and manipulate output datafile to create a database. To deal with the first two functions the “GenericCode interface” module (already implemented in RAVEN) has been coupled with a module that runs MELGEN and MELCOR executable. To allow RAVEN storing output data coming from MELCOR, a Python output parser has been developed.

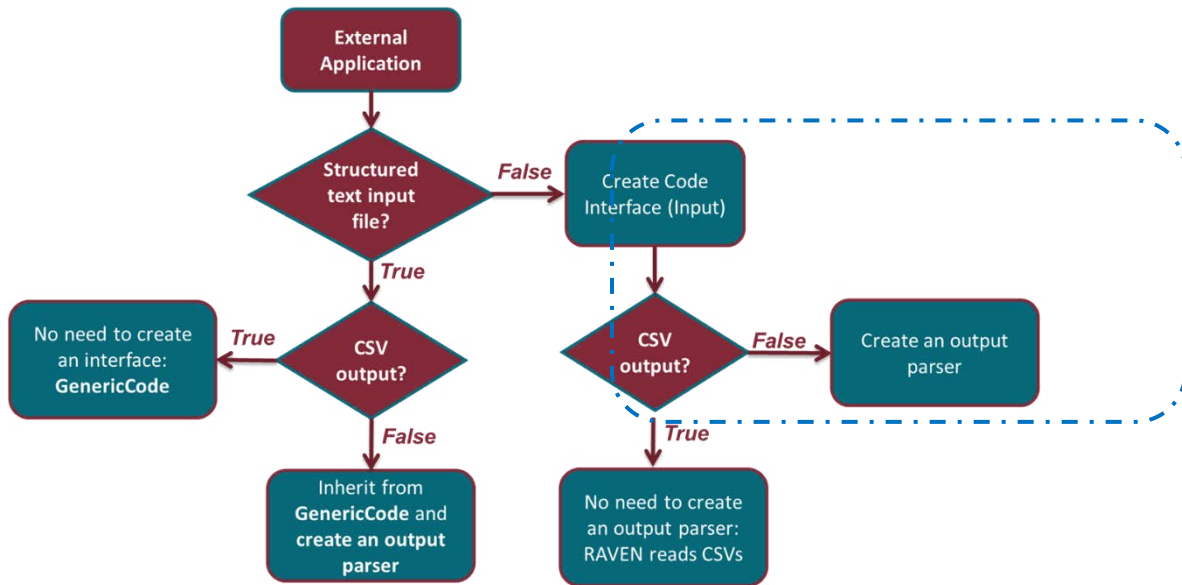


Figure 4-1 – Coupling External Application with RAVEN

The aim of this parser is to convert the PTF binary file generated by MELCOR into a single CSV file. The Python struct module has been used to read the binary plot file allowing MELCOR data handling and conversion in CSV format.

To overcome the handling of large datafiles the interface allows to create a CSV file with only variables required by the users. So is possible to obtain an HDF5 database which comprises variables from all MELCOR packages (CVH, FL, COR, RN etc.) and perform analysis on the specified variables.

Figure below shows the procedural framework used for the uncertainty quantification. A MELCOR input deck is used as template, the chosen parameters are specified as string with special characters. In such a way RAVEN can identify such parameters and replace the string with values sampled from a specified distribution. Consequently N-MELCOR input decks are generated. Once the HDF5 database has been generated statistical analysis of the output sets can be performed.

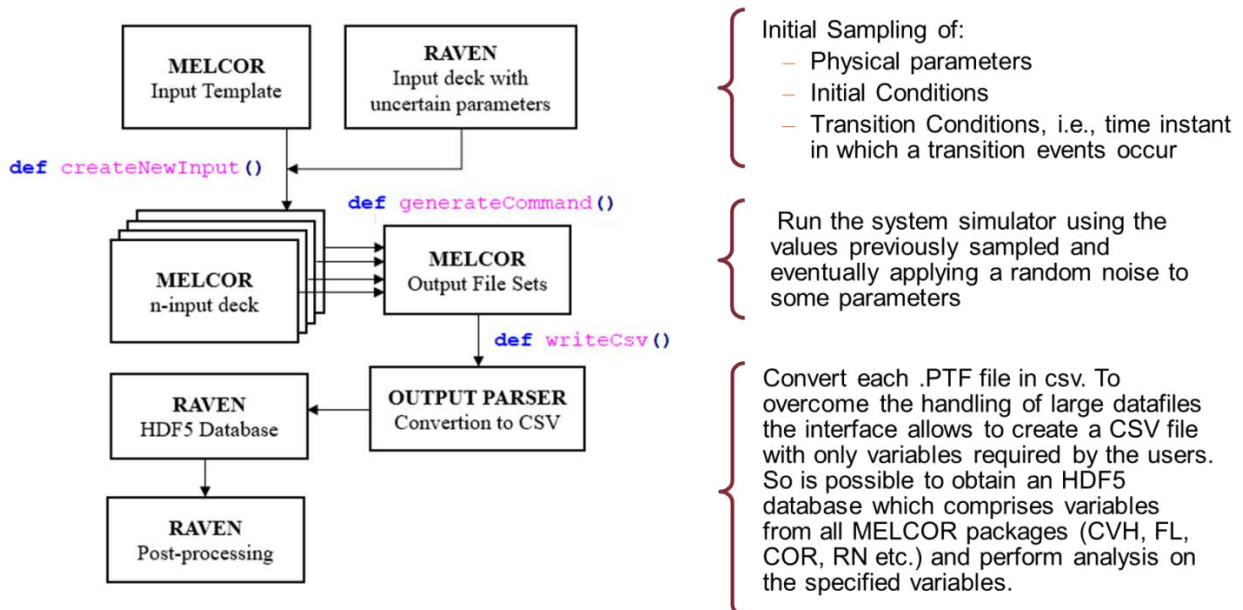


Figure 4-2 - RAVEN-MELCOR flow diagram and description

4.1 Variables and sampling

A set of 7 parameters have been chosen to perform this uncertainty study in order to test the implemented code coupling between RAVEN and MELCOR. The parameters treated in this analysis are the recirculation pump seals leak flow area, plant parameter not available to the code user, and 6 MELCOR modeling parameters chosen in the list of modeling parameters and sensitivity coefficient investigated in [50]. To facilitate uncertainty analyses and sensitivity studies, MELCOR code allows code-users to modify some important parameters model directly through code input as Sensitivity Coefficient (SC). The parameters selected are listed in the Table 4-1.

Once all the variables have been selected a sampling strategy needs to be employed. The sampling strategy is used to perturb the input space in relation to variable distributions. In this analysis the Monte Carlo sampling strategy has been performed setting a limit of 600 calculations. The Monte Carlo method is one of the most-used sampling methodology because doesn't use a structured discretization of the input space but cumulative probability and probability distribution function to compute the different values of the concerned variables.

Variable	Description	RAVEN Distribution
Area_Seal	Recirculation pump seals leak flow area	Triangular Mode: $0.12 E^{-3} [m^2]$ Min: $0.06 E^{-3} [m^2]$ Max: $0.4 E^{-3} [m^2]$
vfall	Velocity of falling debris	Triangular Mode: $0.1 [m/s]$ Min: $0.05 [m/s]$ Max: $1.2 [m/s]$
hdblh	Heat transfer coefficient from debris to lower head	Triangular Mode: $1000 [W/m^2 K]$ Min: $50 [W/m^2 K]$ Max: $1100 [W/m^2 K]$
SC1132(1)	Core Component Failure Parameters - Temperature to which oxidized fuel rods can stand in the absence of unoxidized Zr in the cladding.	Normal Mean: $2700 [K]$ Sigma: $120 [K]$
SC1141(2)	Core Melt Breakthrough Candling Parameters - Maximum melt flow rate per unit width after breakthrough	Triangular Mode: $0.083 [Kg/s]$ Min: $0.01 [Kg/s]$ Max: $1.0 [Kg/s]$
SC1502(2)	Minimum Component Masses - Minimum total mass of component subject to the maximum temperature change criterion for timestep control	Normal Mean: $5 [Kg]$ Sigma: $1.0 [Kg]$
SC1250(1)	Conduction Enhancement for Molten Components - Temperature above which enhancement is employed	Normal Mean: $2800 [K]$ Sigma: $150.0 [K]$

Table 4-1 MELCOR perturbed variables in input-deck

5. RESULTS

Results have been statistically analyzed through the RAVEN BasicStatistic post-processor. A dynamic statistical analysis has been performed setting time as pivot parameter.

To give a better visualization of uncertainty the 0.05, 0.5 and 0.95 quantiles have been selected. Figure 5-1 and Figure 5-2 show quantiles and expected value (0.5 quantile) of predicted drywell and wetwell pressure, respectively. In the early stage of the accident, the gradual increase of pressure is due to steam ejection from recirculation pumps seal leak. In-vessel Hydrogen production process, due to massive Zircalloy oxidation, starts about 2,22 hours after the reactor SCRAM. The Hydrogen reaches the drywell and wetwell containment together with steam through leaks from RPV, causing a pressure peak in the primary containment at about 3,33 hours.

Pressure continues to increase until 0.84 MPa when a break in the drywell is simulated causing steam and non-condensables flowing in the secondary containment buildings. The wetwell venting valves were opened about 23 h 30 min after the earthquake and the containment pressure started to decrease. The venting was modeled by opening a flow path from the top of the wetwell to the environment for this time period, as reported in the TEPCO documents [46]. It is to underline that the results of the calculated data coupled with the related uncertainty band envelope mostly of the TEPCO plant data available related to the drywell and wetwell pressure (Figure 5-1 and Figure 5-2 respectively).

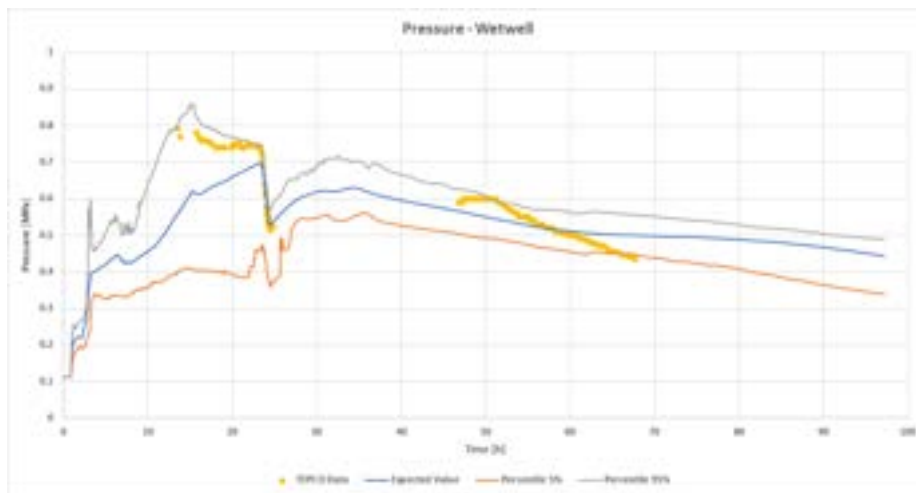


Figure 5-1 - Drywell Pressure predicted by MELCOR

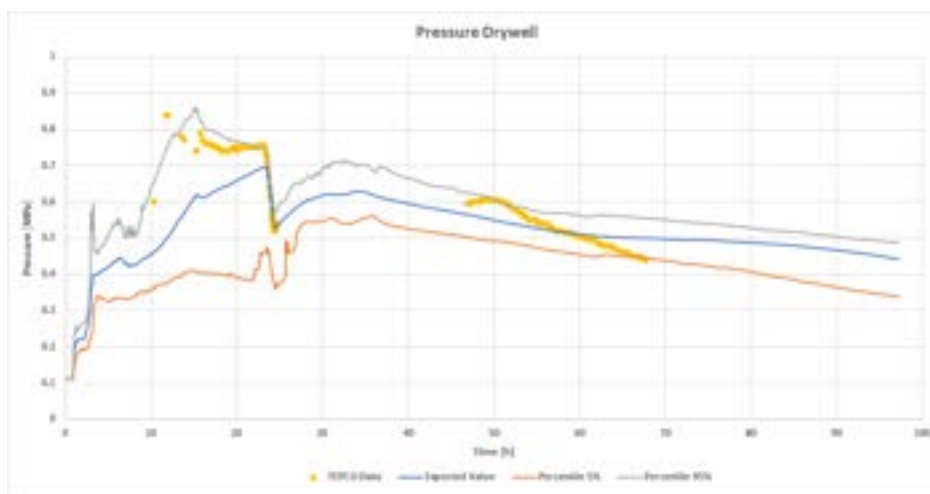


Figure 5-2 - Wetwell pressure predicted by MELCOR

From the analyses of the calculated data, lower head failure and debris ejection from the vessel take place between 7 and 17 hours after the scram. This event influences the wetwell and drywell behavior as reported in Figure 5-1 and Figure 5-2.

To describe the correlation between the variables, the Pearson's coefficient has been used. It is defined between -1 and 1 and measures the strength of the linear relationship between two variables. In Figure 5-3 is possible to see the strong correlation between the recirculation pump seal leak area and the pressure in the drywell containment. The strong positive relationship highlights that as the leak area increases the pressure in containment increases, as expected. Therefore, the lower head failure uncertainty is mainly related to the pump seal leak area uncertainty while the MELCOR modeling parameters and sensitivity coefficient, under investigation in this uncertainty application (Vfall, hdblh, SC1132, SC1141, SC1502, SC1250), have a low ranked influence.



Figure 5-3 - Drywell containment pressure Pearson coefficient

The results of statistical analysis results for pressure in RPV is shown in Figure 5-4. The first notable depressurization is caused by the IC operation in the first hours after the SCRAM. The large pressure drop is predicted between 4 and 5.8 hours and it is associated with gas ejection from RPV.

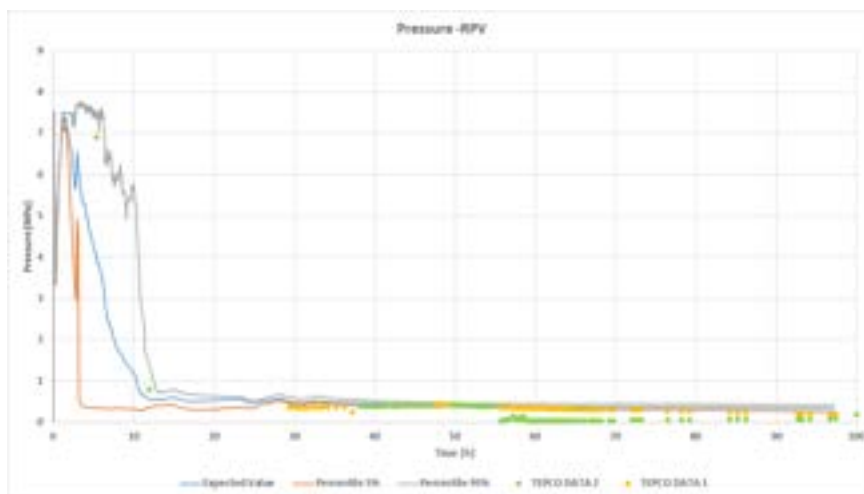


Figure 5-4 - RPV Pressure predicted by MELCOR

Also in this case the Pearson correlation coefficients have been employed to detect the main variables that affect the transient. Figure 5-5 shows that the area of seal leak is strongly correlated with the RPV pressure trend, in particular in the first 6 hours after the reactor SCRAM. However, in this case the trend is strongly negative, in fact an increase in leak area will cause a decrease in RPV pressure, as expected. Therefore, the RPV pressure is mainly related to the pump seal leak area uncertainty while the MELCOR modeling parameters and sensitivity coefficient, under investigation in this uncertainty application (Vfall, hdblh, SC1132, SC1141, SC1502, SC1250), have a low ranked influence. It is to underline that the results of the calculated data coupled with the related uncertainty band contains mostly of TEPCO plant data available related to the RPV pressure (Figure 5-4). A statistical comparison, as in [55], will be carried out in the continuation of this research.

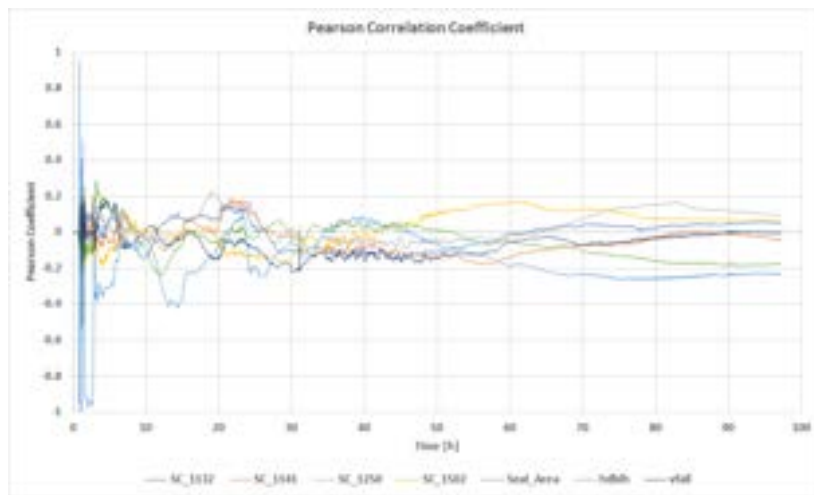


Figure 5-5 - RPV pressure Pearson coefficient

6. UNMITIGATED LOSS OF FEED WATER TRANSIENT ANALYSIS IN A GENERIC PWR THREE LOOPS DESIGN LIKE of 900 MWe

The aim of the present work is the analysis of an unmitigated LFW – Loss of Feed Water sequence in a generic PWR 3-loops 900MWe type reactor. Since the transient is postulated unmitigated and the actions of the operator are assumed to fail, it is a BDBA and evolves as a Severe Accident. The analysis focuses mainly in the characterization of the thermal hydraulic behavior, the in-vessel phenomena, the core degradation and corium behavior in the lower head.

The study of such a complex sequence, involves many fields of study like thermal-hydraulic, source term, core degradation, etc. requiring powerful analytical tools. In this work has been used severe accident code MELCOR 2.2, with user's interface SNAP (Symbolic Nuclear Analysis Package).

This work is a continuation of the PAR 2015 and 2016 activity, ADP ENEA-MiSE. A new and more detailed MELCOR thermal hydraulic nodalization of the PWR has been developed in order to reproduce the accident scenario. Moreover, dealing with the MELCOR best practices, some input parameters have been changed to better represent the plant response to the severe accident.

The reference reactor considered for this analysis is a generic PWR three loops design like of 900 MWe, western type. The main reference plant design parameters are capted from [5][6][7] [51].

6.1 Unmitigated LFW - Loss of feedwater transient

This accident is caused by postulated equipment failures that lead to simultaneous unavailability of the Main Feed Water System (MFWS) and the Emergency Feed Water System (EFWS). Since the transient is postulated unmitigated and the actions of the operator are assumed to fail, it is a BDBA that can evolve as a severe accident if significant core degradation takes place.

Unmitigated loss-of-feed water transient is a high-pressure scenario with decreased capacity of heat removal from the SGs with both primary and secondary circuits still intact.

The SGs will be suddenly drying, and the reactor will scram due to the low SGs level. The RCS heats up and its pressure rises to the set pressure of the PRZ safety valves. The RCS empties and remains at high pressure until core uncover and melt occur. Core melt can thus occur while the RCS is pressurized. This poses a short-term threat for containment of the radioactivity released during core melt (ejection of corium into the containment during pressure-induced rupture of the vessel, resulting in “direct heating” of the containment, SG tube breaks).

Since LPI and HPI are not available, the passive discharge of the accumulators is the only inflow water entering the core to compensate the loss of water coolant. The containment sprays are available.

7. MELCOR nodalization

In the framework of severe accident research activity developed by ENEA, funded by the Italian Ministry of Economic Development (Accordo di Programma ENEA-MiSE), a MELCOR nodalization of a generic PWR of 900 MWe [68], [69] has been developed, by using SNAP, based on public information's available from the scientific technical literature [68], [69], [70], [71], [72], [73].

This work is an extension of the PAR 2015 and 2016 activity, ADP ENEA-MiSE: a more detailed MELCOR thermal hydraulic nodalization of the PWR have been developed in order to reproduce the accident scenario. Moreover, dealing with the MELCOR best practices, some input parameters have been changed to better represent the plant response to the severe accident, following the Best Practice Guidelines given in SOARCA [74].

In particular, this new control volume hydrodynamic nodalization, compared to previous one on which is based, has following mains differences:

- Single CVH core volume splitted in five concentric ring and five axial level;
- Single CVH upper plenum splitted in five concentric ring and two axial level;
- Single CVH hot leg splitted in upper and lower halves and in mid length;

- Single CVH SG ascending side is splitted in 3 parts SG inner plenum and 2 halves CVHs U-tube ascending side;
- Single CVH SG descending side is splitted in SG outlet plenum and 2 halves CVHs U-tube descending side;
- A CVH is added to pressurizer SRVs to check valves temperature;

These changes are described below. Together with, also flow paths and heat structures have been updated to better reproduce accident scenario and control functions are added to better simulate plant control system, thermal hydraulic behavior, accident scenario and phenomena.

The MELCOR model consist of 114 control volumes, 217 flow paths and 131 heat structures.

7.1 RPV – Reactor Pressure Vessel

MELCOR model include representation of RPV component as core, lower plenum, upper plenum, upper head, downcomer, bypass region. They are all build up in CVH - Control Volume Hydrodynamics package, responsible for modelling the thermal-hydraulic behavior of liquid water, water vapor, and gases in MELCOR, giving boundary conditions to all other packages.

Core and lower plenum structures, including their thermal response and relocation during degradation, melting, slumping, and debris formation, are modelled in COR package.

The bottom of RPV has been taken as the reference level.

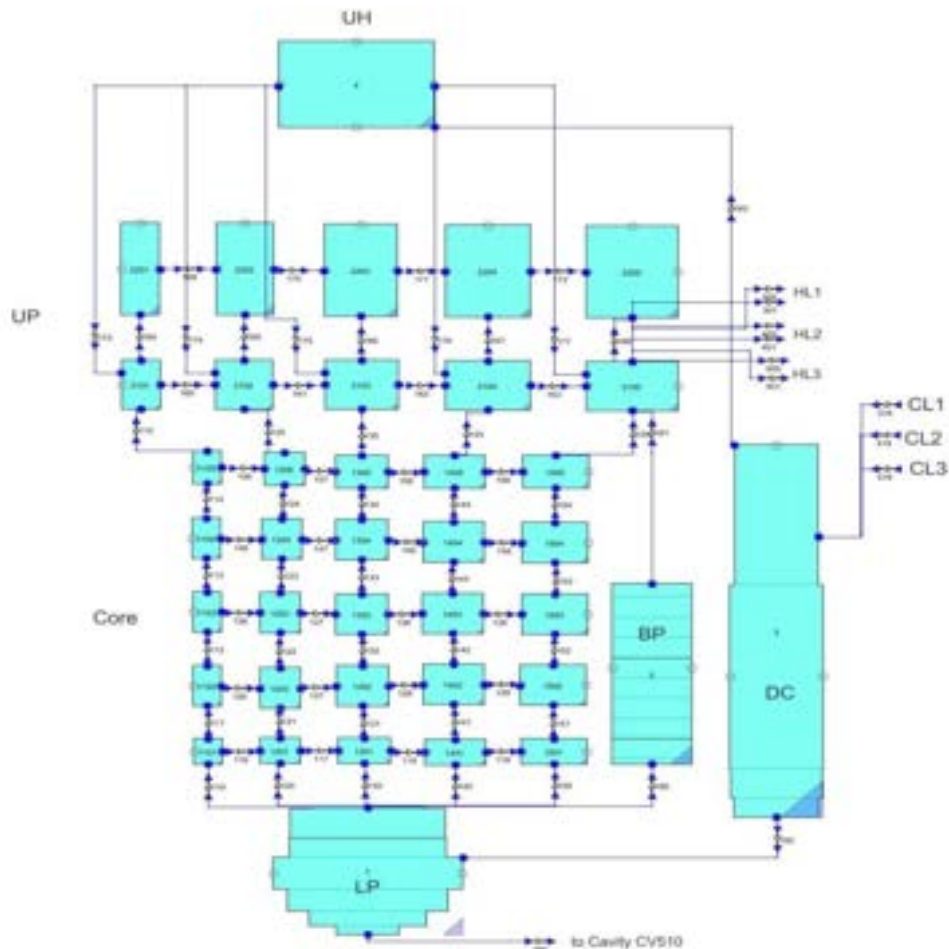


Figure 7-1 - RPV nodalization visualization made by using SNAP

7.1.1 Core

Core is represented by five concentric rings of hydrodynamic control volumes and core structures (Figure 7-3, Figure 7-4 - Core CVH nodalization

). Each ring is divided into five vertical hydrodynamic control volumes and ten core axial levels, coupled two by two with one CVH control volume. Each of the five core rings and ten core levels models the response and relative power of the included fuel assemblies, giving a more accurate and continuous representation of the local fuel collapses and subsequent degradation.

The sixth outer region, models the bypass region between the core shroud around the fuel and the core barrel.

A matrix of axial and radial flow paths simulates two-dimensional flow patterns in the core region during natural circulation. In each flow path in the core and lower plenum nodalization the flow blockage model is activated and then changes in flow resistance during core degradation.

7.1.1.1 Power factors

The 157 fuel assemblies are divided in COR package into 5 radial ring regions. Axial core region included in COR package goes from axial level 8 to 17. Active region is of 3.66m and goes from axial level 9 to 16, with outermost parts modelled as non-active regions of fuel elements [69].

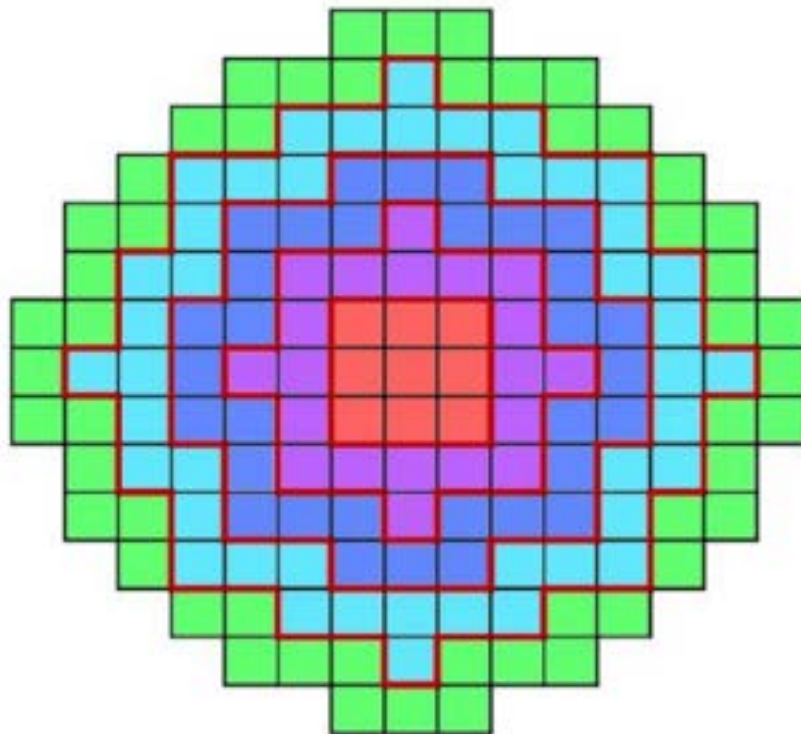


Figure 7-2 – COR package radial ring regions

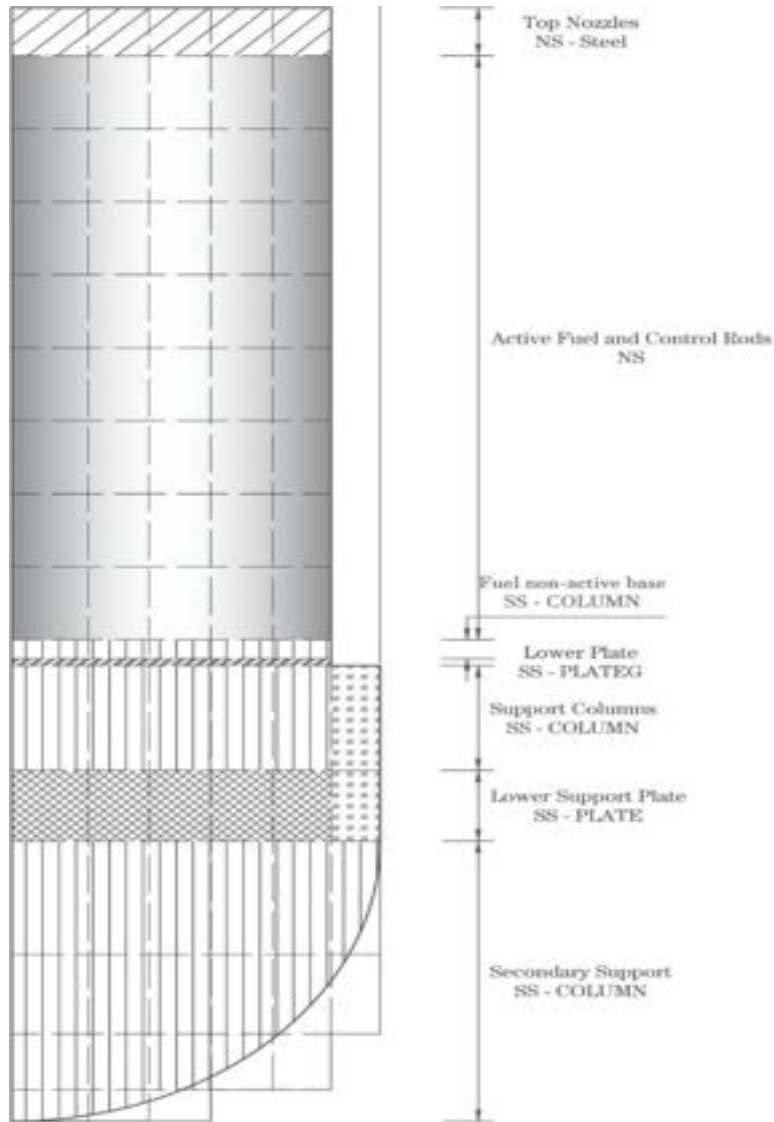


Figure 7-3 - Core COR package nodalization

7.1.2 Upper Plenum

Upper plenum has same 5-ring nodalization scheme of core's CVH extended upward, divided into two axial levels with radial flow between each ring. Axial levels are divided at the hot legs symmetry axis height to separate natural circulation flow outward to the hot legs versus the returning flow (Figure 7-5).

Gas or water can flow through the control rod guide tubes between the upper plenum and the upper head. The leakage pathways between the downcomer and the upper plenum and from the downcomer to the upper head are also represented.

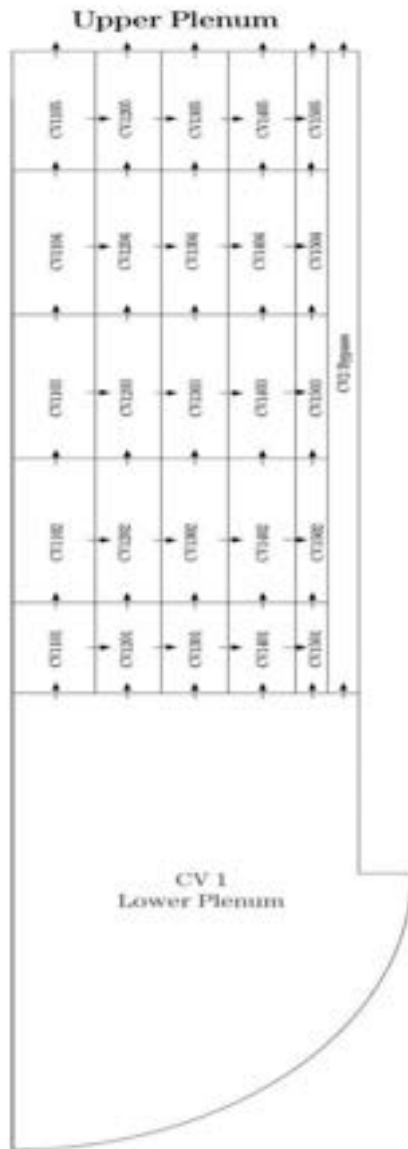


Figure 7-4 - Core CVH nodalization

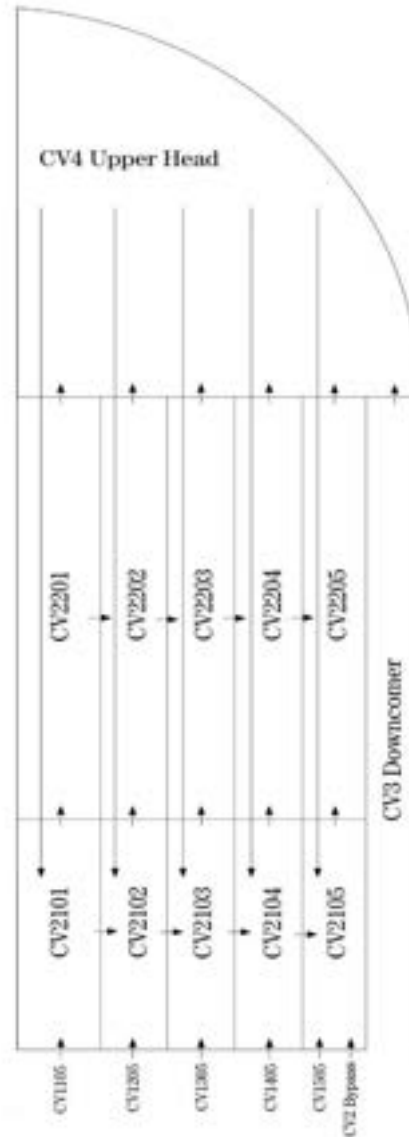


Figure 7-5 - Upper Plenum, Upper Head nodalization

7.2 Hot Legs, Pressurizer, Steam Generator, Cold Leg

The Hot Legs (HL) and SGs need to be modeled in detail (Figure 7-6) because they must simulate conditions ranging from normal operating conditions, single-phase liquid and two-phase accident conditions, and single-phase gas natural circulation conditions, as discussed later. The related HS are made of Carbon Steel, with an internal liner of Stainless Steel.

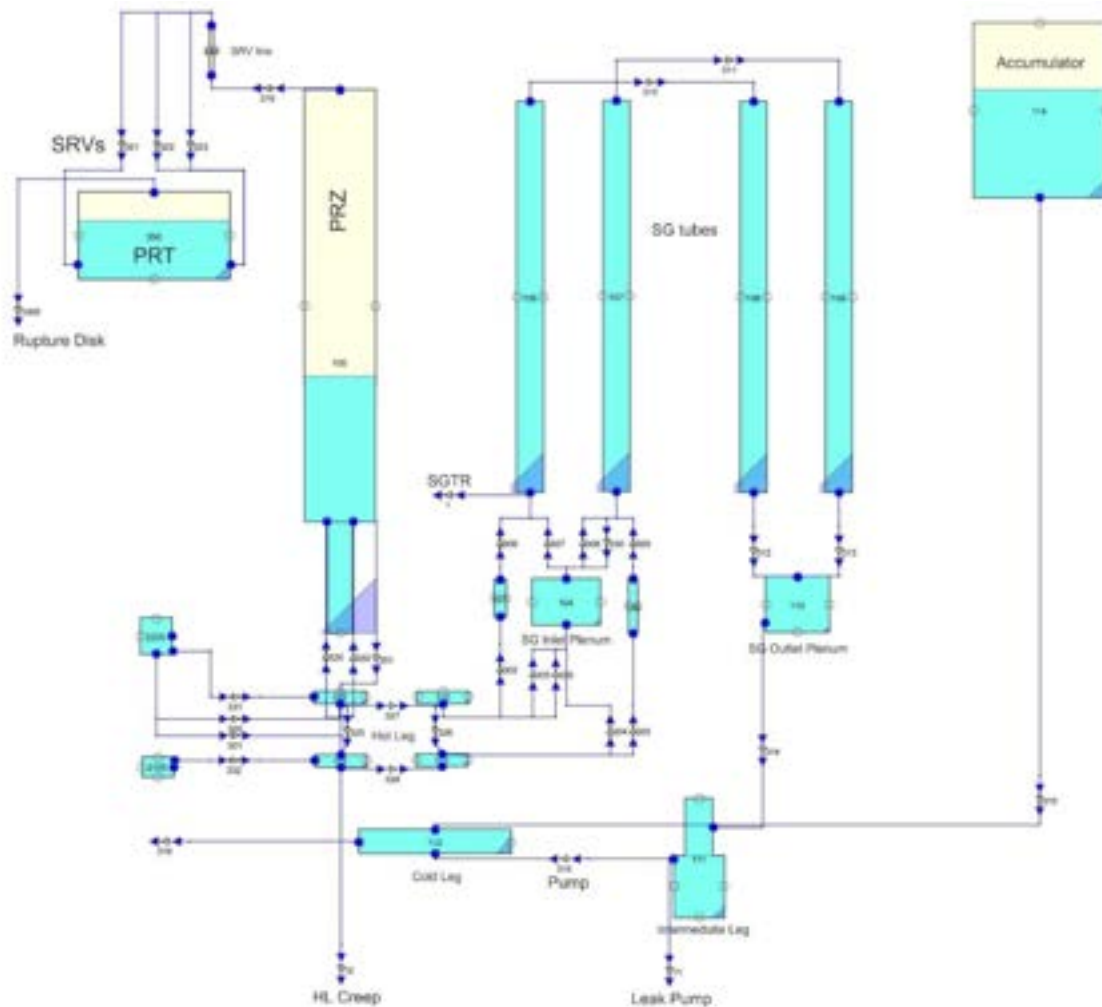


Figure 7-6 - Loop 1 nodalization visualization made by using SNAP

HLs are split in upper and lower halves and in mid length to permit counter-current natural circulation flows. Possible HL creep failure is calculated by Larson-Miller lifetime damage model, opening flow path connection with containment.

PRZ is connected with loop 1 HL with a side-mounted surge line. PRZ has 3 SRV – Safety Relief Valves connected with PRT – Pressurized Relief Tank spargers, connected in turn by a rupture disk to containment atmosphere.

Optional MELCOR pool scrubbing logic (SPARC) was enabled in the flow path representing spargers, removing radionuclide aerosols and vapors from a gas as it flows through a pool of water.

SG tube bundles are split in ascending and descending U-tube side, each one split in two halves with same purpose of HL split.

SG inlet plenum to outlet plenum data is taken from [28]. Flow paths between ascending and descending CVHs are tuned to match the results obtained in [77] in natural circulation condition.

SGTR – SG Tube Rupture is calculated by Larson-Miller lifetime damage model, opening flow path connection with SG riser, with a 100% SG tube flow area of $3.07 \cdot 10^{-4} \text{m}^2$.

7.3 Secondary System

MELCOR model of secondary system include 3 loops Feed Water Tank (FWT), feed water line, SG riser/cavity, SG downcomer, SG steam line, SG steam header (Figure 7-7).

Boundary conditions are used to represent the turbine pressure and feedwater flow to allow direct calculation of the nominal, full-power steady state operating conditions.

SG Secondary side is modelled with two CVH representing riser and downcomer, the former thermally coupled with U-tube primary side. Water level at 100% power is set at about 41.5% of SG narrow range [75]. Each steam line has 3 SRVs, connecting environment, set to open at proper pressure.

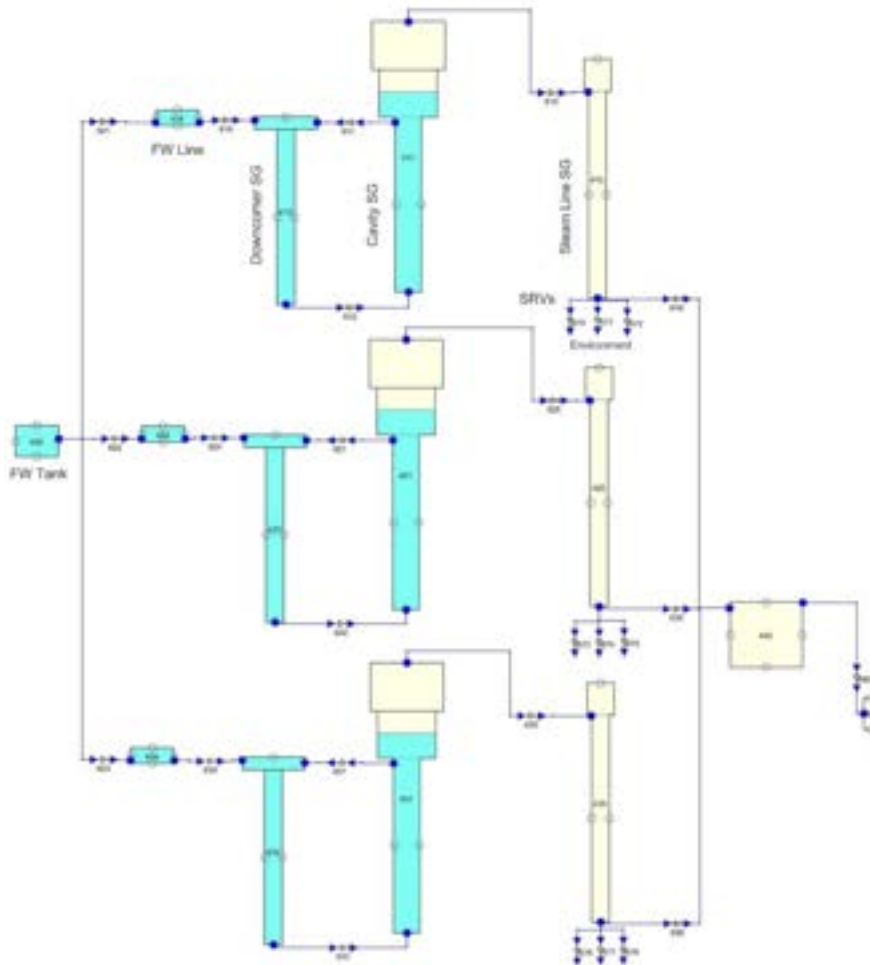


Figure 7-7 - Secondary System nodalization

7.4 Containment

The containment is divided into a total of ten control volumes, representing the basement sump, two reactor cavity zones, reactor pit, the loops cubicle, the PRZ cubicle, the PRZ relief tank cubicle, the annular zone, the pool zone and the upper dome.

The walls, floors and ceilings in the containment are modelled as heat conducting structures. The structures will absorb and release heat during the course of an accident. Fission products can deposit on any structures. However, gravitational settling only occurs on horizontal structures.

The major walls include the outer walls of the containment that are shared with the environment with an internal carbon steel liner and air annular space, and containment basement.

The reactor cavity and pit are represented using special physics models for core-concrete interactions (CCI). The concrete floor is a Standard concrete CORCON generic, with an ablation temperature of 1550 K and an initial temperature of 390 K. The reactor cavity is represented with a flat-bottom cylindrical. If reactor cavity fail radially, reactor pit will receive overflowing material.

There is a Refueling Water Storage Tank (RWST) filled with a water volume at 350 K, used by CSS - Containment Spray System as water reservoir.

7.5 Natural Circulation Flows

MELCOR is a lumped parameter system analysis codes, able to predict the thermal-hydraulic behavior of the entire RCS over extended periods of time. In order to simulate potential three-dimensional fluid phenomena along the severe accident progression, considering the expected flow conditions determined from experimental correlations and/or suitable multidimensional code predictions, the following nodalization approaches have been used:

- In the reactor core, the crossflow junctions between rings, provide an approximation of the multidimensional flow;
- To model HL countercurrent single-phase flow, the HLs were divided into top and bottom halves: the top half provided the flow path for hot vapor to move from the reactor vessel to the SGs, while the cooler vapor flowed from the SGs back to the reactor vessel through the bottom half of the HL pipe. Because the HL flows are artificially separated, some of the interactions between the hot and cool vapor like mixing and heat transfer are not modelled but are taken into account with system code modelling parameters, discussed below. This also separates pipe heat structures, so that large temperature gradients can occur between the top and bottom of the pipe, with no heat transfer between them;
- The SG tubes were also separated into two groups, one to allow the hot vapor to flow from the inlet plenum toward the outlet plenum, while the remainder provided the path for flow from the outlet plenum to return to the inlet plenum.
- The SG inlet plenum modelling was also changed from a single control volume to simulate the mixing that occurs. Most of the plenum volume was contained in a mixing volume that allowed the hot vapor from the HLs and the cool vapor from the SG tubes to mix. While the mixing volume provided most of the flow to the hot SG tubes and to the bottom of the HL, there were also smaller volumes used to allow hot vapor from the top of the HL to pass directly to the hot flowing SG tubes, and to allow cool vapor returning to the inlet plenum from the SG tubes to flow directly to the bottom of the HL.

7.5.1 HL Flow Rates and a Discharge Coefficient

In general, the prediction of the natural circulation flow rates in the HL and SG tube bundle is fundamental to characterize system code transient prediction. So, the mass flow in the HL and the SG tube bundle must be accurately predicted by the code.

The proposed approach establishes the HL flow rates in a system code model using a discharge coefficient C_d [82]. This method is adapted from a paper by Leach and Thompson [83] that uses scaling arguments to establish that the flow rate is proportional to a densimetric Froude number¹.

For application to the system code model for a HL from Figure 7-8, the following assumptions are made i.e. for loop 1 (same assumptions are made for others loops) [77]:

¹ Densimetric Froude number is the ratio of inertial to buoyancy forces: $Fr = v/\sqrt{g\Delta\rho/\bar{\rho}}$

- the hot density ρ_h , is obtained from cell 2205 that feeds the upper HL. The flow conditions entering the HL from cell 2205 are assumed to represent the average conditions in the upper plenum. Similarly, the properties of the flow from the inlet plenum to the lower HL are used to determine the cold density ρ_c . A mass-weighted cold density is obtained from the flows entering the lower HL from inlet plenum volumes 104 and 105. The density difference and average density are computed from these values.
- the full HL diameter is used in the correlation (not the smaller diameter of the individual upper and lower pipes).
- the volumetric flow rate, q , is determined by dividing the mass flow rate by the average density. A net mass flow from the vessel to the SG is used, and this value is obtained at the junction between volumes 102 and 122, FL 327.

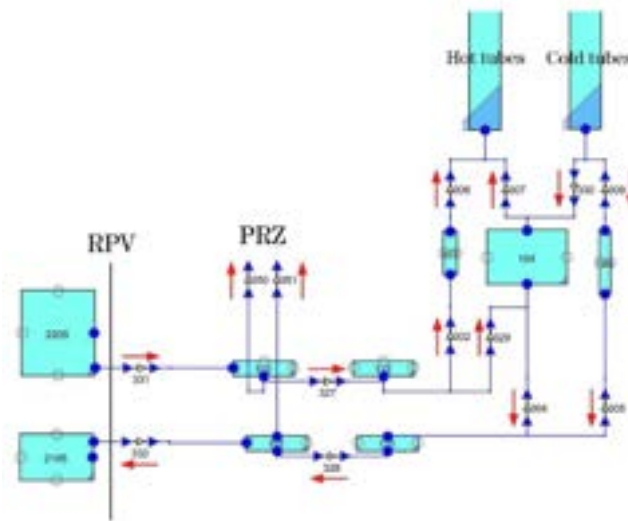


Figure 7-8 - Active nodalization of Loop 1 HL and SG inlet plenum during natural circulation conditions

Flow-loss coefficients can be adjusted to ensure q equation is satisfied.

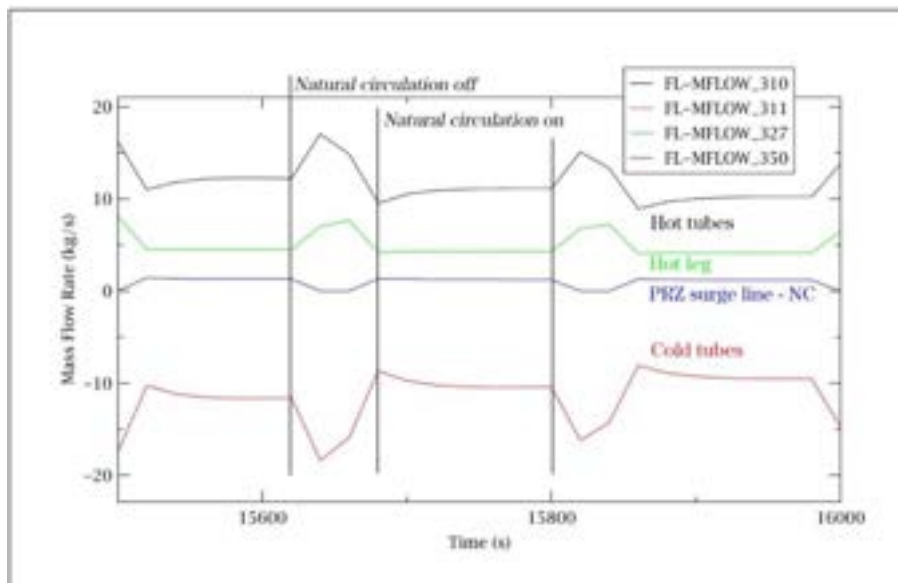


Figure 7-9 - NC mass flow rate


 Ricerca Sistema Elettrico	Sigla di identificazione	Rev.	Distrib.	Pag.	di
	ADPFISS-LP1-122	0	L	39	56

Figure 7-9 shows the results of mass flow rates during natural circulation phase in the accident transient progression.

7.6 Core Degradation Modelling

The core melt progression modelling options have been set to be consistent with current best-practices guidelines [74]. The fuel rod cladding ruptures at relatively low temperature (i.e., modelled at 800°C in MELCOR) and 55 releases fission gases from the fuel-cladding gap. As the fuel temperature increases, an oxide shell forms on the outer surface of the fuel cladding. Since the oxide shell has a higher melting temperature than the unoxidized Zircaloy inside of the fuel rod, the Zircaloy on the interior of the cladding will become molten once the temperature rises above the melting temperature. The molten Zircaloy flows through cracks in the cladding and relocates downward, which leaves a thin Zircaloy oxide shell holding the fuel pellets. Following the relocation of the molten Zircaloy, the local power due to Zircaloy oxidation ceases. The subsequent local thermal response is governed by decay heat and any relocation of molten material from above.

The calculated failure rod collapse mechanisms include:

- failure collapse due to melting the oxidized shell;
- failure collapse of the supporting structure;
- time-at-temperature model that calculates the failure collapse of the oxidized Zircaloy shell holding the fuel rods;

7.6.1 Core blockage model

A “flow blockage” model was added to account for redistribution of flow through a reactor core as a result of changed flow resistance, reduction of area, or even a total blocking of flow, within various parts of the core when intact geometry is lost and a debris bed or pool forms.

The distinction between particulate debris above and below the blockage is maintained by adding the former to the “intact” (as distinct from “conglomerate”) portion of the molten pool component [87]. Therefore, the relocating particulate debris is thermally equilibrated with the existing molten pool.

7.7 Vessel Lower Head Failure and Debris Ejection

MELCOR models heat transfer between lower head, molten pools, debris and penetrations, with a two-dimensional radial and azimuthal conduction through the vessel wall [74].

Lower Head Failure – LHF has modelled only with gross creep rupture, measured to be the most likely in the SNL LHF tests [90]. The lower head creep rupture model uses the code’s default settings. A Larson-Miller parameter is calculated using a one-dimensional temperature profile through the lower head. A cumulative strain is calculated using a lifetime rule and failure occurs with an 18% strain. Penetration failure is not modelled as a mechanism for vessel failure, setting a failure temperature of the penetrations (TPFAIL) of 9999 K [74].

Upon vessel failure, molten and solid debris are assumed to discharge simultaneously.

7.8 Reactor SCRAM

Once LFW occur, SGs water levels go down. When SGs level decreases to 25% of SG narrow range, reactor SCRAM takes place and also the turbine is isolated via MSVI valves. Below (Figure 7-10 and Figure 7-11) reactor power versus time and control function SCRAM logic are shown. LFW takes place at 0s, SG level fall below 25% at 22 s, so reactor SCRAM will be at the same time.

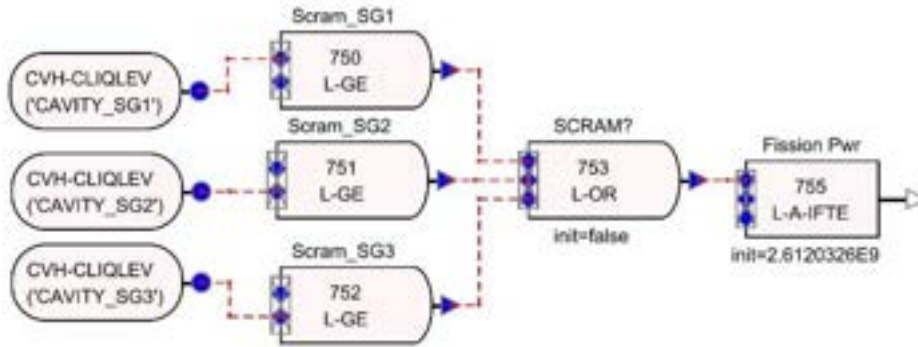


Figure 7-10 - Reactor power / SCRAM control function

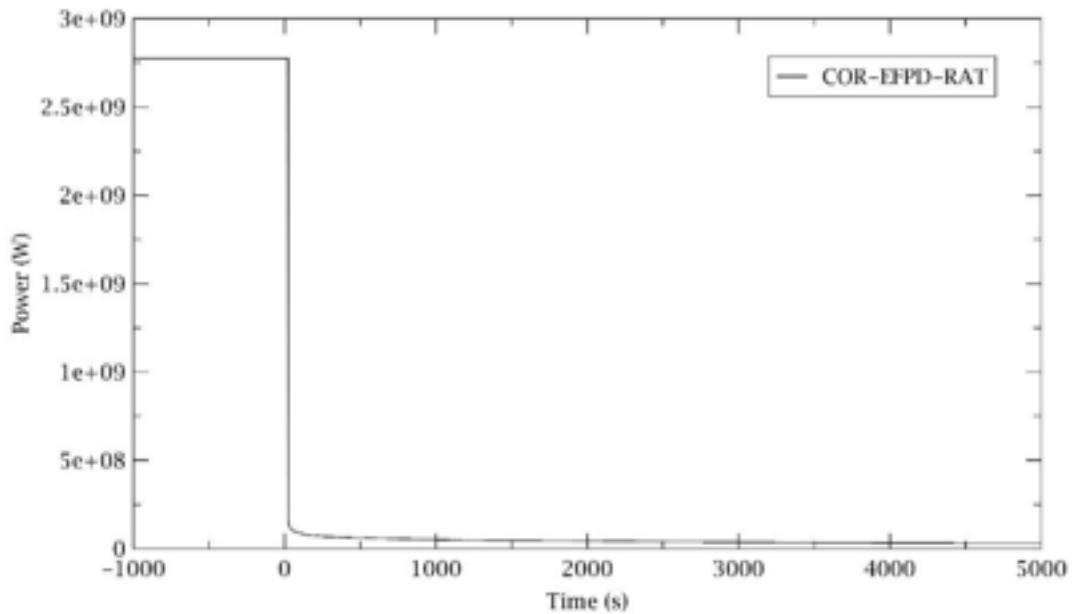


Figure 7-11 - Reactor power vs time

8. Steady State Results

Initial conditions of transient are given by a steady state MELCOR calculation, performed for 3000s. After a stabilization period, about 1000s, variation versus time of all parameters are negligible. Values are in general agreements with reference operational status.

Based on level 1 PSA deterministic analysis, an assessment is made for steady state qualification with following reference value[7] [51][52][69] (Table 8-1):

	Reference value	MELCOR	Acceptable error	Actual error
Reactor thermal power (MWth)	2775	2775	0.50%	0.00%
Primary coolant flowrate (Kg/s)	13734	13700	1.00%	0.25%
HL Pressure (bar)	155.1	155.1	0.10%	0.00%
Core Inlet Temperature (K)	564.85	563.8	1.00%	0.19%
Core Outlet Temperature (K)	601.75	598.3	1.00%	0.57%
Feedwater temperature (K)	499.85	499.85	1.00%	0.00%
Steam pressure turbine inlet (bar)	57.8	57.8	1.00%	0.55%
Steam temp turbine inlet (K)	543	546	1.00%	0.86%
Steam flowrate turbine inlet (Kg/s)	1517	1530	0.10%	0.00%
Heat-transfer area in a SG (m ²)	4746	4746	2.00%	0.00%
Containment free volume (m ³)	50400	50400	0.50%	0.00%

Table 8-1 - Steady State qualification

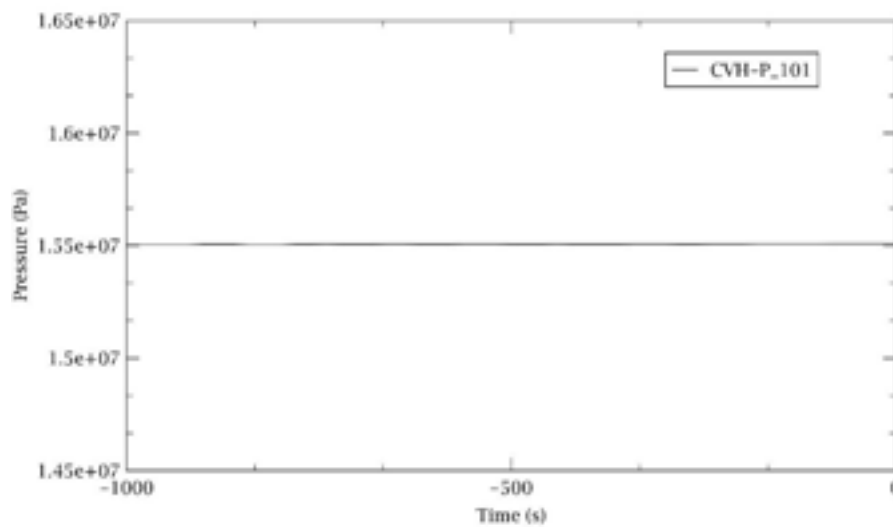


Figure 8-1 – HL Pressure

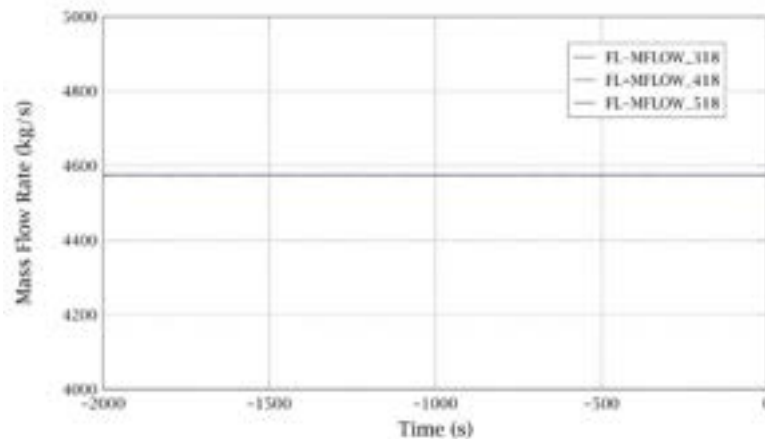


Figure 8-2 – Cold Legs mass flow rate

9. RESULTS

Unmitigated LFW is assumed to take place at reactor full power. This scenario is implemented in MELCOR using the following initiator events and limiting conditions:

- Time = 0 s Main feed water loss
- Time = 0 s Auxiliary feed water unavailable
- HPIS and LPIS, low and high-pressure safety injection unavailable during the whole transient

SCRAM take place when SG liquid level falls below 25% narrow range. MSIV – Mean Steam Isolation Valve close at SCRAM. RCPs tripped when low secondary side SG liquid minimum level is reached. The main event description table is reported below.

Event Description	Time	
	Seconds	hh:mm
Initiating event LFW – Loss of Feedwater	0	0s
Reactor SCRAM MSVI close	22	22s
First SGs SRV opening	30	30s
RCPs trip	3154	00:52
SG dryout	3320	00:55
PRZ SRV opens	3696	01:01
PRZ relief tank rupture disk opens	5170	01:26
Start of fuel rods uncover	5584	01:33
Start of containment sprays	6902	01:55
Start of fuel heatup	7580	02:06
First fission product gap releases	10642	02:57
Start of candling (ring 1)	12683	03:31
Start of particulate debris formation (ring 1)	12765	03:32
Start of failure of supporting structures	13666	03:47
Start of natural circulation in loop n1	15160	04:12
Creep rupture failure of the loop n1 HL	16350	04:32
Containment at design pressure	16360	04:32
Accumulators start discharging	16360	04:32
Isolation of accumulators	16430	04:33
Vessel lower head failure by creep rupture	31262	08:41
End of calculation	36600	10:10

Table 9-1 Chronological event time history

After a MELCOR steady state analysis, in agreement with the full power operation values of the reference reactor, the LFW event takes place at 0s (SOT – Start of transient).

When the level decreases to less than 25% in the SGs, the reactor scram takes place at 22s and also the turbine is isolated. At 3154 s, RCPs trip because of low secondary side SG liquid mass.

The loss of the main feed water, with the auxiliary feed water unavailable, lead to a dry-out in the SGs at 3320s. The secondary system loses gradually the capability to remove the heat and, after more than one hour after SOT, at 3696s (during this time the reactor is into a subcritical condition), the primary circuit reaches the maximum allowable pressure and the PRZ SRVs open. The pressure in both systems, as shown in Figure 9-1, is anchored between the on/off range of the respective SRVs.

Then the PRT failure takes place at 5170s after the SOT; The core collapsed level falls below the top of active core at 5584s and fuel starts to heat up at 7580s.

Core degradation phases start at 10642s with fission product gap releases, then at 12683s starts candling and debris formation at 12765s.

The natural circulation phenomena are important because the steam created in the core circulates along all the RCS transferring its energy and causing thermal stress and creep rupture in the RCS structures: in particular the MELCOR code, by using the Larson-Miller model, predicts loop 1 HL creep at 16350s after the SOT. Figure 9-2 shows the creep rupture index for the HL. The HL temperature profile is showed in the Figure 9-4. The HL creep mass flow rate is reported in Figure 9-5.

So, when the pressure is lower than 43 bar, the accumulators start to discharge water. In this simulation, the vessel fail is predicted at 31262 s with mass ejected to vessel breach (Figure 9-6), after the depressurization of the primary circuit.

At the rupture of the vessel, the fission products are released, first in the containment, and after, through the small leakage, part of those are released in the atmosphere.

Containment pressure is shown in Figure 9-3.

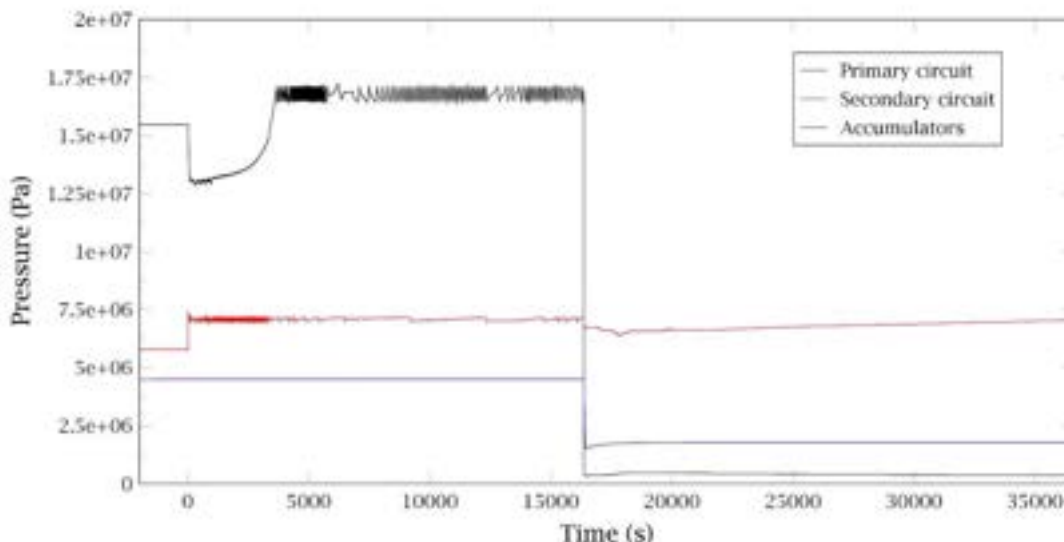


Figure 9-1 - Pressure profile in primary and secondary circuit and accumulators

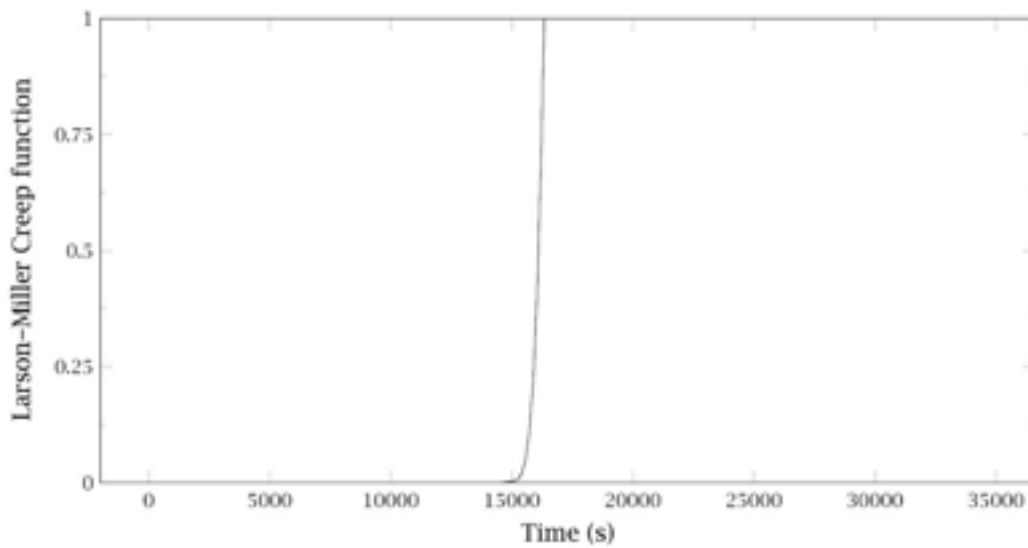


Figure 9-2 - Loop 1 Hot leg Larson-Miller creep function

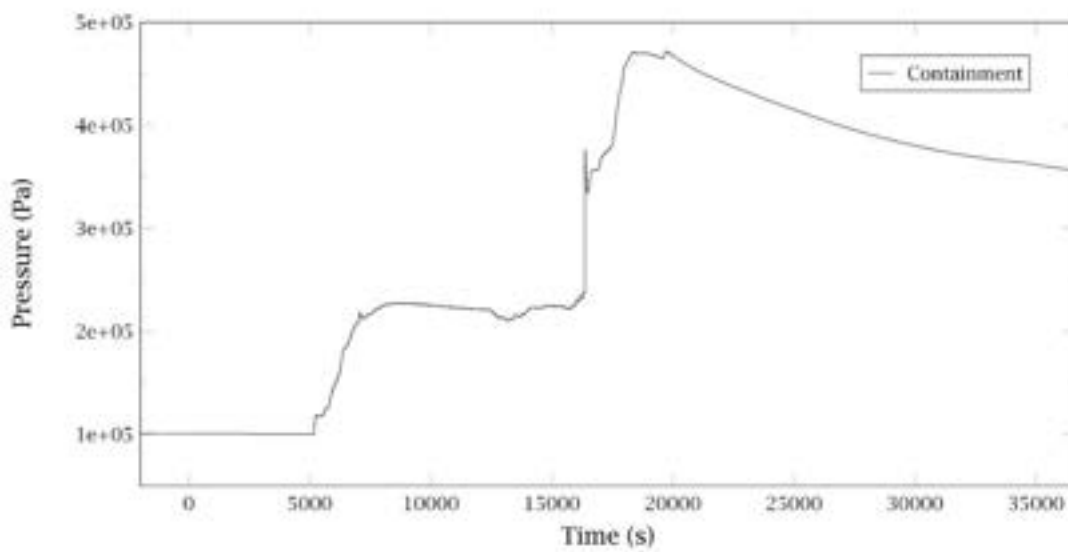


Figure 9-3 – Containment pressure

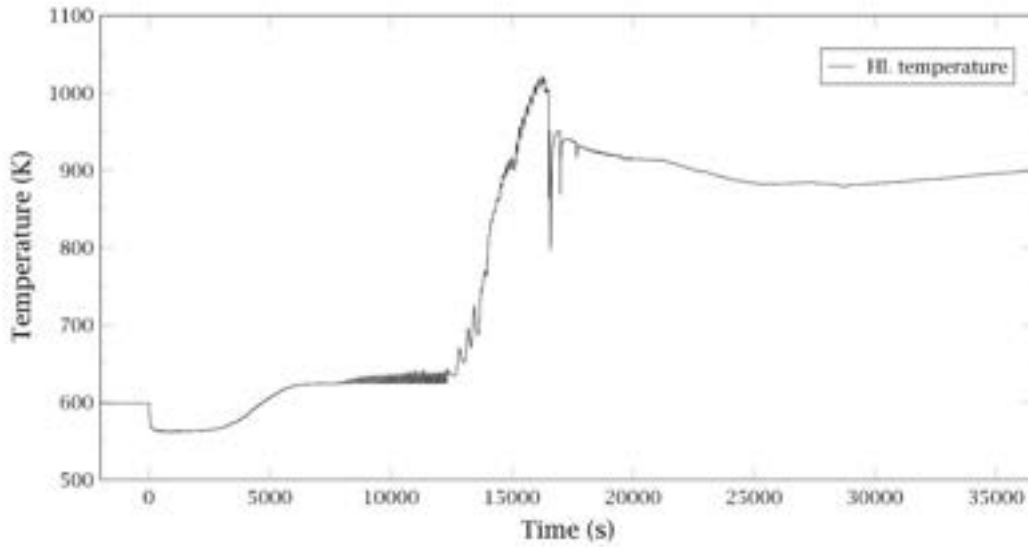


Figure 9-4 - Loop 1 Hot leg temperature profile

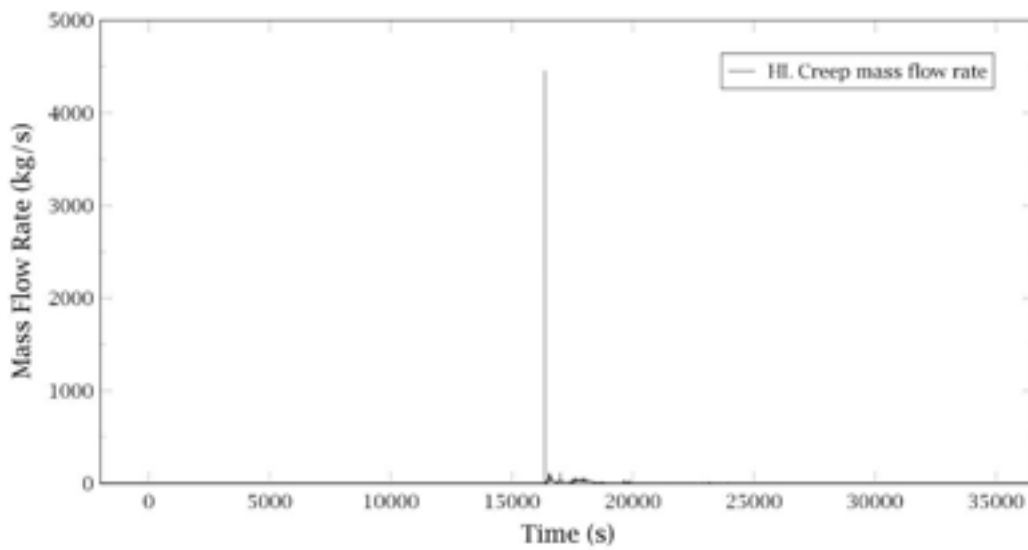


Figure 9-5 - Loop 1 HL creep mass flow rate

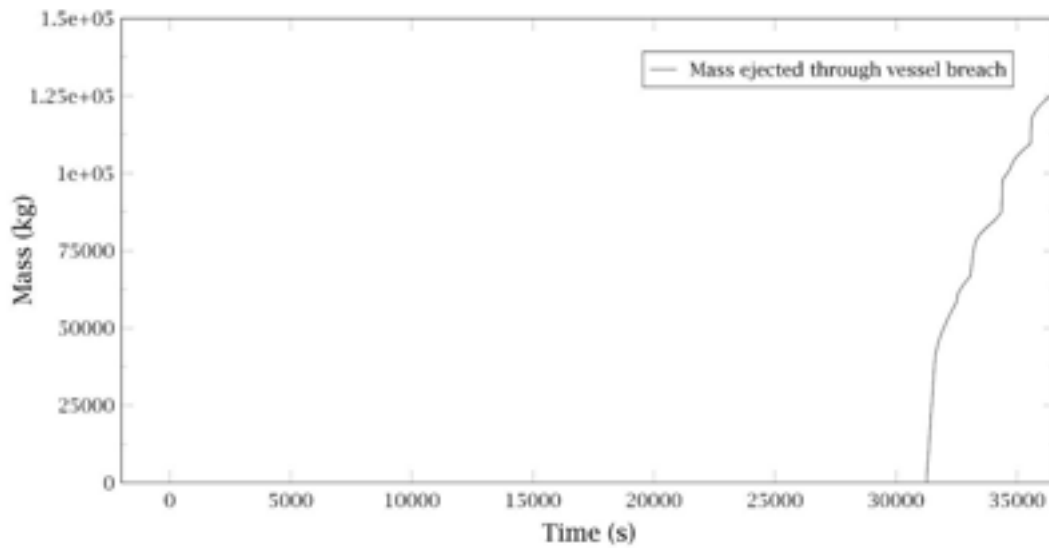


Figure 9-6 - Mass ejected through vessel breach

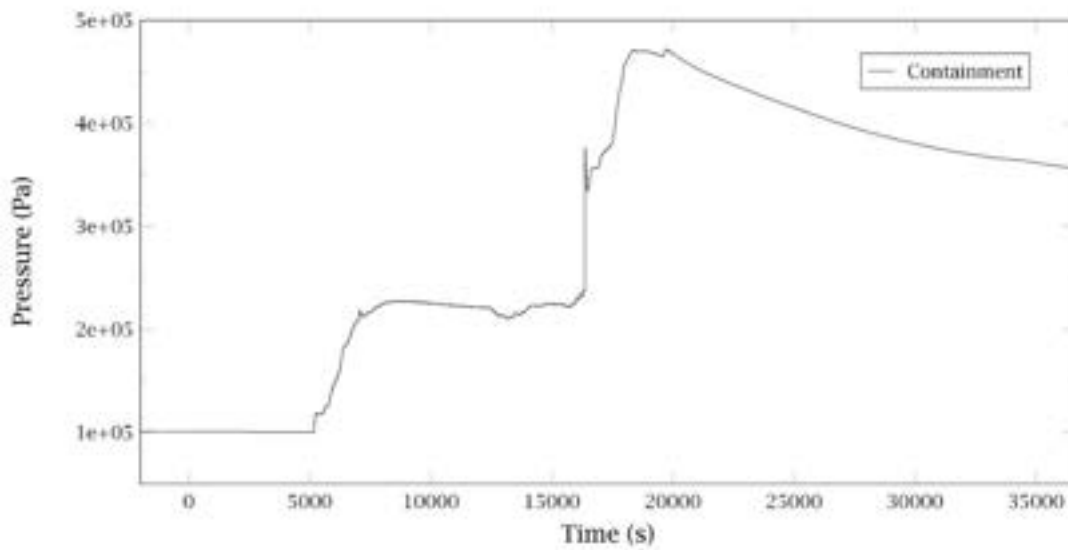



Figure 9-7 - Containment pressure

	Ricerca Sistema Elettrico	Sigla di identificazione ADPFISS-LP1-122	Rev. 0	Distrib. L	Pag. 47	di 56
---	----------------------------------	--	------------------	----------------------	-------------------	-----------------

10. Conclusions

Sapienza University of Rome together with ENEA plans to conduct sensitivity and uncertainty analyses on the Fukushima Daiichi unit 1 plant with the MELCOR code. The MELCOR model to be used was developed for previous deterministic safety analyses reported in [29], [30] and [31]. In order to perform this sensitivity and uncertainty study Sapienza University of Rome has developed a new Python interface to couple the MELCOR code with the RAVEN (Reactor Analysis and Virtual control ENvironment) software tool. The goal of this study is to evaluate the effects of some selected parameters on the melt progression behavior of the core during the BWR Fukushima Daiichi Unit I Severe Accident. Results have been statistically analyzed through the RAVEN BasicStatistic post-processor. A dynamic statistical analysis has been performed setting time as pivot parameter.


The implemented code coupling between RAVEN and MELCOR has been successfully tested in the uncertainty analysis here discussed. The present analysis shows there are some uncertainty that produce differences in timing of the major events such as lower head failure and pressure behaviors. Considering the uncertainty band chosen (0.05, 0.5 and 0.95 quantiles have been selected) the TEPCO plant data, publically available and selected for this analysis, are in general contained on it. Sensitivity analyses are in progress to study the effect of the nodalization detail on the calculated data. Focusing the attention on the lower head failure, it is to underline that its uncertainty is mainly related to the pump seal leak area uncertainty while the MELCOR modeling parameters and sensitivity coefficients, under investigation in this application, have a low ranked influence. Same considerations for the pressure behaviors here investigated. In the future a more detailed analysis will be performed, through the models implemented in RAVEN, by increasing the number of variables affected by uncertainty and including the uncertainty of the TEPCO plant data publically available.

The second simulation carried out in this work is the unmitigated loss of feedwater for a generic PWR 3 loop 900 MWe. The MELCOR 2.2 analysis shows a transient evolution similar in comparison with other analysis existing in literature. In comparison with the results obtained in the previous simulations presented in the past years, the new detailed TH core model permits a better evaluation, but the global results follow the same trend, with small differences in timing. The influence of the new HL nodalization, capable to more accurately predict the natural circulation, is positive and permits a better evaluation of the severe accident behavior.


11. ABBREVIATIONS

ASTEC	Accident Source Term Evaluation Code
BDBA	Beyond Design Basis Accident
BEPU	Best Estimate Plus Uncertainty
BWR	Boiling Water Reactor
CL	Cold Leg
CR	Control Rod
CRGT	Control Rod Guide Tube
CVH	Control Volume Hydrodynamics
ECCS	Emergency Core Cooling System
DBA	Design Basis Accident
DW	DryWell
FL	Flow Path
HL	Hot Leg
HPI	High Pressure Injection system
HS	Heat Structure
IC	Isolation Condenser
LBLOCA	Large Break Loss Of Coolant Accident
LFW	Loss of Feedwater
LH	Lower Head
LOCA	Loss Of Coolant Accident
LPI	Low Pressure Injection system
LWR	Light Water Reactor
MAAP	Modular Accident Analysis Program
MCP	Main Coolant Pump
MSIV	Main Steam Isolation Valves

MELCOR	Methods for Estimation of Leakages and Consequences Of Releases
MFW	Main Feedwater Pump
NPP	Nuclear Power Plant
NS	Non-supporting Structure
PCS	Primary Cooling System
PORV	Pilot-Operated Relief Valve
PRT	Pressurized Relief Tank
PRZ	Pressurizer
PWR	Pressurized Water Reactor
RCP	Reactor Coolant Pump
RCS	Reactor Coolant System
RCV	Reactor Coolant Vessel
RPV	Reactor Pressure Vessel
RN	RadioNuclide
SAM	Severe Accident Management
SIS	Safety Injection Systems
SBLOCA	Small Break LOCA
SBO	Station Blackout
SCRAM	Safety Control Rod Axe Man
SCS	Secondary Cooling System
SG	Steam Generator
SGTR	Steam Generator Tube Rupture
SNAP	Symbolic Nuclear Analysis Package
SNL	Sandia National Laboratories
SOT	Start Of the Transient
SS	Supporting Structure


 Ricerca Sistema Elettrico	Sigla di identificazione ADPFISS-LP1-122	Rev. 0	Distrib. L	Pag. 50	di 56
--	--	------------------	----------------------	-------------------	-----------------

SRV	Safety Relief Valve
TDAFW	Turbine-Driven Auxiliary Feed-Water pump
USNRC	US Nuclear Regulatory Commission
WW	WetWell

 Ricerca Sistema Elettrico	Sigla di identificazione	Rev.	Distrib.	Pag.	di
	ADPFISS-LP1-122	0	L	51	56

12. REFERENCES


- [1] Severe Accident Management Programmes for Nuclear Power Plants, IAEA Safety Standards, Safety Guide No. NS-G-2.15
- [2] Bentaïb, H. Bonneville, G. Cénérino, B. Clément, F. Corenwinder, M. Cranga, G. Ducros, F. Fichot, D. Jacquemain, C. Journeau, V. Koundy, D. Leteinturier, D. Magallon, R. Meignen, F. Monroig, G. Nahas, F. Pichereau, E. Raimond, J-M. Seiler, B. Tourniaire, J-P. Van-Dorsselaere; D. Jacquemain, Coordinator; Nuclear Power Reactor Core Melt Accidents, Current State of Knowledge, IRSN, EDP Sciences, France (2015).
- [3] M. Pescarini, F. Mascari, D. Mostacci, F. De Rosa, C. Lombardo, F. Giannetti, Analysis of unmitigated large break loss of coolant accidents using MELCOR code, 35th UIT Heat Transfer Conference (UIT2017), IOP Conf. Series: Journal of Physics: Conf. Series 923 (2017) 012009.
- [4] F. Mascari, J. C. DE LA ROSA BLUL, M. Sangiorgi, G. Bandini, ASTEC, MAAP AND MELCOR benchmark code analysis of an unmitigated SBO transient in A PWR-900 like reactor, IAEA Technical Meeting on the Status and Evaluation of Severe Accident Simulation Codes for Water Cooled Reactors", from 9 to 12 October 2017, IAEA's Headquarters in Vienna, Austria.
- [5] F. Mascari, M. D'onorio, F. Giannetti, G. Caruso, A. Naviglio, Analisi di Transitori Non Mitigati: Perdita di Refrigerante da Piccola Rottura in PWR, Perdita D'acqua di Alimento del GV in PWR e SBO in BWR (Analyses of Unmitigated Transients: Small Break LOCA in PWR, Loss of Feedwater in PWR and SBO in BWR), ADPFISS-LP1- 103, 2017" <http://openarchive.enea.it/handle/10840/9211>
- [6] F. Mascari, Marco Pescarini, F. Giannetti, I. Luciani, G. Caruso, Integral Calculations of Severe Accident Scenarios in PWRs and BWRs, ADPFISS-LP1-075, 2016. <http://openarchive.enea.it/bitstream/handle/10840/8170/ADPFISS-LP1-075.pdf?sequence=1>
- [7] C. Lombardo, F. Mascari, P. Buffa, F. Castiglia, M. Giardina, G. Palermo, Nodalizzazione MELCOR per lo Studio Integrato di Sequenze Incidentali su Reattori PWR da 900 MWe e Valutazioni Preliminari D'impatto a Breve e Medio Raggio, ADPFISS-LP1-026, Italy (2014).
- [8] Chatelard P., Belon S., Bosland L., Carénini L., Coindreau O., Cousin F., Marchetto C., Nowack H., Piar L., Chailan L, Main modelling features of ASTEC V2.1 major version, Annals of Nuclear Energy (on Press), January 2016
- [9] MELCOR Computer Code Manuals, Vol.1: Primer and Users' Guide, SAND 2015-6691 R; Vol. 2: Reference Manual, SAND 2015-6692 R; Vol. 3: MELCOR Assessment Problems, SAND 2015-6693 R; Sandia National Laboratories, USA (2015).
- [10] J.P. Van Dorsselaere, M. Barrachin, S. Power, M. Adorni, M. Hrehor, F. Mascari, A. Schaffrath, I. Tiselj, E. Uspuras, Y. Yamamoto, D. Gumenyuk, N. Fedotova, O. Cronvall, P. Liska, The Summary of ETSON strategic orientations on research activities, ETSON Research Group activity, atw Vol. 63 (2018), issue 1 January
- [11] M. D'Onorio, F. Giannetti, F. Mascari, G. Caruso, UNCERTAINTY ANALYSES USING THE RAVEN SOFTWARE TOOL COUPLED WITH MELCOR SEVERE ACCIDENT CODE, ANS Best Estimate Plus Uncertainty International Conference (BEPU 2018) Real Collegio, Lucca, Italy, May 13-19, 2018, BEPU2018-282
- [12] A. Bersano, F. Mascari, Evaluation of a Double-Ended Guillotine Break Transient in a Three-Loop PWR-900 Like with TRACE Code Coupled with DAKOTA Uncertainty Analysis, 12th International Topical Meeting on Nuclear Reactor Thermal-Hydraulics, Operation and Safety (NUTHOS-12) Qingdao, China, October 14-18, 2018
- [13] Source term uncertainty, recent development in understanding fission product behaviour, NEA/CSNI/R(92)2

	Sigla di identificazione ADPFISS-LP1-122	Rev. 0	Distrib. L	Pag. 52	di 56
---	--	------------------	----------------------	-------------------	-----------------


- [14] SOAR on Containment Thermalhydraulics and Hydrogen Distribution, NEA/CSNI/R(1999)16
- [15] In-Vessel Core Degradation Code Validation Matrix, Update 1996-1999, NEA/CSNI/R(2000)21, France (2001).
- [16] State-Of-The-Art Report On Nuclear Aerosols, NEA/CSNI/R(2009)5
- [17] Containment code validation matrix, NEA/CSNI/R(2014)3
- [18] F. Mascari, H. Nakamura, K. Ummlinger, F. De Rosa, F. D'Auria, Scaling issues for the experimental characterization of reactor coolant system in integral test facilities and role of system code as extrapolation tool, Proceeding of International Topical Meeting on Nuclear Reactor Thermal Hydraulics 2015, NURETH 2015.
- [19] J. P. Van Dorsselaere, J. Mustoe, S. Power, M. Adorni, A. Schaffrath, A. Nieminen, ETSO views on R&D priorities for implementation of the 2014 Euratom Directive on safety of nuclear installations, Kerntechnik: Vol. 81, No. 5, pp. 527-534.
- [20] .Humphries, MELCOR Code Development Status EMUG 2018, 10th Meeting of the European MELCOR User Group, University of Zagreb, Zagreb, Croatia, Faculty of Electrical Engineering and Computing – FER, April 25-27, 2018
https://www.psi.ch/emug/Emug2018EN/EMUG_2018_01.pdf
- [21] Electric Power Research Institute, "Modular Accident Analysis Program (MAAP) MELCOR Crosswalk, Phase 1 – Study", EPRI report, 2014
- [22] D. L. Luxat, D. A. Kalanich, J. T. Hanophy, R. O. Gauntt, R. M. Wachowiak, MAAP-MELCOR Crosswalk Phase 1 Stud, Nuclear Technology · volume 196, 2016.
- [23] S. Belon, C. Bouillet, H. Bonneville, N. Andrews, C. Faucett, "Insight of Core Degradation Simulation in Integral Codes Throughout ASTEC/MELCOR Crosswalk Comparisons and ASTEC Sensitivity Studies", Proceedings of ERMSAR 2017, Warsaw, Poland, May 16-18, (2017).
- [24] NEA/CSNI/R(98)22: Good Practices for User Effect Reduction, Status Report, November 1998
- [25] Approaches and Tools for Severe Accident Analysis for Nuclear Power Plants, IAEA Safety Reports Series No. 56, IAEA, Vienna, 2008
- [26] CESAM, Deliverable, D40.44 – Synthesis of Evaluation of the Impact of SAM Actions Through ASTEC NPP Calculations, (2017).
- [27] F. Mascari, J.C. De La Rosa Blul, M. Sangiorgi, G. Bandini, Analyses of an Unmitigated Station Blackout Transient with ASTEC, MAAP and MELCOR Codes, SICNUC – PC28 – 001, Italy (2017).
- [28] F. Mascari, J.C. De La Rosa Blul, M. Sangiorgi, G. Bandini, "Analyses of an Unmitigated Station Blackout Transient with ASTEC, MAAP and MELCOR Code, 9th Meeting of the "European MELCOR User Group", Madrid, Spain, April 6-7, (2017).
- [29] C. Parisi, F. Mascari, P. Balestra, F. Giannetti, G. Caruso, Fukushima Dai-ichi Unit 1 Accident Simulation by Best Estimate and Integral Codes & Accident Management Procedures Identification Focusing on BWR close to the Italian Borders. ADPFISS – LP1 – 044
<http://hdl.handle.net/10840/5032>
- [30] F. Mascari, F. Giannetti, G. Caruso, Integral study of accident sequences with reference to NPPs next to the Italian borders. ADPFISS-LP1-059 <http://hdl.handle.net/10840/7061>
- [31] F. Mascari, M. D'Onorio, F. Giannetti, G. Caruso, A. Naviglio, Analisi di transitori non mitigati: perdite di refrigerante da piccola rottura in PWR, perdita d'acqua di alimento del GV in PWR e SBO in BWR. ADPFISS-LP1-103

- [32] Fauske & Associates, LLC “Transmittal Document for MAAP5 Code Revision MAAP 5.02”, FAI/13-0801, 2013.
- [33] MELCOR Computer Code Manuals, Vol.1: Primer and Users’ Guide, SAND 2015-6691 R; Vol. 2: Reference Manual, SAND 2015-6692 R; Vol. 3: MELCOR Assessment Problems, SAND 2015-6693 R; Sandia National Laboratories, USA (2015).
- [34] <http://melcor.sandia.gov/about.html>
- [35] Symbolic Nuclear Analysis Package (SNAP), User’s Manual. Applied Programming Technology, Inc., (2012).
- [36] Safety of Nuclear Power Plants: Design, IAEA Safety Standards, Specific Safety Requirements, No. SSR-2/1SOARCA 1 2
- [37] C. Rabbit, A. Alfonsi, J. Cogliatti, D. Mandelli, and R. Kinoshita, “REACTOR ANALYSIS AND VIRTUAL CONTROL ENVIRONMENT (RAVEN) FY12 REPORT,” Tech. Rep. INL/EXT-12-27351, Idaho National Laboratory (INL) (2012).
- [38] C. Rabbit, A. Alfonsi, J. Cogliatti, D. Mandelli and R. Martineau, “RAVEN as Control Logic and Probabilistic Risk Assessment Driver for RELAP-7,” in “Proceeding of American Nuclear Society (ANS), San Diego (CA),” (2012), vol. 107, pp. 333–335
- [39] Cristian Rabiti, Andrea Alfonsi, Joshua Cogliati, Diego Mandelli, and Robert Kinoshita. RAVEN, a New Software for Dynamic Risk Analysis. United States: N. p., 2014. Web.
- [40] Safety of Nuclear Power Plants: Design, IAEA Safety Standards, Specific Safety Requirements, No. SSR-2/1SOARCA 1 2
- [41] IAEA, The Fukushima Daiichi accident — Vienna: International Atomic Energy Agency, 2015 ISBN 978–92–0–107015–9
- [42] https://www.nirs.org/wp-content/uploads/fukushima/naic_report.pdf
- [43] State-of-the-Art Reactor Consequence Analyses Project Volume 1: Peach Bottom Integrated Analysis. NUREG/CR-7110, Vol. 1
- [44] Randall Gauntt et al., Fukushima Daiichi Accident Study (Status as of April 2012) SAND2012-6173
- [45] J. J. Carbajo, Severe Accident Source Term Characteristics for Selected Peach Bottom Sequerices Predicted by the MELCOR Code. NUREG/CR-5942
- [46] TEPCO, Plant Specifications of Unit 1, https://fdada.info/docdata/accident_analysis/PS-Unit1-01.pdf (updated 02.12.13).
- [47] <https://www.nrc.gov/docs/ML1423/ML14234A136.pdf>
- [48] TEPCO, Fukushima Nuclear Accidents Investigation Report, http://www.tepco.co.jp/en/press/corp-com/release/betu12_e/images/120620e0104.pdf (2012).
- [49] BOILING WATER REACTOR TURBINE TRIP (TT) BENCHMARK, Volume I: Final Specifications, NEA/NSC/DOC(2001)1
- [50] MELCOR Best Practices as Applied in the State-of-the-Art Reactor Consequence Analyses (SOARCA) Project, NUREG/CR-7008, USNRC, 2014 <https://www.nrc.gov/docs/ML1423/ML14234A136.pdf>
- [51] Lillington J N et al., “Main Characteristics of Nuclear Power Plants in the European Union and Candidate Countries” EUR 20056, 2001;
- [52] D. Jacquemain, et.al., “Nuclear power reactor core melt accidents - State of knowledge” IRSN, 2015;

- [53] B. Clément, N. Hanniet-Girault, G. Repetto, D. Jacquemain, A.V. Jones, M.P. Kissane, M.P. von der Hardt, "LWR severe accident simulation: synthesis of the results and interpretation of the first Phebus FP experiment FPT0", Nuclear Engineering and Design 226 (1), 5-82, 2003;
- [54] L. Sepold, P. Hofmann, W. Leiling, A. Miassoedov, D. Piel, L. Schmidt, M. Steinbrück, "Reflooding experiments with LWR-type fuel rod simulators in the QUENCH facility", Nuclear Engineering and Design 204 (1-3), 205-220, 2001;
- [55] Ivan Rinaldi, Andrea Alfonsi, Joshua Cogliatti, Cristian Rabiti, Fabio Giannetti, Gianfranco Caruso, A Comprehensive Validation Approach Using The RAVEN Code. 2015 ANS Annual Meeting: "Nuclear Technology: An Essential Part of the Solution"
- [56] F. Fichot, J.M. Seiler, V. Strizhov, "Applications of the OECD MASCA Project Results to Reactor Safety Analysis" MASCA Application Report, OECD-NEA, 2003;
- [57] J.M. Seiler, K. Froment "Material effects on multiphase phenomena in late phases of severe accidents of nuclear reactors", Multiphase Science and Technology 12, 117-257, 2000;
- [58] M. Saito et al., "Melting attack of solid plates by a high-temperature liquid jet – effect of crust formation", Nuclear Engineering and Design 121 (1), 11-23, 1990;
- [59] A. Stewart, A.T Pieczynski, V. Srinivar, "Natural Circulation Experiments for PWR Degraded Core Accidents," EPRI Project No. RP2177-5 Final Report, 1990;
- [60] Stewart, W.A., Pieczynski, A.T., and Srinivar, V., "Natural Circulation Experiments for PWR High Pressure Accidents," EPRI Report TR 102815, 1993.
- [61] P. D. Bayless, et.al., "Severe Accident Natural Circulation Studies at the INEL", NUREG/CR-6285, February 1995;
- [62] C.F. Boyd, K. Hardesty, "CFD Analysis of 1/7th Scale Steam Generator Inlet Plenum Mixing During a PWR Severe Accident," NUREG-1781, U.S. NRC, October 2003;
- [63] C.F. Boyd, D.M. Helton, K. Hardesty, "CFD Analysis of Full Scale Steam Generator Inlet Plenum Mixing During a PWR Severe Accident," NUREG-1788, U.S. NRC, May 2004;
- [64] P. B. Bayless, "Analysis of Natural Circulation During A Surry Station Blackout Using SCDAP/RELAP5," NUREG/CR-5214, EGG-2547, Idaho National Engineering Laboratory, Idaho Falls, Idaho, September 1988.
- [65] K. C. Wagner, "MELCOR 1.8.5 Analysis of Natural Circulation Flow in the Westinghouse High-Pressure SF6 Experiments," Draft SAND Report, Sandia National Laboratories, June 2001
- [66] C.D Fletcher, R.M. Beaton, "SCDAP/RELAP5 Base Case Calculation for the Station Blackout Uncertainty Study," Letter report to D. M. Helton, US NRC, August 2006.
- [67] C.D Fletcher, R.M. Beaton "Evaluation of Uncertainties in SCDAP/RELAP5 Station Blackout Simulations," Letter report to D. M. Helton, US NRC, August 2006.
- [68] C. Lombardo, F. Mascari, P. Buffa, F. Castiglia, M. Giardina, G. Palermo, "Nodalizzazione MELCOR per lo Studio Integrato di Sequenze Incidentali su Reattori PWR da 900 MWe e valutazioni preliminari d'impatto a breve e medio raggio", ENEA, ADPFISS-LP1-026, 09/09/2014
- [69] F. Mascari, Marco Pescarini, F. Giannetti, I. Luciani, G. Caruso, "Integral Calculations of Severe Accident Scenarios in PWRs and BWRs", ADPFISS-LP1-075, 2016
- [70] ENEL Direzione delle Costruzioni DIR-PUN 1986 Progetto Unificato Nucleare - I Quaderni dell'Energia No. 12
- [71] CSNI Report No 166: Containment for Pressurized Water Reactors, a State-of-the-Art Report, December 1989

	Ricerca Sistema Elettrico	Sigla di identificazione ADPFISS-LP1-122	Rev. 0	Distrib. L	Pag. 55	di 56
---	----------------------------------	--	------------------	----------------------	-------------------	-----------------

- [72] NEA/CSNI/R(2000)21: In-Vessel Core Degradation Code Validation Matrix, Update 1996-1999, February, 2001
- [73] F. D'Auria, M. Frogheri, W. Giannotti, RELAP5/MOD3.2 Post Test Analysis and Accuracy Quantification of SPES Test SP-SB-04, NUREG/IA-0155, February 1999.
- [74] K. Ross, J. Phillips, R. O. Gauntt, K. C. Wagner, "MELCOR Best Practices as Applied in the State-of-the-Art Reactor Consequence Analyses (SOARCA) Project," NUREG/CR-7008, U.S. NRC, August 2014
- [75] U.S. NRC, "Westinghouse Technology Systems Manual", 1993;
- [76] R. J. Roark, W. C. Young "Formulas for Stress and Strain", McGraw-Hill Book Company, New York, NY, 1982;
- [77] C. Boyd, K. Armstrong, "Computational Fluid Dynamics Analysis of Natural Circulation Flows in a Pressurized-Water Reactor Loop under Severe Accident Conditions", NUREG-1922, March 2010;
- [78] J. Couturier, M. Schwarz, "Current State of Research on Pressurized Water Reactor Safety" IRSN, 2018;
- [79] U.S. NRC, "State-of-the-Art Reactor Consequence Analyses Project. Volume 2: Surry Integrated Analysis," NUREG/CR-7110 Volume 2, Rev. 1, 2013;
- [80] E.R Lindgren, S.G. Durbin, "Measurement of pressure drops in prototypic BWR and PWR fuel assemblies in the laminar regime" Nuclear Energy Agency of the OECD (NEA), Jan 2012;
- [81] J. Peybernès, "Evaluation of the forces generated by cross-flow on PWR fuel assembly", IAEA-TECDOC-1454, 2005;
- [82] C.F. Boyd, "Prediction of Severe Accident Counter Current Natural Circulation Flows in the Hot Leg of a Pressurized Water Reactor" U.S. NRC, Proceedings of ICONE 14, International Conference on Nuclear Engineering, 17-20 July 2006, Miami, Florida.
- [83] S.J. Leach and H. Thompson, "An Investigation of Some Aspects of Flow Into Gas Cooled Nuclear Reactors Following an Accidental Depressurization," J. Br. Nuclear Energy Society, July 14, 1975, No. 3, 243-250;
- [84] Y. Liao, S. Guentay, "Correlation of Steam Generator Mixing Parameters for Severe Accident Hot-Leg Natural Circulation" IYNC 2008, Paper No. 122, September 2008;
- [85] T. Boardman, N. Jeanmougin, R. Lofaro, J. Prevost, "Leak Rate Analysis of the Westinghouse Reactor Coolant Pump" NUREG/CR-4294, U.S. NRC, 85-ETEC-DRF-1714, 1985;
- [86] Dominion, "Operator Response Times for a Total Loss of RCP Seal Cooling," ET-CME-05-0020, Revision 2, December 5, 2006;
- [87] "MELCOR Computer Code Manuals", Vol. 2: Reference Manual, Version 2.2.9541 2017, SAND2017-0876 O, January 2017;
- [88] "MELCOR Computer Code Manuals", Vol. 1: Primer and Users' Guide, Version 2.2.9541 2017, SAND2017-0455 O, January 2017.
- [89] A. Annunziato, D. Magallon, et al., "Progress of the FARO/KROTOS programme," Cooperative Severe Accident Research Meeting, U.S. NRC, 1996;
- [90] L.L. Humphries et. al, "Lower Head Failure Experiments and Analyses," NUREG/CR-5582, SAND98-2047, Sandia National Laboratories, 1998;
- [91] M.T. Farmer, S. Lomperski, and S. Basu, "Results of Reactor Material Experiments Investigating 2-D Core-Concrete Interaction and Debris Coolability," Proc. Proc. Int. Conf. Adv. Power Plants, ICAPP'04, Pittsburgh, Pennsylvania, June 2004

 Ricerca Sistema Elettrico	Sigla di identificazione ADPFISS-LP1-122	Rev. 0	Distrib. L	Pag. 56	di 56
--	--	------------------	----------------------	-------------------	-----------------

- [92] T. Nakamura and R.A. Lorenz, "A Study of Cesium and Krypton Releases Observed in HI and VI Tests Using a Booth Diffusion Model," Oak Ridge National Laboratory Research Paper, May 1987
- [93] R. A. Lorenz, M. F. Osborne, "A Summary of ORNL Fission Product Release Tests with Recommended Release Rates and Diffusion Coefficients", U.S NRC, NUREG/CR-6261, 1995;
- [94] Ray A. Berry et al. RELAP-7 Theory Manual (Revision 2) · April 2016 INL/EXT-14-31366 (Revision 2), DOI: 10.13140/RG.2.1.4346.1522
- [95] H. Glaeser, "GRS Method for Uncertainty and Sensitivity Evaluation of Code Results and Applications," Sci. Technol. Nuc. Ins. (2008) 10
- [96] S.S. Wilks, "Determination of sample sizes for setting tolerance limits," Ann. Math. Stat. 12(1), pp. 91-96 (1941) 11.
- [97] S.S. Wilks, "Statistical prediction with special reference to the problem of tolerance limits," Ann. Math. Stat. 13(4), pp. 400-409 (1942)
- [98] IAEA International Atomic Energy Agency "Best Estimate Safety Analysis for Nuclear Power Plants: Uncertainty Evaluation," Safety Reports Series (2008)
- [99] M.E. Stephens, B.W. Goodwin, T.H. Andres, "Deriving parameter probability density functions," Reliab. Eng. Syst. Safe. 42, pp. 271-291 (1993)